Supporting Information

Light-driven chiroptical photoswitchable DNA-assemblies mediated by bioinspired photoresponsive molecules

Marta Dudek,[a,b#] Marco Deiana,[a*#] Ziemowit Pokladek,[a,b] Piotr Mlynarz,[b] Marek Samoc[a] and Katarzyna Matczyszyn[a*]

[a]Advanced Materials Engineering and Modelling Group, Faculty of Chemistry, Wroclaw University of Science and Technology, Wyb. Wyspianskiego 27, 50-370 Wroclaw, Poland

[b]Department of Bioorganic Chemistry, Faculty of Chemistry, Wroclaw University of Science and Technology, Wyb. Wyspianskiego 27, 50-370 Wroclaw, Poland

M.D. and M. D. These authors contribute equally.

*Corresponding authors: katarzyna.matczyszyn@pwr.edu.pl and marco.deiana@pwr.edu.pl

Table of Contents:

Synthesis

Synthesis NMR-spectra were recorded on a Bruker AvanceTM 600 MHz spectrometer. Mass spectra were conducted with a WATERS LCT Premier XE mass spectrometer (ESI). Unless otherwise noted, all reactions were carried out under normal conditions. Materials and solvents obtained from commercial suppliers were used without further purification.

Synthesis of **4,5**

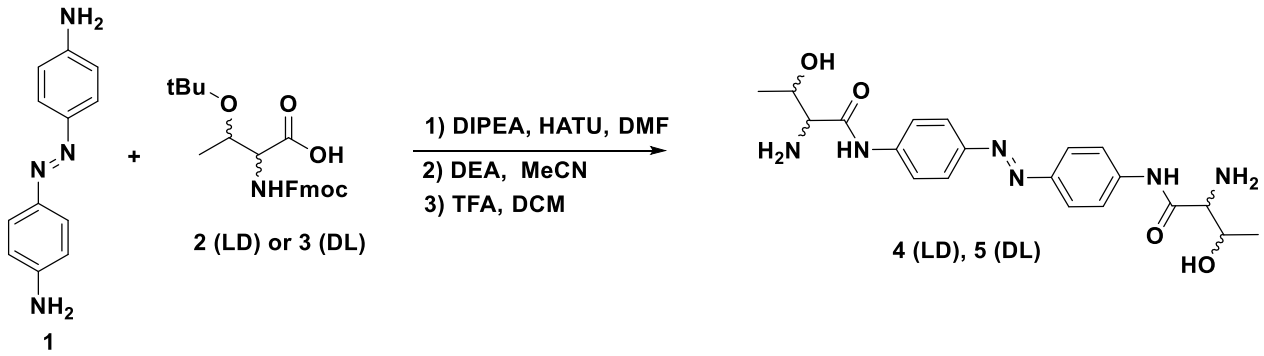

Compound **1** was synthetized according to previous published procedure.[1]

(E)-N,N'-(diazene-1,2-diylbis(4,1-phenylene))bis(2-amino-3-hydroxybutanamide). To a solution of Fmoc-Thr(Boc)-OH (LD for **4** and DL for **5**) (0.4 g, 1 mmol, 2.4 equiv.) in DMF (10 mL), DIPEA (0.26 g, 2 mmol, 4.8 equiv.) and HATU (0.38 g,1 mmol, 2.4 equiv.) were added, after few seconds (E)-4,4'- (diazene-1,2-diyl)dianiline (0.09 g, 0.42 mmol, 1 equiv.) was added. The reaction mixture was stirred overnight at room temperature. Solvent was removed under reduced pressure, then water (100 mL) was added and reaction mixture was filtered through Buchner funnel, solid was washed with water and dried under vacuum. Without further purification F-moc protection group was removed by adding obtained solid to diethylamine (DEA) (0.8 mL) in MeCN (0.8 mL) solution. The mixture was stirred for 2 h and concentrated under reduced pressure. The obtained orange solid was dissolved in DCM (10 mL) and TFA (1 mL) was added to remove tBu group and the reaction mixture was stirred overnight. Solvent was removed under vacuum and crude product was purified by HPLC using gradient from water to water/MeCN (1/1) in 20 minutes. **4**, **5** were obtained as orange powders (**4**: 0.2 g, 48%, **5**: 0.21 g, 51%).

Spectral data for **4**:

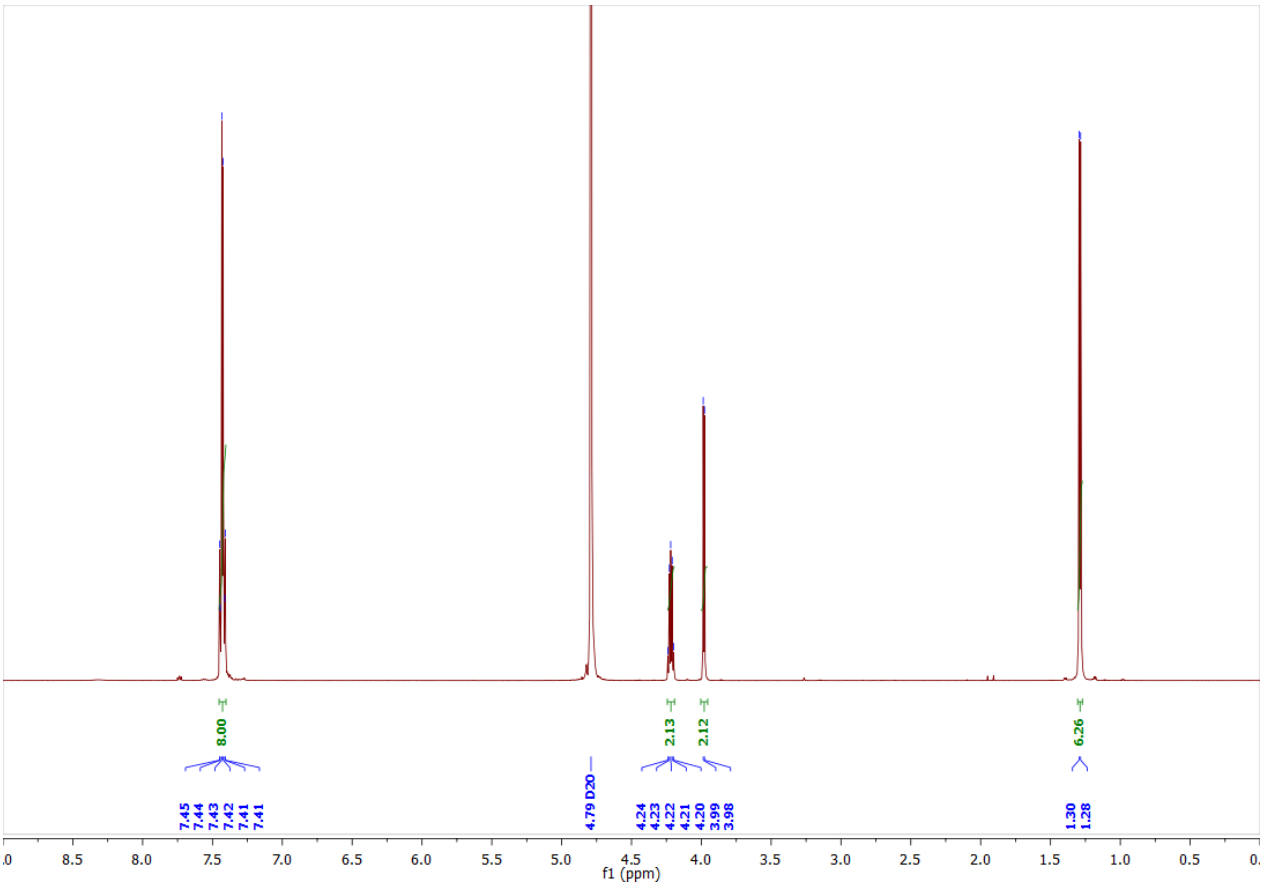

Figure S1. ^{1}H-NMR spectrum of **4**

^{1}H NMR (400 MHz, D2O) δ:

7.47 – 7.39 (m, 8H), 4.22 (p, *J* = 6.4 Hz, 2H), 3.98 (d, *J* = 5.6 Hz, 2H), 1.29 (d, *J* = 6.5 Hz, 6H).

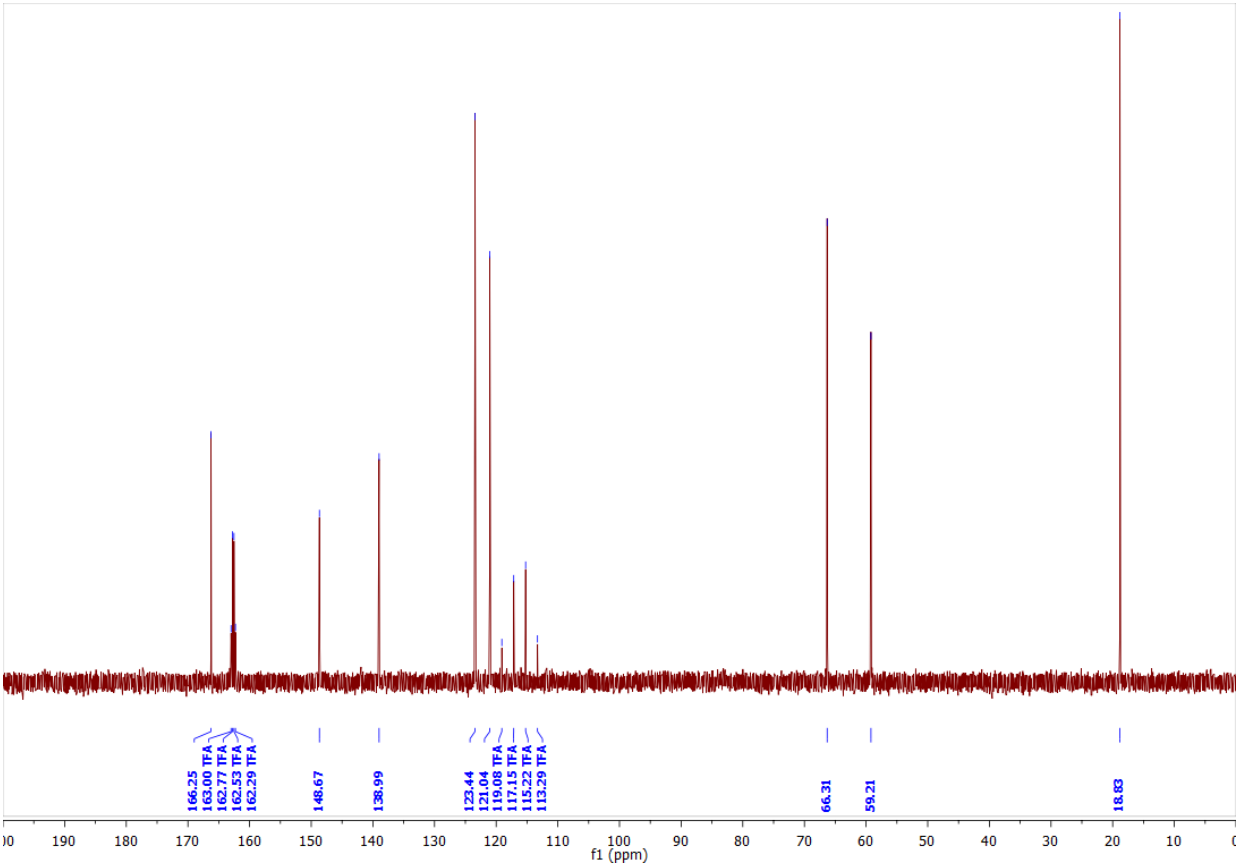

Figure S2. ^{13}C-NMR spectrum of **4**

^{13}C NMR (101 MHz, D2O) δ:

166.25, 148.67, 138.99, 123.44, 121.04, 66.31, 59.21, 18.83

HRMS m/z (ESI): calc. for: $C_{20}H_{26}N_6O_4$: $[M+H]^+$,

Required:415.2094 , found:415.2086

Spectral data for **5**:

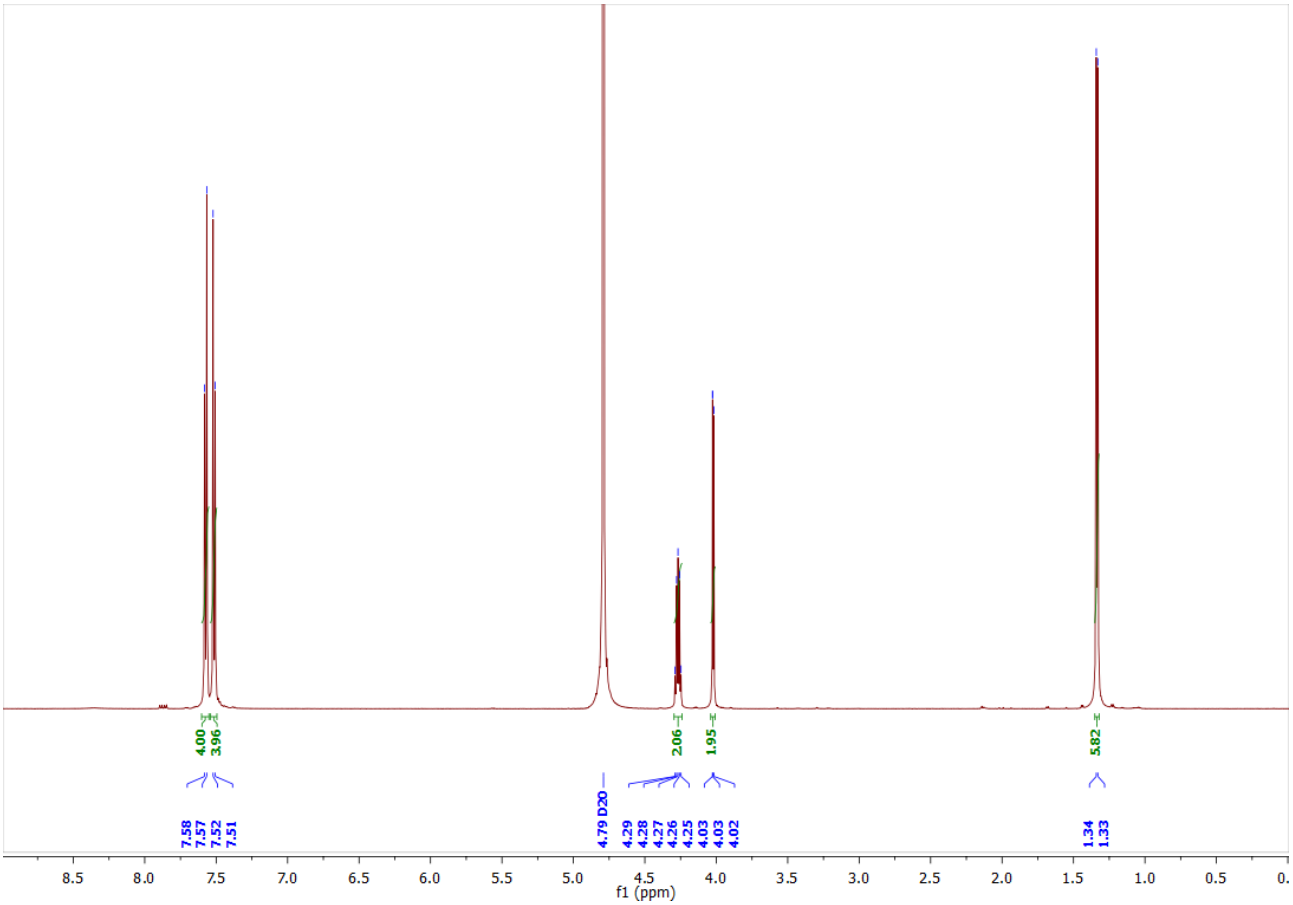

Figure S3. ^{1}H-NMR spectrum of **5**

^{1}H NMR (400 MHz, D2O) δ:

7.57 (d, *J* = 8.9 Hz, 4H), 7.51 (d, *J* = 8.9 Hz, 4H), 4.27 (p, *J* = 6.4 Hz, 2H), 4.05 – 4.00 (m, 2H), 1.34 (d, *J* = 6.5 Hz, 6H).

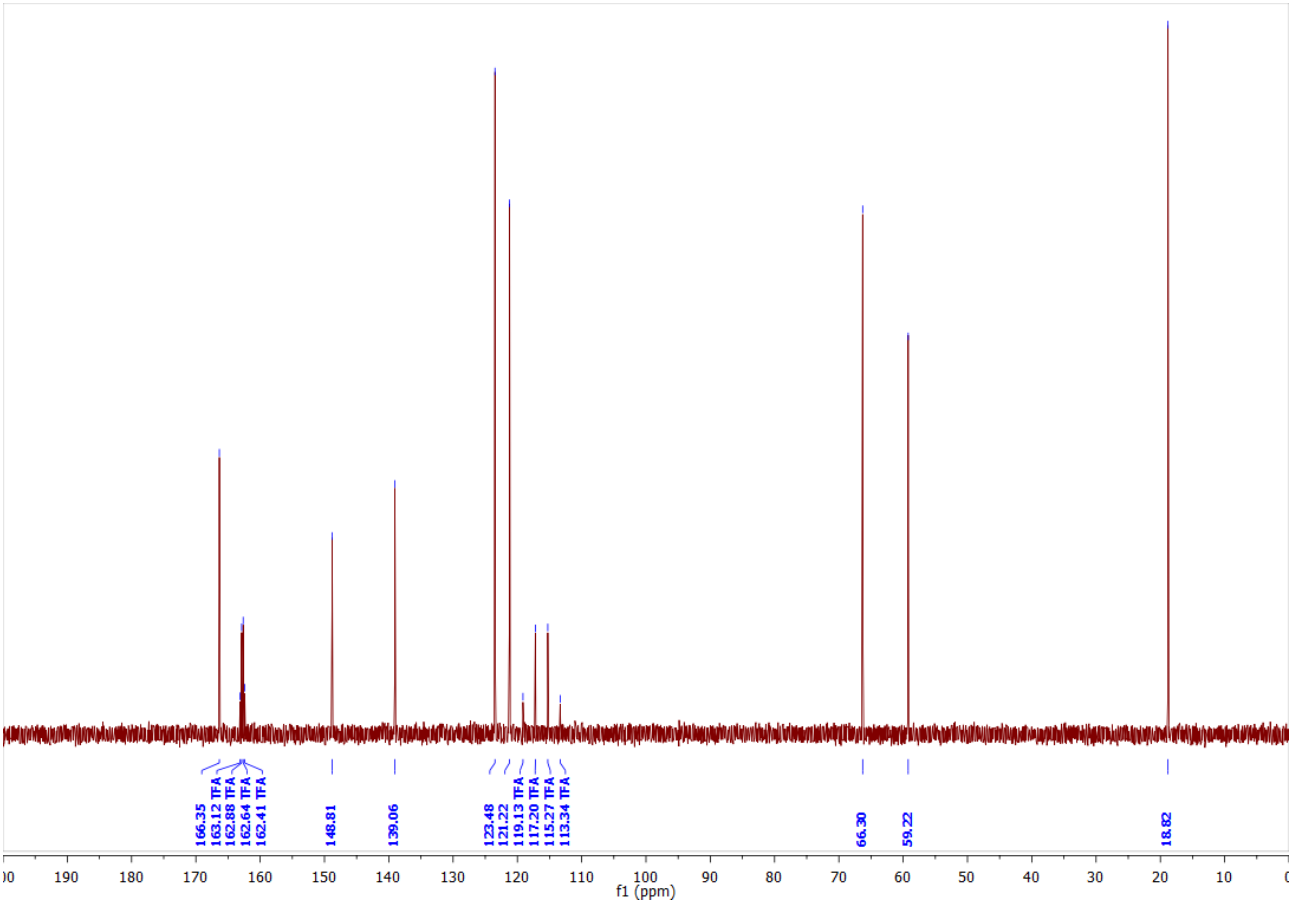

Figure S4. ^{13}C-NMR spectrum of **5**

^{13}C NMR (101 MHz, D2O) δ:

166.35, 148.81, 139.06, 123.48, 121.22, 66.30, 59.22, 18.82

HRMS m/z (ESI): calc. for: $C_{20}H_{26}N_6O_4$: $[M+H]^+$,

Required:415.2094, found:415.2089

Synthesis of 8,9

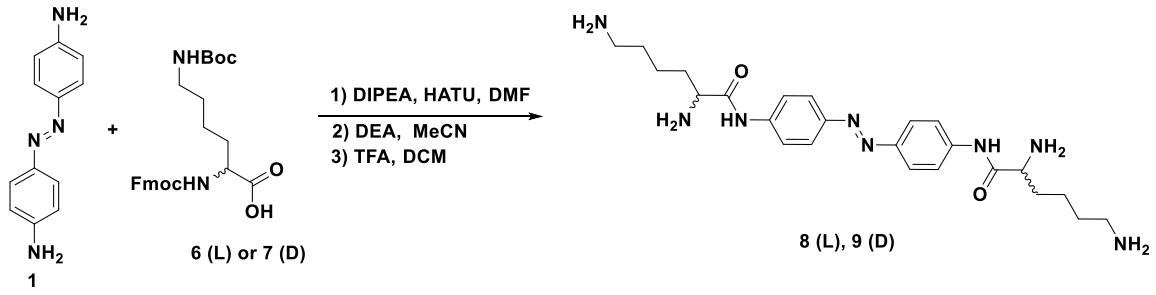

(E)-N,N'-(diazene-1,2-diylbis(4,1-phenylene))bis(2,6-diaminohexanamide). To a solution of Fmoc-Lys(Boc)-OH (LL for **8** and DD for **9**) (0.53 g, 1.13 mmol, 2.4 equiv.) in DMF (10 mL), DIPEA (0.29 g, 2.25 mmol, 4.8 equiv.) and HATU (0.43 g,1.13 mmol, 2.4 equiv.) were added, after few seconds (E)-4,4'- (diazene-1,2-diyl)dianiline (0.10 g, 0.47 mmol, 1 equiv.) was added. The reaction mixture was stirred overnight at room temperature. Solvent was removed under reduced pressure, then water (100 mL) was added and reaction mixture was filtered through Buchner funnel, solid was washed with water and dried under vacuum. Without further purification F-moc protection group was removed by adding obtained solid to diethylamine (DEA) (0.8 mL) in MeCN (0.8 mL) solution. The mixture was stirred for 2 h and concentrated under reduced pressure. The obtained orange solid was dissolved in DCM (10 mL) and TFA (1 mL) was added to remove Boc group and the reaction mixture was stirred overnight. Solvent was removed under vacuum and crude product was purified by HPLC using gradient from water to water/MeCN (1/1) in 20 minutes (1/1) in 20 minutes. **8**, **9** were obtained as orange powders (**8**: 0.19 g, 36%, **9**: 0.2 g, 38%).

Spectral data for **8**:

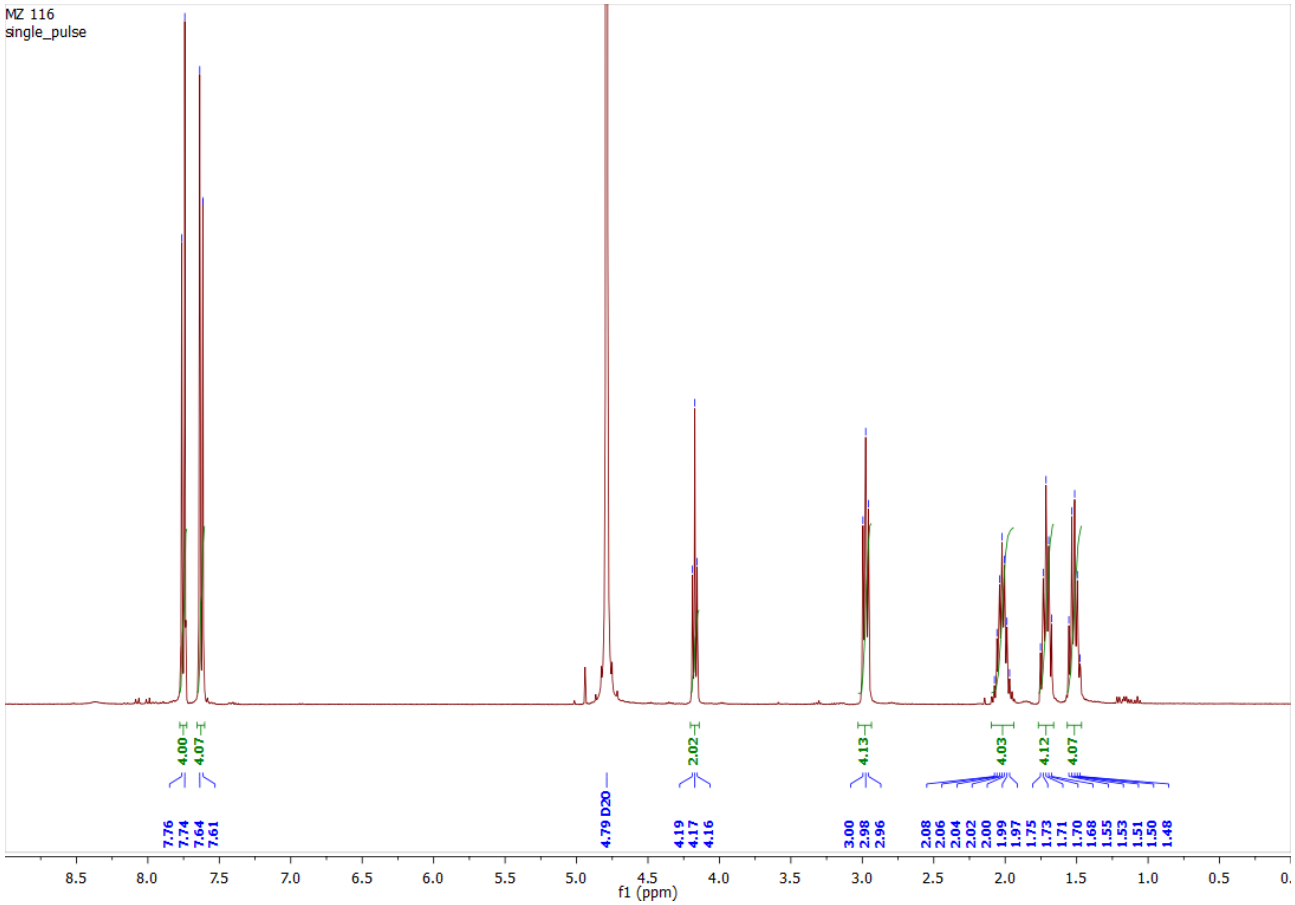

Figure S5. ^{1}H-NMR spectrum of **8**

^{1}H NMR (400 MHz, D_2O) δ:

7.75 (d, *J* = 8.8 Hz, 4H), 7.63 (d, *J* = 8.8 Hz, 4H), 4.17 (t, *J* = 6.6 Hz, 2H), 2.98 (t, *J* = 7.8 Hz, 4H), 2.14 – 1.87 (m, 4H), 1.78 – 1.62 (m, 5H), 1.58 – 1.43 (m, 4H)

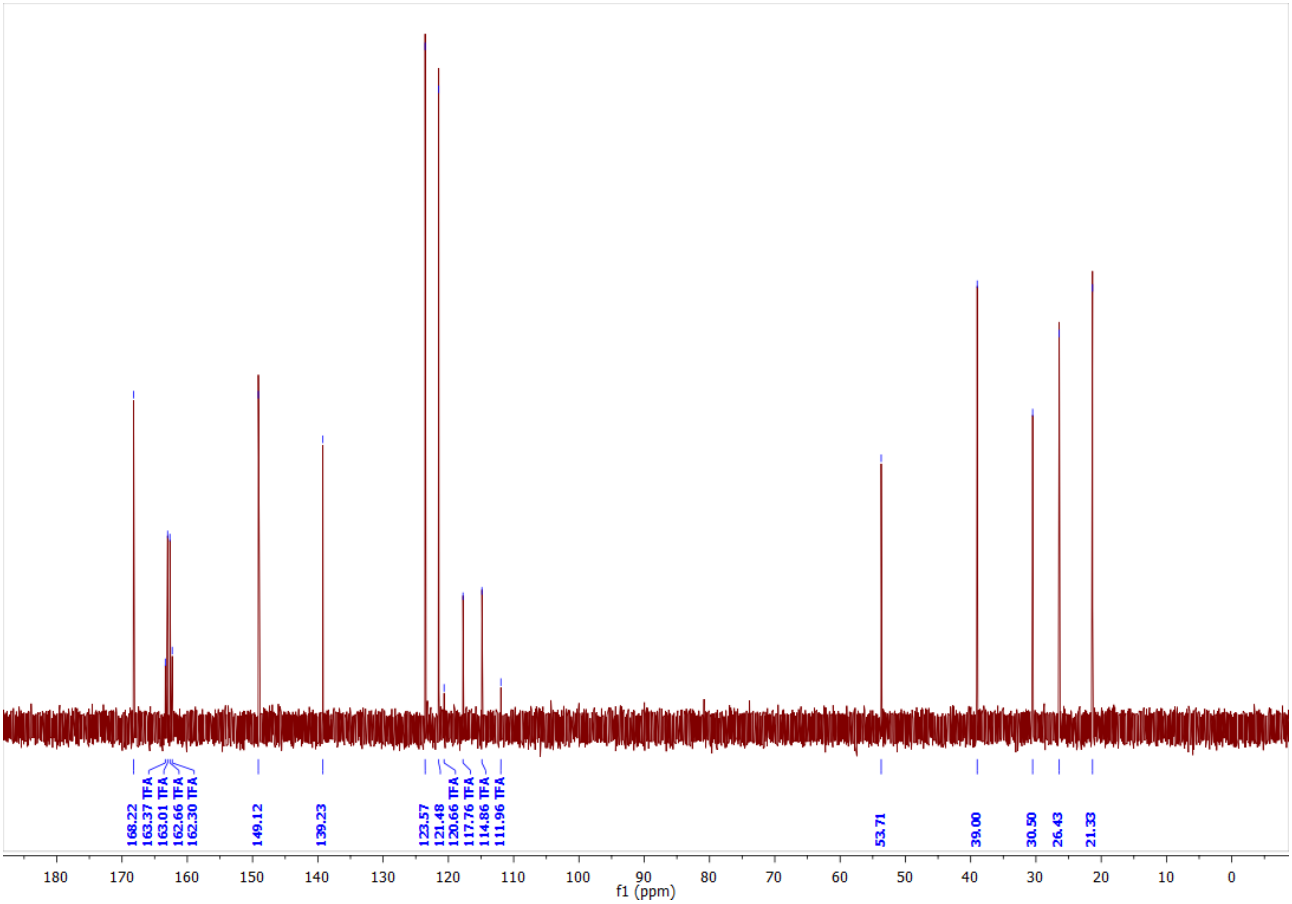

Figure S6. ^{13}C-NMR spectrum of **8**

^{13}C NMR (101 MHz, D2O) δ:

168.2, 149.1, 139.2, 123.6, 121.5, 117.8, 114.9, 53.7, 39.0, 30.5, 26.4, 21.3.

HRMS m/z (ESI): calc. for: $C_{24}H_{36}N_8O_2$: $[M+H]^+$,

Required: 469.3040, found: 469.3030

Spectral data for **9**:

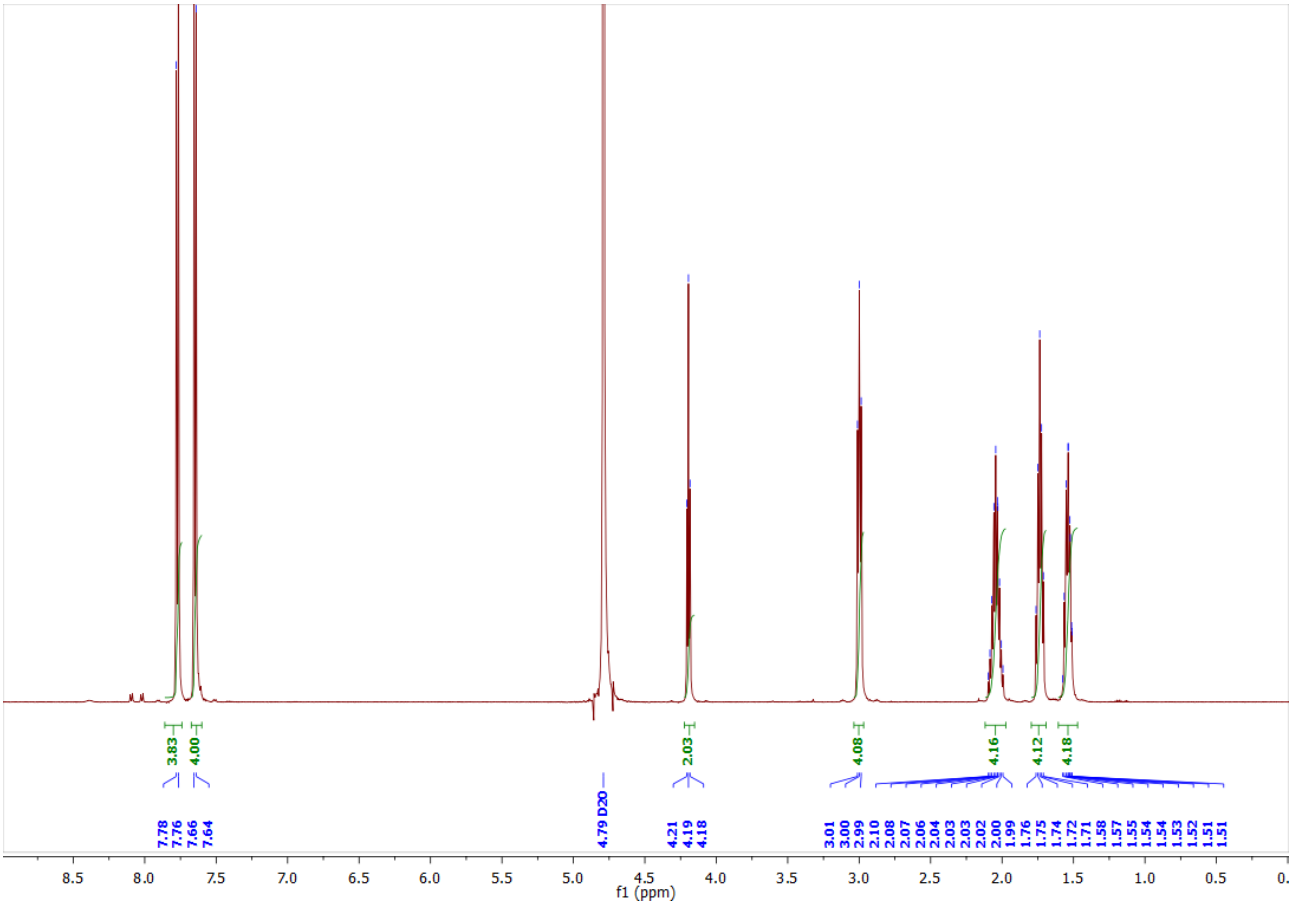

Figure S7. ^{1}H-NMR spectrum of **9**

^{1}H NMR (400 MHz, D_2O) δ:

7.77 (d, *J* = 8.9 Hz, 4H), 7.65 (d, *J* = 8.9 Hz, 4H), 4.19 (t, *J* = 6.6 Hz, 2H), 3.00 (t, *J* = 7.8 Hz, 4H), 2.16 – 1.95 (m, 4H), 1.83 – 1.61 (m, 4H), 1.63 – 1.45 (m, 4H).

:

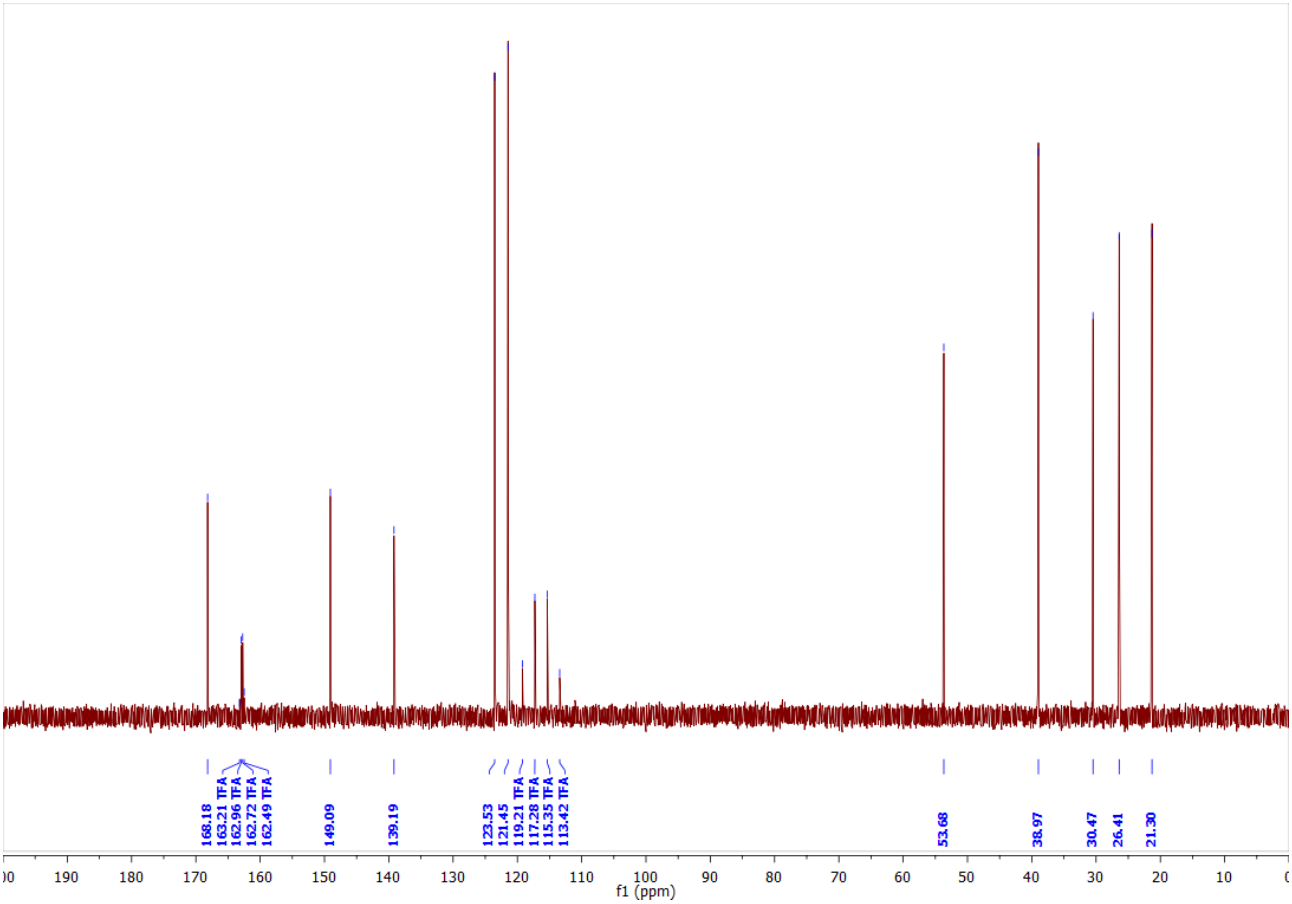

Figure S8. ^{13}C-NMR spectrum of **9**

^{13}C NMR (101 MHz, D_2O) δ

168.18 , 162.96 , 162.72 , 149.09 , 139.19 , 123.53 , 121.45 , 53.68 , 38.97 , 30.47 , 26.41 , 21.30

HRMS m/z (ESI): calc. for: $C_{24}H_{36}N_8O_2$: $[M+H]^+$,

Required: 469.3040, found: 469.3040

Computations

Calculation was done by Gaussian16 package[2], APFD[3] functional with 6-31+G(d,p) basic set. SCRF PCM[4] model of solvent was used with water as a solvent. TD-DFT method was used to calculated UV-Vis absorption spectra with water as a solvent. We used fully protonated amino groups, which is correspondent to the state of molecule at physiological pH. Various conformers were used as a starting point to find global minimum respect to orientations between amide bond and alpha carbon. Lowest energy conformers for all compounds showed hydrogen bond between oxygen of carbonyl atom of amide bond and protonated amine group. All structures were confirmed as stationary points by frequency analysis. TD-DFT results calculated UV-Vis absorption spectra with water as a solvent. Obtained results show good agreement with experimental spectra (Figures S13 and S14), in all cases energy of $\pi_{N=N}^* \leftarrow \pi_{N=N}$ transitions in *trans* forms and $\pi_{N=N}^* \leftarrow (LP)_N$ in *cis* forms were overestimated by 30 nm average (Table. S1). Electrostatic potential showed different space arrangement of amino acids chains which was responsible for the different coordination between DNAs and studied compounds.

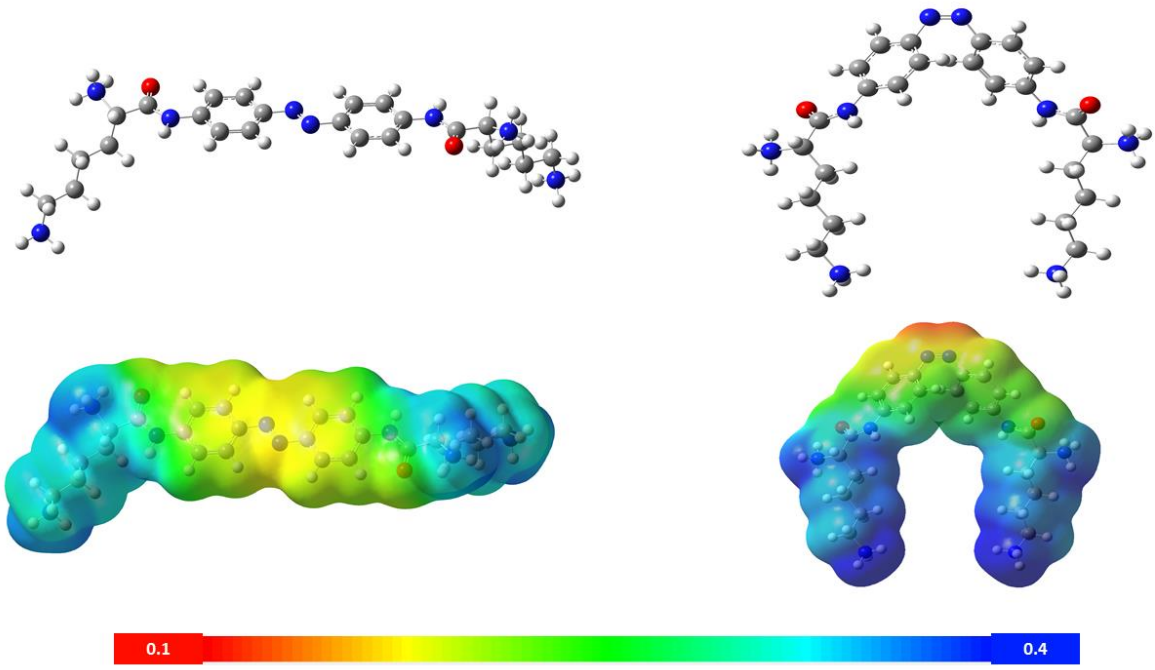

Figure S9. *Trans* and *cis* optimized structures (up) and corresponding electrostatic potential (down) for **8** (**Azo-LL-Lys**)

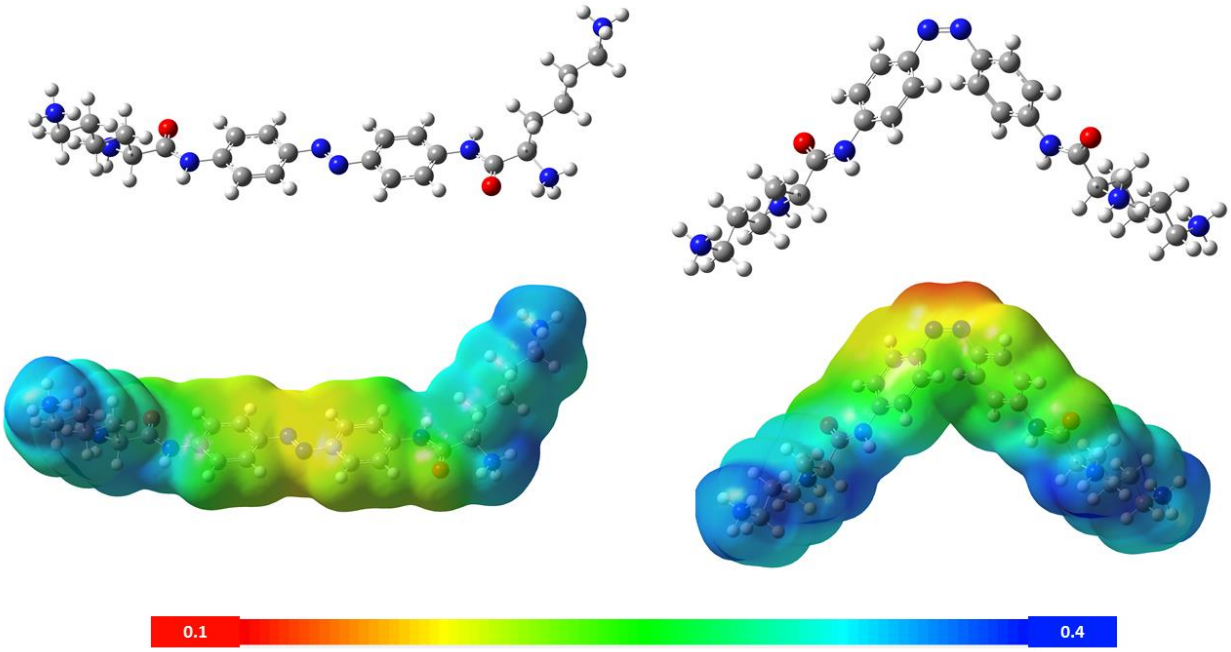

Figure S10. *Trans* and *cis* optimized structures (up) and corresponding electrostatic potential (down) for **9** (**Azo-DD-Lys**)

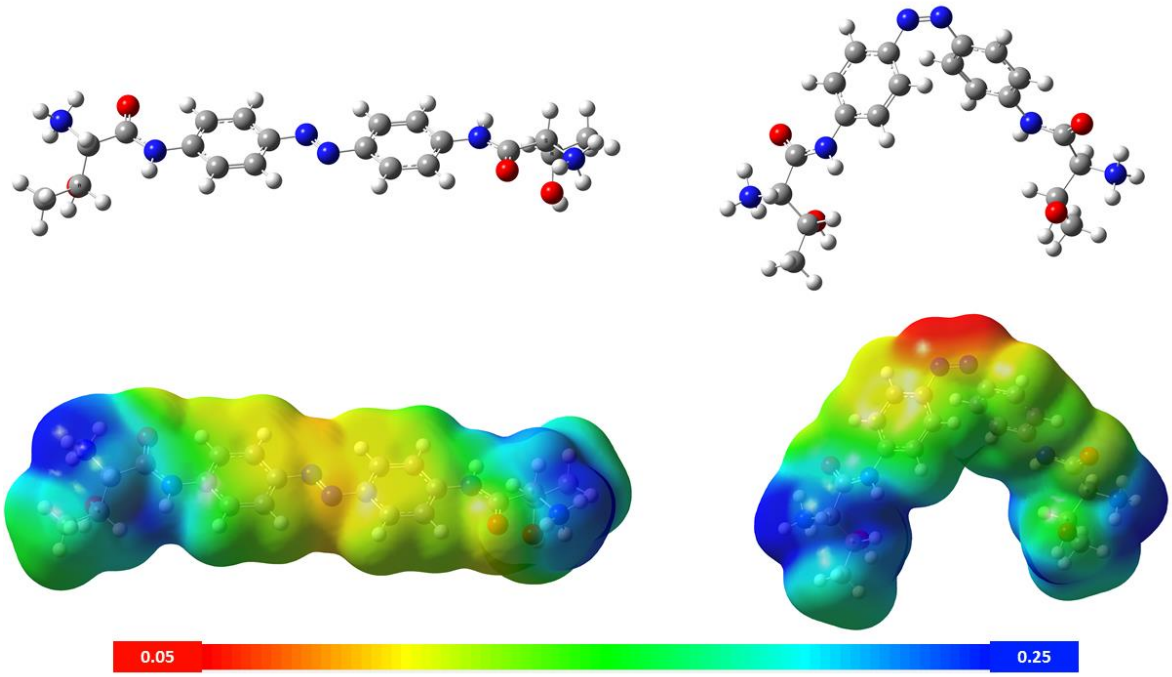

Figure S11. *Trans* and *cis* optimized structures (up) and corresponding electrostatic potential (down) for **4** (**Azo-LL-Thr**)

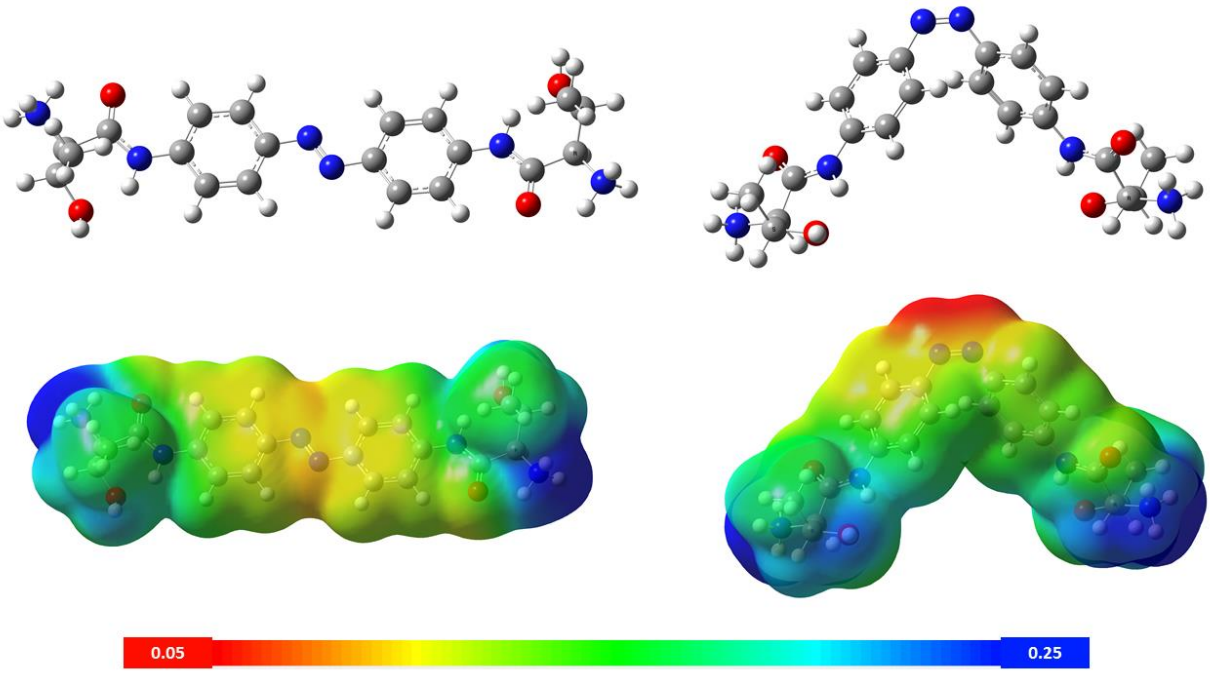

Figure S12. *Trans* and *cis* optimized structures (up) and corresponding electrostatic potential (down) for **5** (**Azo-DD-Thr**)

Cartesian Coordinates of the DFT Optimized Geometries

trans form of **8** (**Azo-LL-Lys** *trans*)

C	3.87728200	-1.03653200	-1.50307600
C	2.48664500	-1.04378000	-1.53717300
C	1.73139300	-1.04616800	-0.35994700
C	2.39107700	-1.04267600	0.88151400
C	3.77292600	-1.03439600	0.92564400
C	4.52647600	-1.02987900	-0.26264900
H	4.44978400	-1.03585200	-2.42047700
H	1.96634700	-1.04706000	-2.49103700
H	1.81142700	-1.04504100	1.79851000
H	4.28017200	-1.03019000	1.88766000
N	0.33512400	-1.04894200	-0.53121000
N	-0.33514100	-1.04924300	0.53062700
C	-1.73141800	-1.04638200	0.35945700
C	-2.39122200	-1.04209000	-0.88193900
C	-2.48656300	-1.04474400	1.53675400
C	-3.77307800	-1.03375800	-0.92592700
H	-1.81166100	-1.04384300	-1.79899300
C	-3.87720200	-1.03744800	1.50280000
H	-1.96617200	-1.04865400	2.49056400
C	-4.52651800	-1.02999000	0.26243600
H	-4.28041600	-1.02888900	-1.88788700
H	-4.44961300	-1.03733500	2.42025400
N	-5.92391600	-1.01173600	0.12000000

N	5.92385300	-1.01168200	-0.12006400
H	6.25523100	-0.98691800	0.83634600
H	-6.25540200	-0.98682900	-0.83636700
C	-6.86922700	-1.01874800	1.08195400
C	-8.30774300	-0.85459200	0.56639000
O	-6.67343800	-1.09935500	2.29368900
C	6.86926600	-1.01868500	-1.08189800
C	8.30771800	-0.85459600	-0.56615000
O	6.67364900	-1.09932000	-2.29366100
C	8.61039500	0.62067000	-0.29021900
H	7.80225900	1.00811300	0.33951000
C	9.94583600	0.85427400	0.41552800
H	9.95498800	0.30426900	1.36479200
H	10.78598100	0.47006900	-0.17737600
N	-9.16410200	-1.38112300	1.67282300
H	-10.05845800	-0.89554500	1.75623700
H	-9.36228300	-2.37889400	1.57301100
N	9.16416500	-1.38130100	-1.67242700
H	9.36219100	-2.37909100	-1.57248500
H	8.62336000	-1.25886300	-2.54681100
H	8.49431500	-1.46479300	0.32143500
H	10.05861400	-0.89589500	-1.75574700
H	-8.62314400	-1.25866600	2.54710500
H	-8.49447300	-1.46482800	-0.32113500
C	-8.61039500	0.62066400	0.29042300
H	-7.80233900	1.00807600	-0.33942700
H	-8.55874700	1.17983300	1.23346300
C	-9.94591500	0.85427700	-0.41516300
H	-10.78600300	0.47000300	0.17778600
H	-9.95512000	0.30430100	-1.36444600
C	-10.16899200	2.34445800	-0.67364300
H	-9.33221300	2.74470300	-1.25953600
H	-10.18532700	2.88508700	0.28104700
C	-11.47299300	2.57069300	-1.41842900
H	-11.46848500	2.09728900	-2.40240100
H	8.55888300	1.17982300	-1.23327900
C	10.16891700	2.34444500	0.67403000
H	9.33214100	2.74472200	1.25990700
H	10.18527100	2.88504900	-0.28067500
C	11.47294300	2.57064300	1.41878200
H	12.33317100	2.20262900	0.85603400
H	-12.33326100	2.20283400	-0.85563300
H	11.46838300	2.09733500	2.40279600
N	11.70895600	4.03383600	1.64874000
H	12.57546100	4.19840300	2.16617000
H	11.78189400	4.54693600	0.76681200
N	-11.70883200	4.03387500	-1.64855400
H	-12.57537800	4.19851800	-2.16588200
H	-11.78160100	4.54708000	-0.76667800
H	10.95073100	4.46095000	2.18675700
H	-10.95060800	4.46083600	-2.18669600

cis form of **8** (**Azo-LL-Lys** *cis*)

N	0.79742600	-5.54318900	-0.22968300
N	-0.44695600	-5.58335800	-0.16208000
C	-1.26390700	-4.41545400	-0.15775800
C	-1.12993300	-3.40285900	-1.11687700
C	-2.33584600	-4.38578500	0.73546000
C	-2.04594000	-2.36315300	-1.15115300
H	-0.32210000	-3.43542600	-1.84102600
C	-3.23466800	-3.32412900	0.73334400
H	-2.45614800	-5.19549300	1.44979300
C	-3.09367400	-2.30797000	-0.22006200
H	-1.94647200	-1.58819200	-1.90756200
H	-4.04693600	-3.29596700	1.44676100
C	1.54694100	-4.33892900	-0.09256200
C	2.63225400	-4.16239000	-0.95238800
C	1.34275700	-3.43820300	0.96156700
C	3.47508300	-3.06374100	-0.82023200
H	2.80794100	-4.88771200	-1.74194500
C	2.20236200	-2.36330400	1.12348700
H	0.52611000	-3.58581900	1.66085900
C	3.26404300	-2.16002100	0.22900400
H	4.29918800	-2.92220800	-1.50605100
H	2.04841600	-1.67663300	1.95239500
N	-3.98317400	-1.22151100	-0.33035500
C	-4.98316200	-0.87065100	0.49819100
C	-5.77517900	0.38371900	0.06944700
O	-5.30482500	-1.46107100	1.53133200
C	-4.94134400	1.66462500	0.05566900
H	-4.05316600	1.49613100	-0.56187100
C	-5.70716900	2.86815500	-0.49456900
H	-4.57142500	1.86388900	1.06962900
H	-6.02934900	2.65417800	-1.52129300
H	-6.62003600	3.05279500	0.08635900
C	-4.84207000	4.12798100	-0.47135900
H	-3.94472100	3.97028200	-1.08321300
H	-4.50587300	4.32354600	0.55470000
C	-5.62250600	5.32090100	-0.99566000
H	-6.50555700	5.52979800	-0.38833500
H	-3.85170800	-0.64721100	-1.15316000
N	4.09481300	-1.05021700	0.47197700
C	5.11210200	-0.58334800	-0.27753300
C	5.77082800	0.69952900	0.25932500
O	5.51889100	-1.06776000	-1.33379300
C	4.92611100	1.93256200	-0.06980900
H	3.90454600	1.73164400	0.27076600
C	5.42852100	3.21492900	0.59392500
H	4.86821400	2.04945200	-1.15958800
H	5.46698900	3.07091300	1.68077300
H	6.45017400	3.45813100	0.27415700
C	4.51456000	4.39311000	0.25788800
H	3.49294500	4.16991000	7 0.59062600

H	4.47870400	4.53307700	-0.82975900
C	5.00662300	5.66516400	0.92613400
H	6.00188600	5.95129000	0.57966300
H	3.89528900	-0.54654300	1.32741100
N	7.09524700	0.75317500	-0.43276400
H	7.84138500	0.32004200	0.11529600
H	6.98897400	0.20354200	-1.30504500
N	-6.88801500	0.47392400	1.06763400
H	-7.81543000	0.40487800	0.64705000
H	-6.74435600	-0.33114300	1.71374100
H	-6.85694400	1.33130100	1.62184300
H	7.39229100	1.70221800	-0.66323900
H	5.95780800	0.63124100	1.33417800
H	-6.22505500	0.20735800	-0.91242500
H	-5.93548300	5.17945100	-2.03199000
H	5.02667500	5.57286900	2.01384900
N	-4.78210300	6.56264600	-0.96847800
H	-5.28556700	7.36894600	-1.34620700
H	-4.49659300	6.80526600	-0.01650700
N	4.09765900	6.81535200	0.61051800
H	4.40873900	7.67753300	1.06385100
H	4.05814300	7.00029700	-0.39486400
H	-3.92932900	6.45296000	-1.52250100
H	3.14029200	6.63785500	0.92431100

trans form of **9** (**Azo-DD-Lys** *trans*)

C	3.87709800	-1.04287200	1.50171000
C	2.48645800	-1.05036400	1.53547400
C	1.73141900	-1.04680400	0.35810400
C	2.39135200	-1.03684500	-0.88318800
C	3.77321300	-1.02821500	-0.92698100
C	4.52654300	-1.02982000	0.26146000
H	4.44940800	-1.04687600	2.41921400
H	1.96595700	-1.05864600	2.48919500
H	1.81190200	-1.03445700	-1.80031000
H	4.28064800	-1.01889200	-1.88885100
N	0.33515200	-1.05063000	0.52916800
N	-0.33509300	-1.04646800	-0.53267500
C	-1.73138300	-1.04464800	-0.36137200
C	-2.39098900	-1.04590100	0.88013600
C	-2.48669000	-1.03806500	-1.53853500
C	-3.77283300	-1.03809100	0.92438800
H	-1.81127000	-1.05155800	1.79707300
C	-3.87733600	-1.03123800	-1.50431900
H	-1.96645700	-1.03764800	-2.49244100
C	-4.52645100	-1.02931000	-0.26383600
H	-4.28002000	-1.03761400	1.88644600
H	-4.44990700	-1.02729200	-2.42167200
N	-5.92382000	-1.01162900	-0.12109100

N	5.92395700	-1.01133900	0.11920800
H	6.25551200	-0.98451800	-0.83709100
H	-6.25508000	-0.98841600	0.83539400
C	-6.86936400	-1.01768800	-1.08281700
C	-8.30776300	-0.85439700	-0.56666600
O	-6.67387800	-1.09686900	-2.29469300
C	6.86917800	-1.01973400	1.08123200
C	8.30780400	-0.85527700	0.56600200
O	6.67326100	-1.10194900	2.29284300
C	8.61052300	0.62012800	0.29092700
H	8.55841100	1.17879900	1.23423800
C	9.94628600	0.85426300	-0.41403500
H	10.78620600	0.46966300	0.17894000
H	9.95583700	0.30490800	-1.36367200
C	-8.61073900	0.62055300	-0.28944200
H	-8.55922500	1.18062400	-1.23195700
H	-7.80270600	1.00752400	0.34071300
C	-9.94627700	0.85334000	0.41639600
H	-9.95540900	0.30251900	1.36519100
H	-10.78633900	0.46952400	-0.17689100
C	-10.16940700	2.34326400	0.67620900
H	-10.18583100	2.88475400	-0.27799600
H	-9.33256700	2.74305200	1.26233300
C	-11.47324600	2.56895400	1.42146100
H	-12.33368500	2.20145800	0.85869800
H	7.80269900	1.00781500	-0.33904900
C	10.16938300	2.34463000	-0.67143700
H	10.18562900	2.88457400	0.28363700
H	9.33266200	2.74534600	-1.25709600
C	11.47345700	2.57135500	-1.41595300
H	11.46895700	2.09871800	-2.40029400
N	-9.16430900	-1.38045100	-1.67317300
H	-9.36182800	-2.37842800	-1.57410100
H	-10.05900000	-0.89535500	-1.75576900
N	9.16389900	-1.38253700	1.67229800
H	9.36266200	-2.38009100	1.57154400
H	10.05795800	-0.89659300	1.75671400
H	8.49458700	-1.46507200	-0.32181400
H	-8.49404200	-1.46532000	0.32046800
H	-8.62384600	-1.25693400	-2.54759500
H	8.62238700	-1.26122900	2.54642400
H	12.33366900	2.20300200	-0.85339100
H	-11.46839300	2.09491200	2.40512700
N	-11.70896600	4.03200300	1.65258700
H	-11.78205700	4.54574800	0.77105300
H	-12.57530300	4.19632000	2.17036000
N	11.70947900	4.03468400	-1.64496200
H	11.78238600	4.54723900	-0.76270900
H	12.57606300	4.19952200	-2.16216900
H	10.95135900	4.46215500	-2.18284600
H	-10.95050600	4.45855900	2.19071900

cis form of **9** (**Azo-DD-Lys** *cis*)

N	-0.59838700	4.73367500	-0.17679900
N	0.59839800	4.73368900	0.17618300
C	1.37043300	3.54182100	0.30090000
C	1.42394700	2.56505800	-0.70283600
C	2.21191900	3.44026400	1.40963300
C	2.27602600	1.48190900	-0.56252200
H	0.80824400	2.65547800	-1.59192900
C	3.04111500	2.33528100	1.57620700
H	2.19601400	4.22342400	2.16246200
C	3.07184000	1.34604800	0.58533700
H	2.32231300	0.73336800	-1.34976700
H	3.66471800	2.24729200	2.45544100
C	-1.37049500	3.54182900	-0.30122600
C	-2.21216300	3.44022600	-1.40982100
C	-1.42393400	2.56515800	0.70260700
C	-3.04145100	2.33528200	-1.57618900
H	-2.19634900	4.22334600	-2.16269500
C	-2.27608600	1.48204400	0.56249700
H	-0.80812200	2.65561400	1.59161900
C	-3.07205800	1.34611700	-0.58524800
H	-3.66520100	2.24726700	-2.45531700
H	-2.32232900	0.73358700	1.34982700
N	3.87720100	0.19520300	0.66366200
C	4.76949600	-0.14479300	1.61427100
C	5.54172800	-1.44340500	1.33035200
O	5.02973000	0.49632400	2.63217800
C	6.68518900	-1.19376300	0.34412900
H	7.39168200	-0.47737800	0.78257200
C	7.39999100	-2.47241000	-0.09220300
H	6.25611400	-0.70292000	-0.53619000
H	7.84474800	-2.99208800	0.76700500
H	6.67097900	-3.16374000	-0.53296100
C	8.50398500	-2.16515400	-1.10374400
H	9.23784000	-1.48457900	-0.65378200
H	8.07241500	-1.65083000	-1.97160000
C	9.19011600	-3.44396700	-1.55169300
H	8.49644100	-4.12695300	-2.04617300
H	3.76246500	-0.45814400	-0.10128500
N	-3.87752100	0.19533900	-0.66333000
C	-4.76931000	-0.14512800	-1.61424600
C	-5.54156600	-1.44368300	-1.33011100
O	-5.02903500	0.49551000	-2.63258500
C	-6.68526100	-1.19384300	-0.34421800
H	-7.39177700	-0.47774500	-0.78308900
C	-7.39995400	-2.47242600	0.09247100
H	-6.25644500	-0.70257800	0.53599400
H	-7.84455300	-2.99243500	-0.76662200
H	-6.67090700	-3.16350700	0.53355100
C	-8.50410100	-2.16495100	1.10379400

H	-9.23792600	-1.48452200	0.65355700
H	-8.07266900	-1.65039100	1.97157500
C	-9.19021100	-3.44368800	1.55197700
H	-8.49656000	-4.12649900	2.04673200
H	-3.76308500	-0.45770500	0.10192200
N	-6.06847700	-1.86625100	-2.66303000
H	-5.41834200	-2.47628600	-3.16264100
H	-6.96375100	-2.35315500	-2.60019300
N	6.06901500	-1.86554900	2.66325400
H	5.41887000	-2.47515700	3.16337700
H	6.96410300	-2.35277600	2.60026400
H	6.18007400	-1.00433900	3.22623400
H	-6.17905100	-1.00522800	-3.22641800
H	-4.88054500	-2.23541900	-0.96686500
H	4.88071700	-2.23533000	0.96748400
H	-9.66255000	-3.96747700	0.71844600
N	-10.27711700	-3.14770700	2.54179300
H	-10.99724000	-2.54094100	2.14229700
H	-10.74405300	-4.00173600	2.85549400
H	-9.91290500	-2.67869800	3.37491600
H	9.66262400	-3.96750100	-0.71809800
N	10.27687000	-3.14813700	-2.54172800
H	10.99679500	-2.54092400	-2.14254900
H	10.74410300	-4.00216700	-2.85498600
H	9.91247500	-2.67969800	-3.37509900

trans form of **4** (**Azo-LL-Thr** *trans*)

C	-3.98479400	-1.18859700	-0.33537000
C	-2.60123300	-1.33334400	-0.33461300
C	-1.75461000	-0.22023400	-0.31459500
C	-2.31325300	1.06957900	-0.29068800
C	-3.68727700	1.22354700	-0.28978400
C	-4.53305500	0.09925600	-0.31383600
H	-4.62826400	-2.05742800	-0.35281100
H	-2.15841600	-2.32541800	-0.34976100
H	-1.66265300	1.93753000	-0.27292300
H	-4.11560200	2.22321200	-0.27121800
N	-0.37640100	-0.50228100	-0.31698100
N	0.37642100	0.50265200	-0.31701200
C	1.75463000	0.22057700	-0.31471200
C	2.31323800	-1.06925400	-0.29095000
C	2.60127100	1.33366600	-0.33469400
C	3.68725500	-1.22325500	-0.29011300
H	1.66261100	-1.93718700	-0.27324300
C	3.98483400	1.18888500	-0.33551900
H	2.15848800	2.32575500	-0.34977100
C	4.53306600	-0.09898100	-0.31409300
H	4.11555900	-2.22293300	-0.27167000
H	4.62832400	2.05770100	-0.35293700
N	5.91507800	-0.35289800	-0.30265600

N	-5.91508100	0.35311100	-0.30227400
H	-6.16471500	1.33160700	-0.23445600
H	6.16467100	-1.33143100	-0.23524600
C	6.93254400	0.52364100	-0.42519300
C	8.33716700	-0.11200900	-0.37285800
O	6.82322900	1.73758000	-0.58979000
C	8.63113500	-0.84836000	0.94115100
H	7.81301600	-1.55694100	1.12580800
C	-6.93248200	-0.52342000	-0.42546500
C	-8.33715300	0.11209500	-0.37287100
O	-6.82306600	-1.73724400	-0.59079600
C	-8.63123600	0.84768800	0.94154200
H	-7.81313100	1.55616200	1.12666800
C	-9.94837900	1.61009100	0.90226400
H	-9.92894100	2.36469500	0.11077600
H	-10.79949900	0.94342400	0.73314400
H	-10.10863100	2.12574600	1.85366000
O	-8.61317000	-0.18508500	1.91676800
C	9.94827400	-1.61077100	0.90158500
H	10.10833100	-2.12703000	1.85268700
H	9.92897300	-2.36486000	0.10960700
H	10.79943900	-0.94400700	0.73307200
O	8.61301300	0.18385900	1.91695200
H	8.94702800	-0.15428200	2.75646500
H	-8.94752800	0.15250500	2.75636500
N	9.28125100	1.03136600	-0.50964700
H	8.72804200	1.84009300	-0.84521000
H	9.64155700	1.28541100	0.41911200
N	-9.28114100	-1.03127800	-0.51032200
H	-10.05971100	-0.85128200	-1.14381200
H	-8.72784200	-1.83978800	-0.84626100
H	-8.46815200	0.78204000	-1.22636500
H	-9.64151100	-1.28581800	0.41827500
H	10.05985900	0.85162300	-1.14315800
H	8.46810200	-0.78147400	-1.22674300

cis form of **4** (**Azo-LL-Thr** *cis*)

N	0.62151900	4.49801400	0.02989700
N	-0.62547600	4.51042800	0.05744200
C	-1.40795600	3.32335900	0.16492500
C	-1.17888300	2.36244500	1.15847900
C	-2.52858500	3.21407500	-0.65920400
C	-2.04427800	1.28783900	1.28694100
H	-0.33294900	2.45881100	1.83162700
C	-3.37912600	2.11718200	-0.56162300
H	-2.72252000	3.98546400	-1.39926600
C	-3.13669400	1.14646400	0.41821000
H	-1.86709200	0.54952700	2.06524900
H	-4.22805500	2.02414400	-1.22509500

C	1.38215300	3.29992000	-0.10398600
C	2.52864700	3.18027100	0.68279000
C	1.11262900	2.33919100	-1.08827000
C	3.36742900	2.07713600	0.55783500
H	2.75288700	3.95036600	1.41559800
C	1.96461600	1.25821400	-1.24473000
H	0.24780300	2.44200400	-1.73559300
C	3.08561900	1.10881300	-0.41398500
H	4.23760500	1.97803900	1.19212900
H	1.75670200	0.52228100	-2.01771100
N	3.88191500	-0.03118400	-0.62921500
C	5.01084200	-0.40044400	0.00440500
C	5.63072700	-1.72452600	-0.49305300
O	5.57427800	0.22850500	0.90022800
C	4.68889800	-2.92986100	-0.38556400
N	6.80774000	-1.94425600	0.39259300
H	5.98033200	-1.59879400	-1.52128400
H	3.75314400	-2.67904200	-0.90254200
C	5.26911500	-4.19126500	-1.01097700
O	4.46029100	-3.05533700	1.01064300
H	7.64723500	-2.24895700	-0.09943400
H	6.98362700	-1.04391500	0.87603200
H	6.56407800	-2.62819300	1.11948400
H	5.47369500	-4.03176100	-2.07346100
H	6.19345900	-4.50637200	-0.51708400
H	4.54912100	-5.01063400	-0.92750100
H	3.99971800	-3.88338000	1.19220100
N	-3.95698700	0.01865600	0.61158200
C	-4.97613900	-0.41784800	-0.15152000
C	-5.66916000	-1.69766400	0.36323100
O	-5.39681900	0.12417400	-1.17379300
C	-4.73035400	-2.89835500	0.53619900
N	-6.68456500	-2.02173800	-0.67613900
H	-6.18286900	-1.47237800	1.30141100
H	-3.87904300	-2.58441500	1.15467000
C	-5.41177800	-4.08339200	1.20710500
O	-4.29550000	-3.18092600	-0.78621300
H	-7.59290300	-2.29038600	-0.29916200
H	-6.77977500	-1.17532800	-1.26780900
H	-6.32433200	-2.77090800	-1.28062400
H	-5.75179500	-3.81018400	2.20996600
H	-6.26931200	-4.44286800	0.62998900
H	-4.70303800	-4.91072600	1.30774700
H	-3.83917800	-4.03072100	-0.80414800
H	-3.74187000	-0.52652700	1.43639400
H	3.56197300	-0.63524400	-1.37507400

trans form of **5** (**Azo-DD-Thr** *trans*)

C	3.94148700	-1.32261200	-0.32840000
C	2.55417000	-1.42064700	-0.34488000
C	1.74630300	-0.27936400	-0.38509100
C	2.34930700	0.99048600	-0.41869100
C	3.72778700	1.09780000	-0.40510900
C	4.53496300	-0.05442800	-0.35655700
H	4.55539900	-2.21231000	-0.29316900
H	2.07710400	-2.39665700	-0.32287900
H	1.72859800	1.87959200	-0.45397400
H	4.19229600	2.08076800	-0.43093200
N	0.35963700	-0.51486900	-0.38642200
N	-0.35963400	0.51462700	-0.38642600
C	-1.74631000	0.27916600	-0.38504600
C	-2.34936800	-0.99066900	-0.41834700
C	-2.55413100	1.42049000	-0.34505200
C	-3.72785500	-1.09792600	-0.40473100
H	-1.72869800	-1.87981100	-0.45341000
C	-3.94144900	1.32251500	-0.32854100
H	-2.07701800	2.39648300	-0.32323400
C	-4.53497500	0.05435200	-0.35644400
H	-4.19240500	-2.08087900	-0.43029700
H	-4.55533400	2.21224000	-0.29344400
N	-5.92133000	-0.15385800	-0.34111600
N	5.92130800	0.15389800	-0.34123500
H	6.24508800	1.12266800	-0.36352500
H	-6.24527300	-1.12257300	-0.36354800
C	-6.90391600	0.75652700	-0.22838200
C	-8.32878400	0.16514100	-0.26478500
O	-6.77138000	1.97829300	-0.13285600
C	-8.57566700	-1.05966300	0.63273700
C	6.90398200	-0.75637900	-0.22837200
C	8.32883100	-0.16491800	-0.26482600
O	6.77156300	-1.97817100	-0.13300200
C	8.57556100	1.05986000	0.63277300
H	9.65000200	1.28670100	0.58835300
O	-7.84749600	-2.09544600	-0.02044800
H	-7.86990900	-2.89496400	0.52042400
N	9.22751900	-1.29764800	0.08353300
H	10.05773900	-1.34715500	-0.50861500
H	9.53960700	-1.27908400	1.05664700
H	8.54836500	0.12184900	-1.29801300
H	8.65592900	-2.15768900	-0.03632300
O	7.84679100	2.09544500	-0.02000800
H	7.87097900	2.89556500	0.51988300
C	8.14456200	0.87013500	2.08157600
H	7.07855500	0.63708600	2.15382700
H	8.71051000	0.07698500	2.58056400
H	8.33772600	1.78771200	2.64493400
N	-9.22740800	1.29791100	0.08366700
H	-10.05776100	1.34734700	-0.50830100

H	-9.53928500	1.27944400	1.05685000
H	-8.54836600	-0.12153600	-1.29799000
H	-8.65588700	2.15794700	-0.03635800
C	-8.14424500	-0.87028500	2.08141700
H	-8.33804700	-1.78772200	2.64480500
H	-7.07806000	-0.63803700	2.15360500
H	-8.70963100	-0.07680400	2.58050900
H	-9.65021900	-1.28605800	0.58863000

cis form of **5** (**Azo-DD-Thr** *cis*)

N	0.62151900	4.49801400	0.02989700
N	-0.62547600	4.51042800	0.05744200
C	-1.40795600	3.32335900	0.16492500
C	-1.17888300	2.36244500	1.15847900
C	-2.52858500	3.21407500	-0.65920400
C	-2.04427800	1.28783900	1.28694100
H	-0.33294900	2.45881100	1.83162700
C	-3.37912600	2.11718200	-0.56162300
H	-2.72252000	3.98546400	-1.39926600
C	-3.13669400	1.14646400	0.41821000
H	-1.86709200	0.54952700	2.06524900
H	-4.22805500	2.02414400	-1.22509500
C	1.38215300	3.29992000	-0.10398600
C	2.52864700	3.18027100	0.68279000
C	1.11262900	2.33919100	-1.08827000
C	3.36742900	2.07713600	0.55783500
H	2.75288700	3.95036600	1.41559800
C	1.96461600	1.25821400	-1.24473000
H	0.24780300	2.44200400	-1.73559300
C	3.08561900	1.10881300	-0.41398500
H	4.23760500	1.97803900	1.19212900
H	1.75670200	0.52228100	-2.01771100
N	3.88191500	-0.03118400	-0.62921500
C	5.01084200	-0.40044400	0.00440500
C	5.63072700	-1.72452600	-0.49305300
O	5.57427800	0.22850500	0.90022800
C	4.68889800	-2.92986100	-0.38556400
N	6.80774000	-1.94425600	0.39259300
H	5.98033200	-1.59879400	-1.52128400
H	3.75314400	-2.67904200	-0.90254200
C	5.26911500	-4.19126500	-1.01097700
O	4.46029100	-3.05533700	1.01064300
H	7.64723500	-2.24895700	-0.09943400
H	6.98362700	-1.04391500	0.87603200
H	6.56407800	-2.62819300	1.11948400
H	5.47369500	-4.03176100	-2.07346100
H	6.19345900	-4.50637200	-0.51708400
H	4.54912100	-5.01063400	-0.92750100
H	3.99971800	-3.88338000	1.19220100
N	-3.95698700	0.01865600	0.61158200

C	-4.97613900	-0.41784800	-0.15152000
C	-5.66916000	-1.69766400	0.36323100
O	-5.39681900	0.12417400	-1.17379300
C	-4.73035400	-2.89835500	0.53619900
N	-6.68456500	-2.02173800	-0.67613900
H	-6.18286900	-1.47237800	1.30141100
H	-3.87904300	-2.58441500	1.15467000
C	-5.41177800	-4.08339200	1.20710500
O	-4.29550000	-3.18092600	-0.78621300
H	-7.59290300	-2.29038600	-0.29916200
H	-6.77977500	-1.17532800	-1.26780900
H	-6.32433200	-2.77090800	-1.28062400
H	-5.75179500	-3.81018400	2.20996600
H	-6.26931200	-4.44286800	0.62998900
H	-4.70303800	-4.91072600	1.30774700
H	-3.83917800	-4.03072100	-0.80414800
H	-3.74187000	-0.52652700	1.43639400
H	3.56197300	-0.63524400	-1.37507400

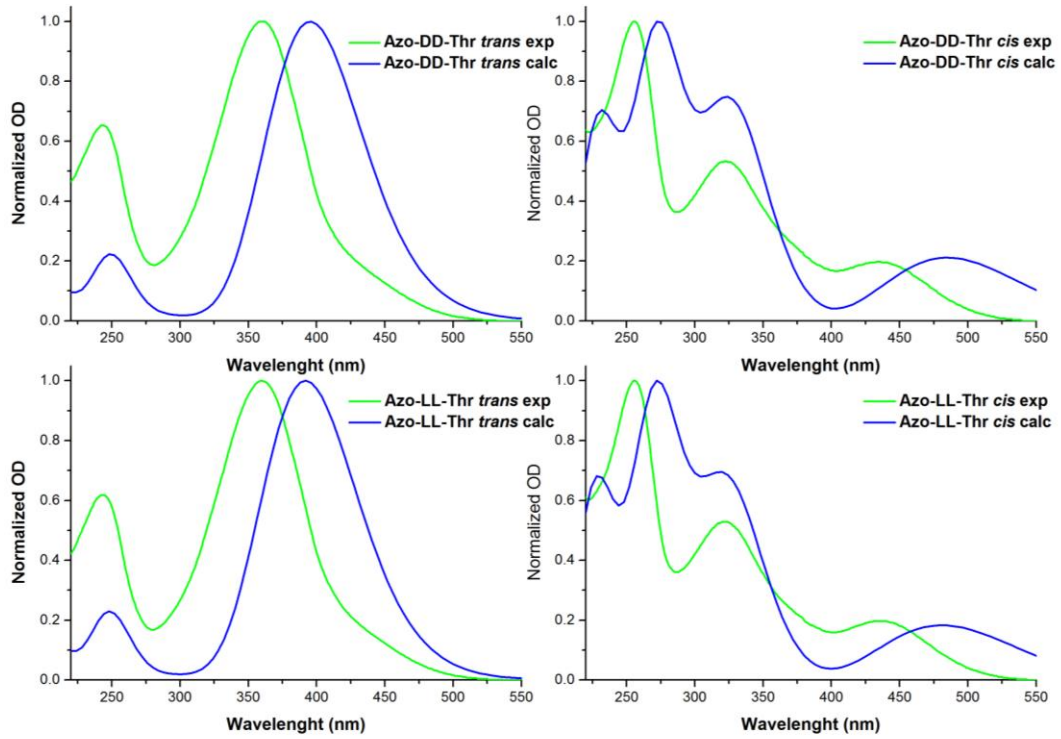

Figure S13. Normalized **e**xperimental and calculated UV-Vis spectra of **Azo-DD-Thr** and **Azo-LL-Thr** in *trans* and *cis* form.

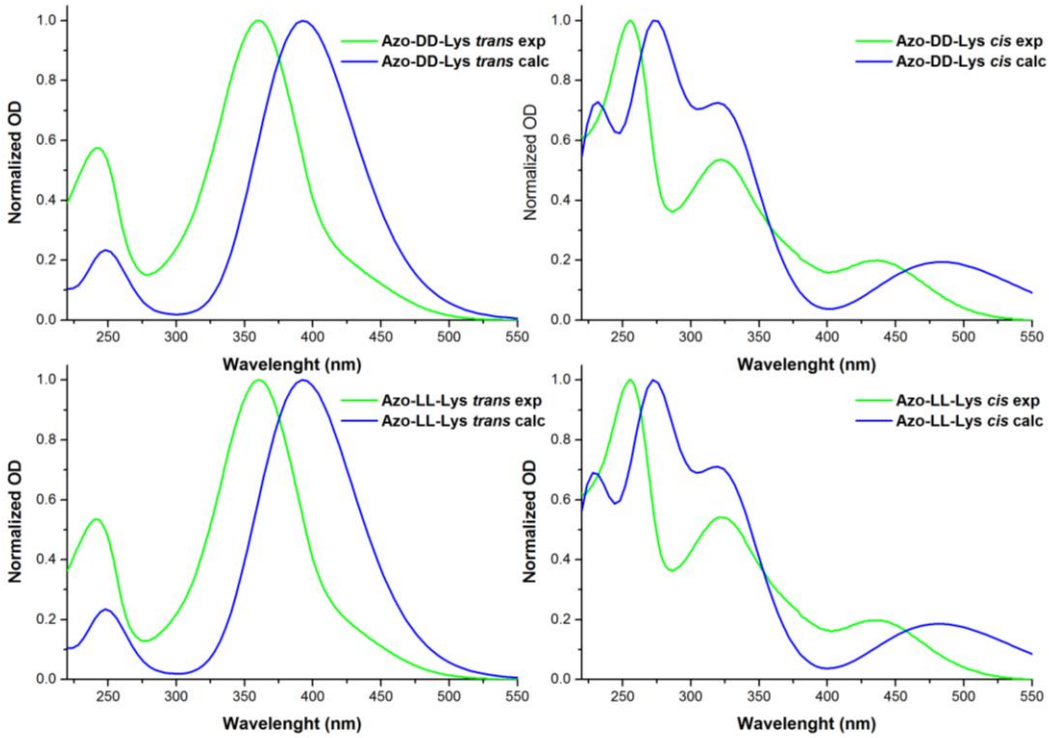

Figure S14. Normalized experimental and calculated UV-Vis spectra of **Azo-DD-Lys** and **Azo-LL-Lys** in *trans* and *cis* form.

Table S1. Computed transitions (nm) energy and composition of the first Singlet Excited States (Wavelength, Oscillator Strength *f*, Transition Percentage) for studied Compounds.

Compounds	Calculated λ_{max} [*f*]	Composition	Major Assignment
Azo-DD-Lys *trans*	474 [0.00]	125 → 127 (95%)	$\pi_{N=N}^* \leftarrow (LP)_N$
	392 [1.59]	126 → 127 (100%)	$\pi_{N=N}^* \leftarrow \pi_{N=N}$
	249 [0.35]	126 → 129 (85%)	
Azo-DD-Lys *cis*	483 [0.14]	126 → 128 (85%)	
	327 [0.36]	124 → 127 (85%)	
	273 [0.25]	126 → 129 (60%)	
	273 [0.23]	126 → 128 (65%)	
	237 [0. 20]	125 → 129 (80%)	
	225 [0.13]	124 → 129 (80%)	
Azo-LL-Lys *trans*	473 [0.00]	125 → 127 (95%)	$\pi_{N=N}^* \leftarrow (LP)_N$
	392 [1.59]	126 → 127 (100%)	$\pi_{N=N}^* \leftarrow \pi_{N=N}$
	249 [0.35]	126 → 129 (85%)	
Azo-LL-Lys *cis*	482 [0.13]	126 → 128 (85%)	
	326 [0.34]	124 → 127 (85%)	
	273 [0.29]	126 → 129 (60%)	
	273 [0.20]	126 → 128 (65%)	
	237 [0. 17]	125 → 129 (80%)	
	225 [0.12]	124 → 129 (80%)	
Azo-DD-Thr *trans*	473 [0.00]	109 → 111 (95%)	$\pi_{N=N}^* \leftarrow (LP)_N$
	395 [1.59]	110 → 111 (100%)	$\pi_{N=N}^* \leftarrow \pi_{N=N}$
	249 [0.33]	110 → 113 (95%)	
Azo-DD-Thr *cis*	480 [0.12]	110 → 111 (85%)	
	326 [0.31]	108 → 111 (80%)	
	273 [0.21]	110 → 112 (60%)	

	272 [0.28]	110 → 113 (65%)	
	237 [0. 18]	109 → 112 (85%)	
Azo-LL-Thr *trans*	473 [0.00]	109 → 111 (95%)	$\pi_{N=N}^* \leftarrow (LP)_N$
	395 [1.57]	110 → 111 (100%)	$\pi_{N=N}^* \leftarrow \pi_{N=N}$
	249 [0.32]	110 → 113 (95%)	
Azo-LL-Thr *cis*	480 [0.14]	110 → 111 (85%)	
	329 [0.36]	108 → 111 (90%)	
	274 [0.24]	110 → 112 (40%) 110 → 113 (25%)	
	238 [0.21]	109 → 112 (90%)	
	225 [0. 18]	108 → 113 (70%)	

Frontier MOs for studied molecules

Contour values are ± 0.02 $(e/bohr^3)^{1/2}$.

Azo-DD-Lys *trans*

129

LUMO+2

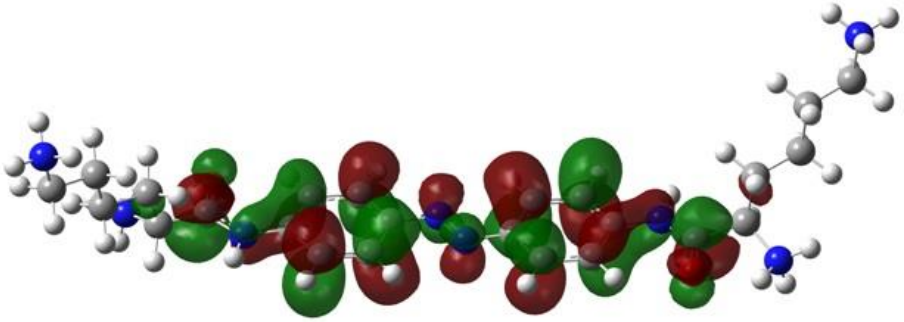

127

LUMO
(π N=N*)

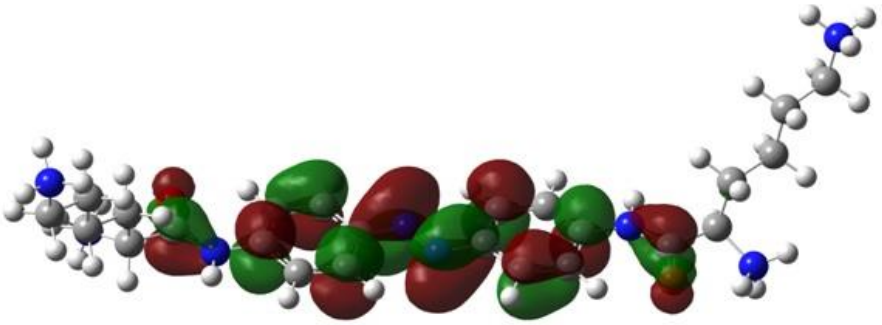

126

HOMO

(π N=N)

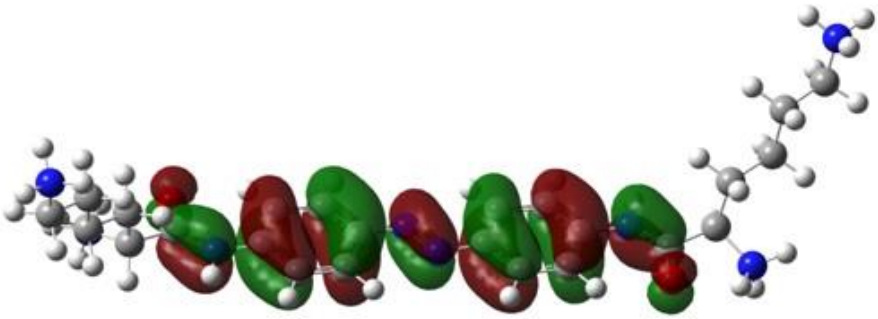

125

HOMO - 1 (LP_N)

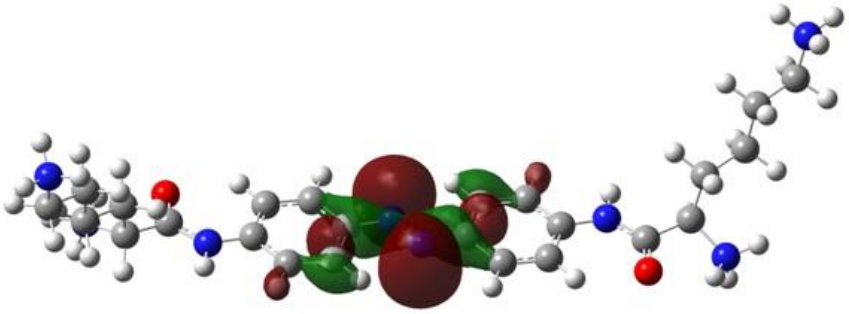

Azo-DD-Lys *cis*

129

LUMO+2

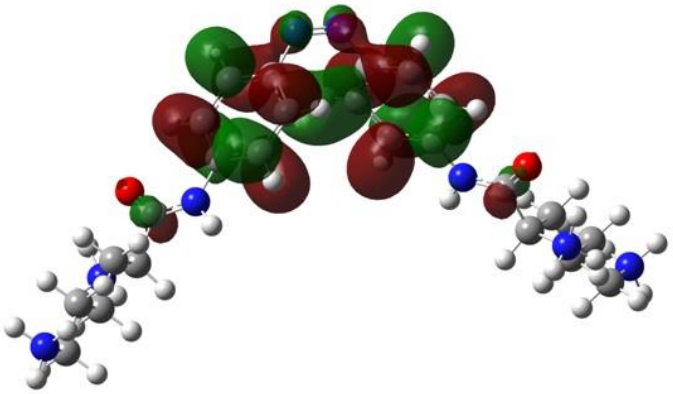

128

LUMO+1

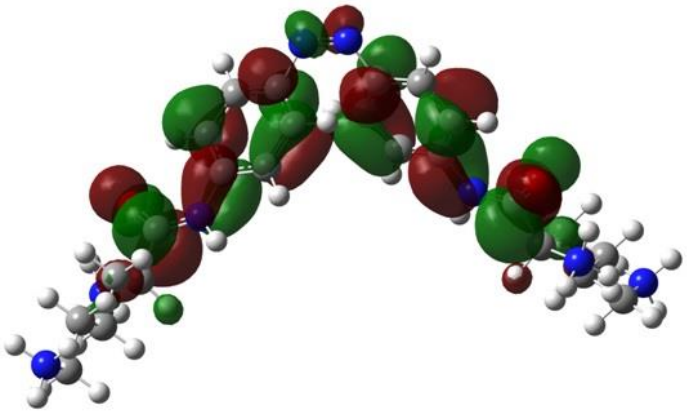

127

LUMO+1

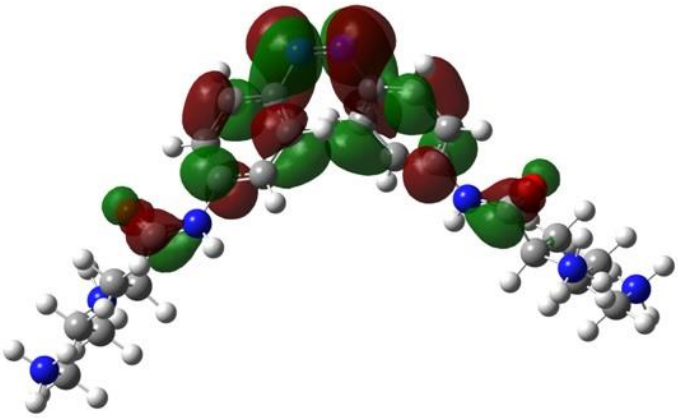

126

HOMO

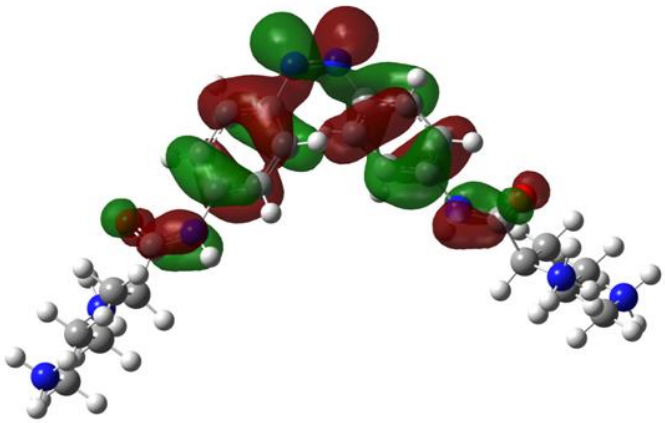

125

HOMO - 1

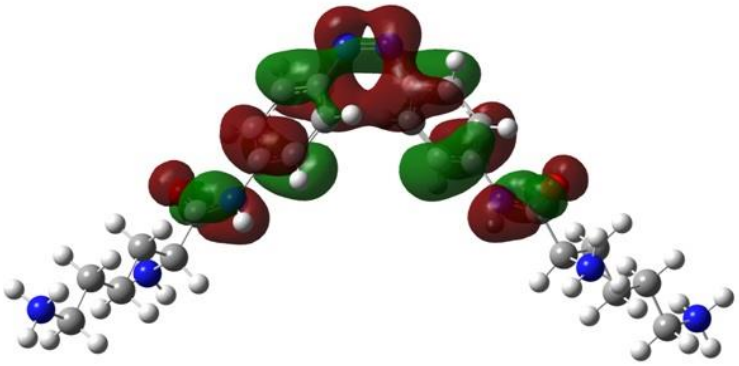

124

HOMO - 2

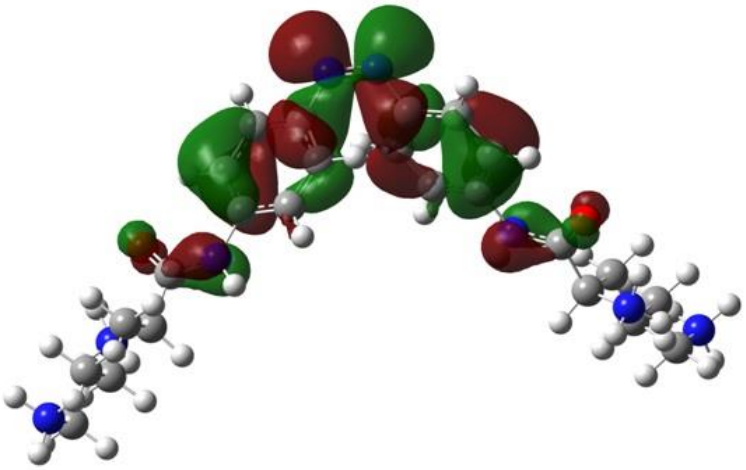

Azo-LL-Lys *trans*

129

LUMO+2

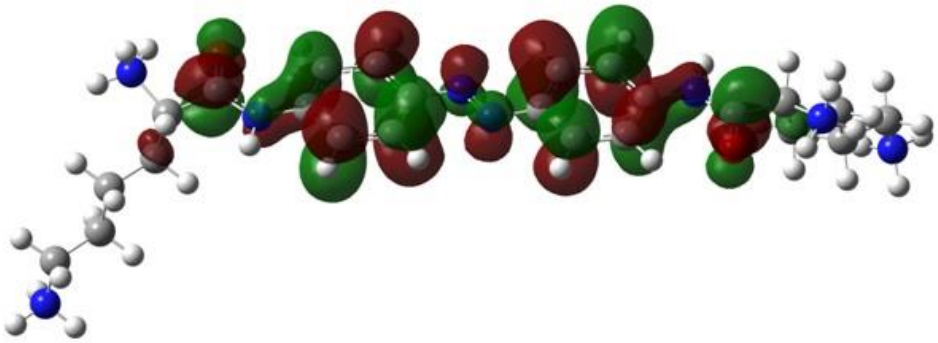

127

LUMO (π N=N*)

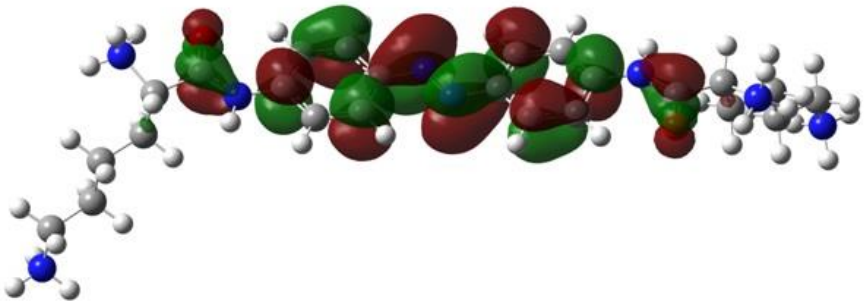

126

HOMO

(π N=N)

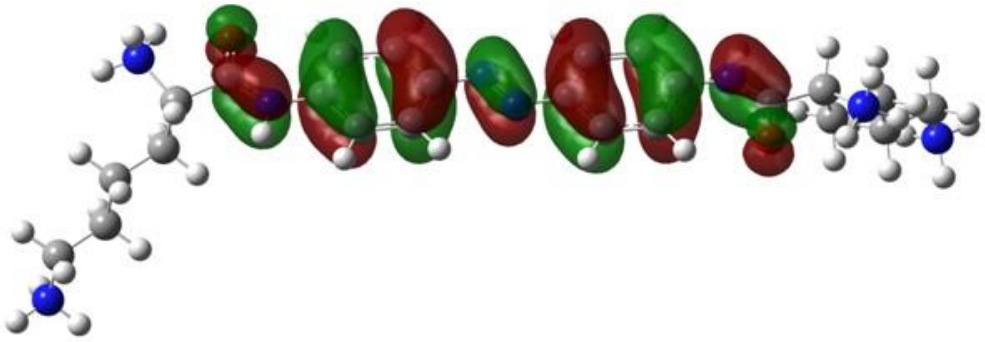

125

HOMO - 1 (LP_N)

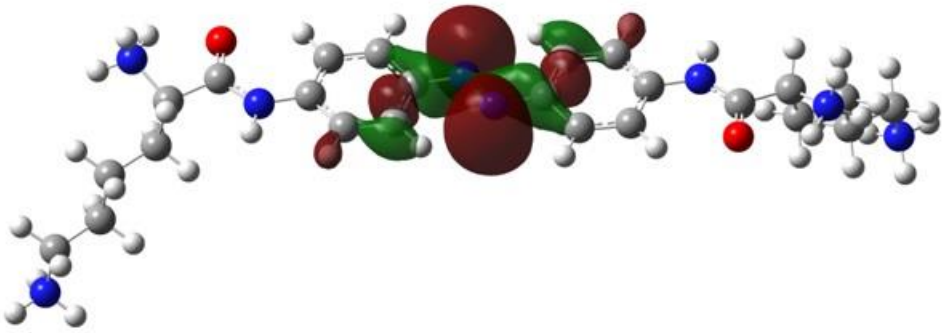

Azo-LL-Lys *cis*

129

LUMO+2

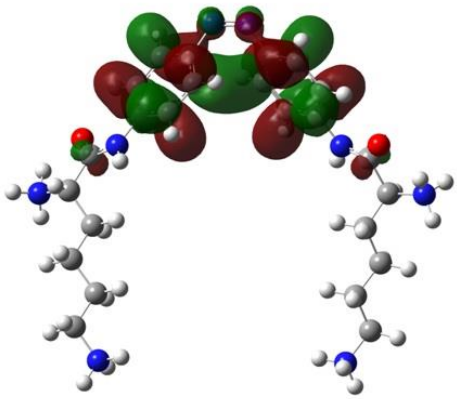

128

LUMO+1

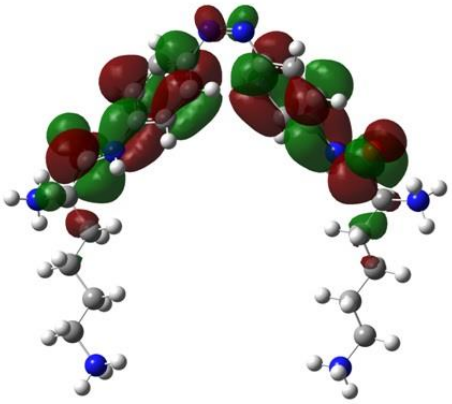

127

LUMO+1

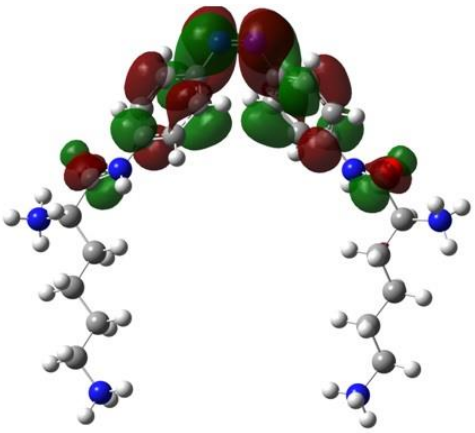

126

HOMO

(π N=N)

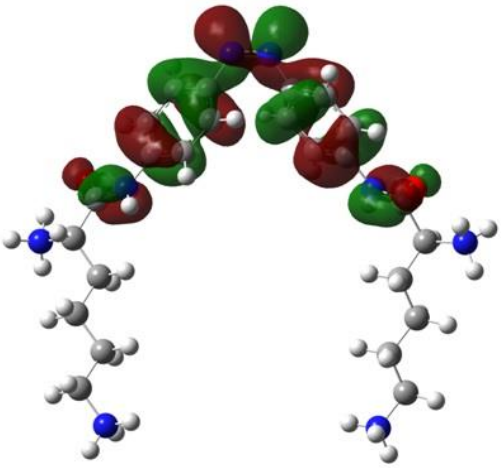

125

HOMO-1

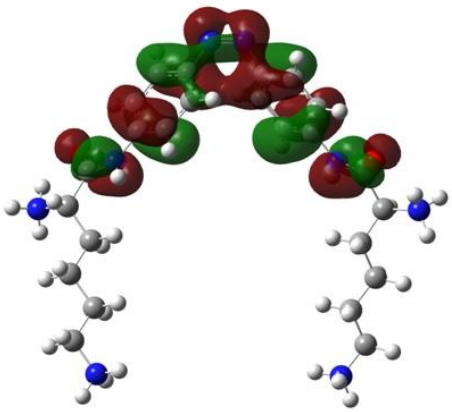

124

HOMO - 2

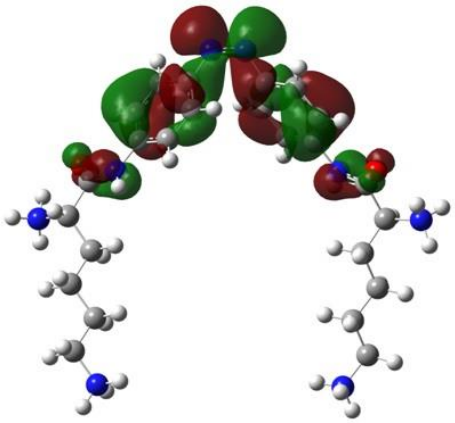

Azo-LL-Thr *trans*

113
LUMO+2

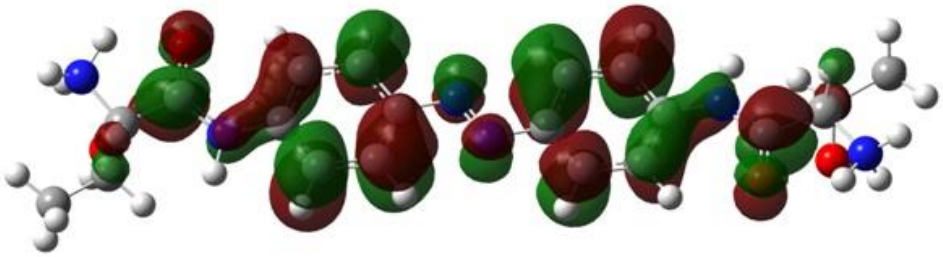

111
LUMO
(π N=N*)

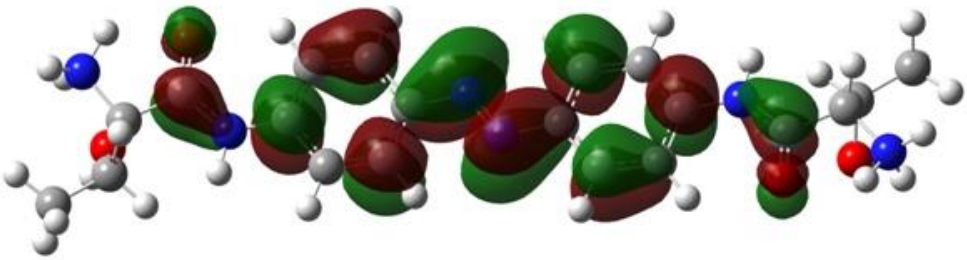

110

HOMO

(π N=N)

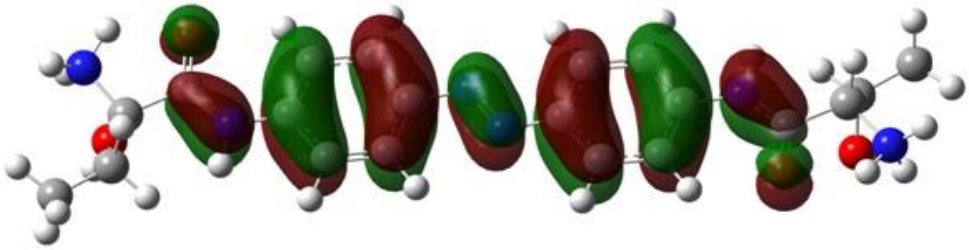

109

HOMO - 1 (LP_N)

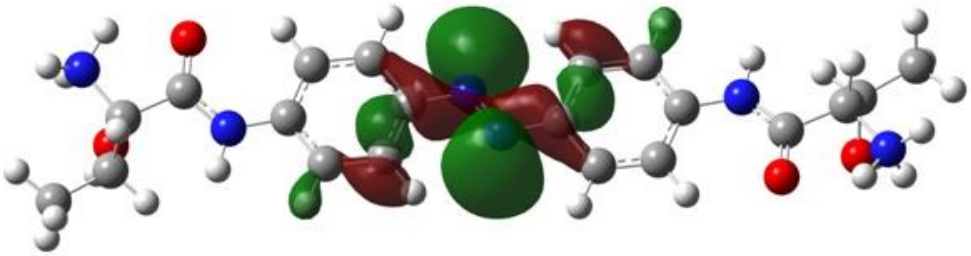

Azo-LL-Thr *cis*

113
LUMO+2

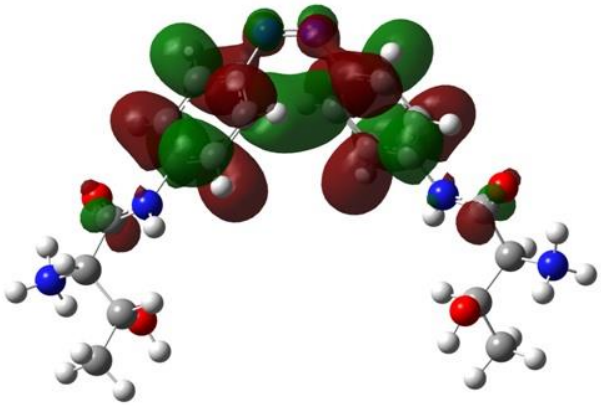

112
LUMO+1

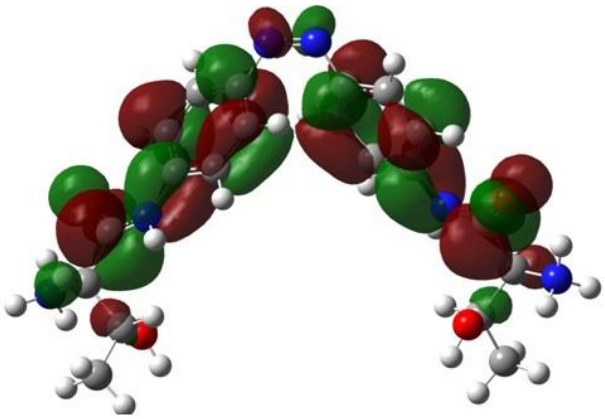

111
LUMO

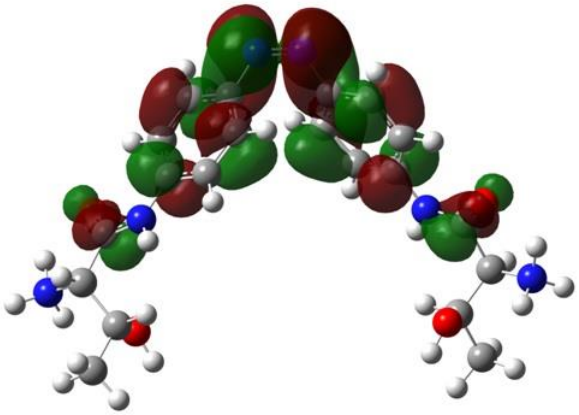

110

HOMO

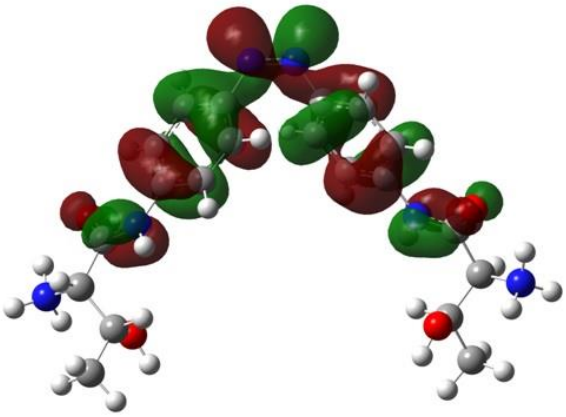

109

HOMO - 1

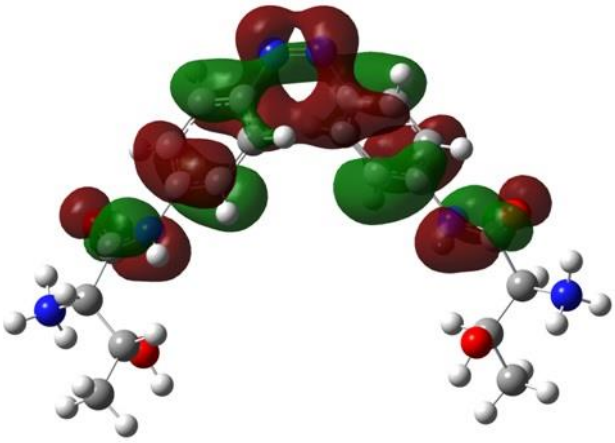

108

HOMO - 2

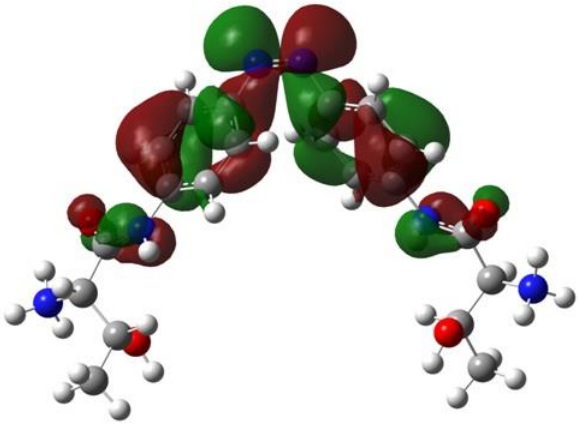

Azo-DD-Thr *trans*

113
LUMO+2

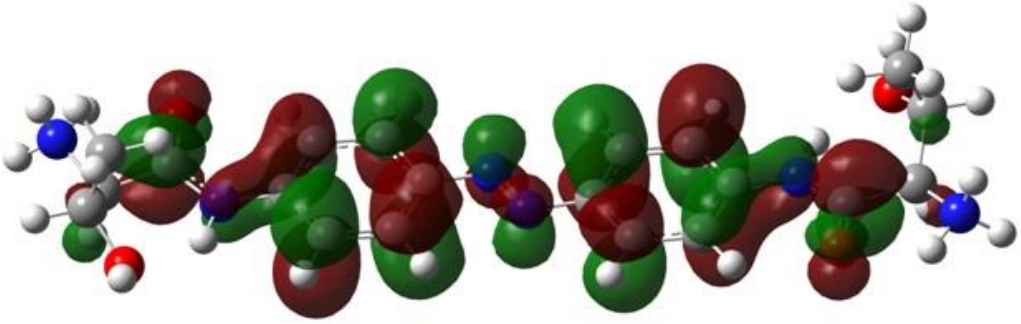

1

111
LUMO
(π N=N*)

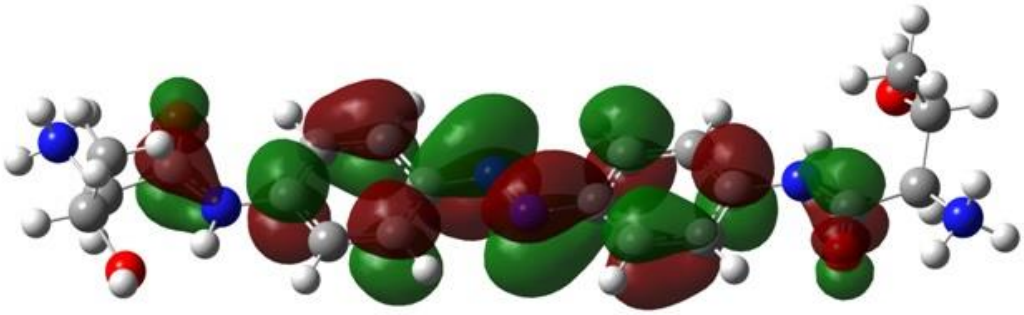

110

HOMO

(π N=N)

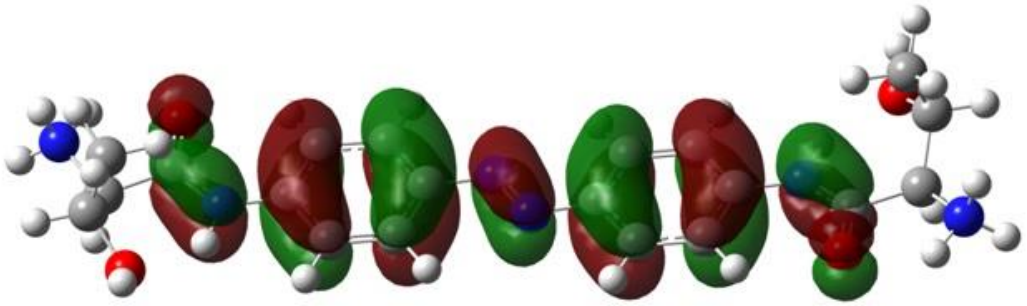

109

HOMO - 1 (LP_N)

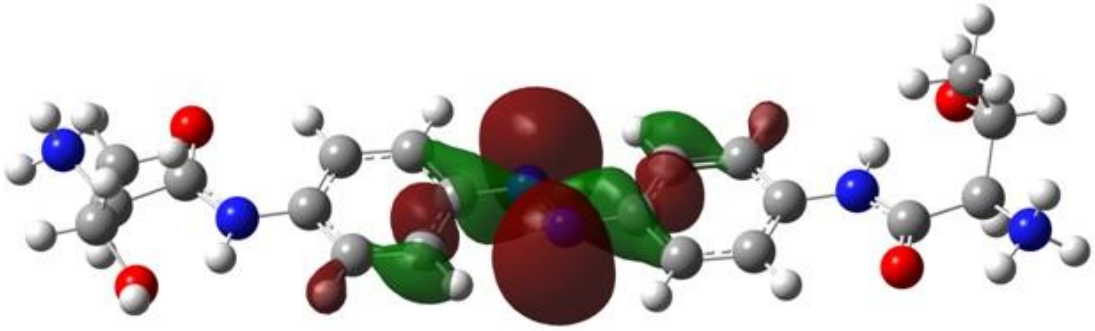

Azo-DD-Thr *cis*

113
LUMO+2

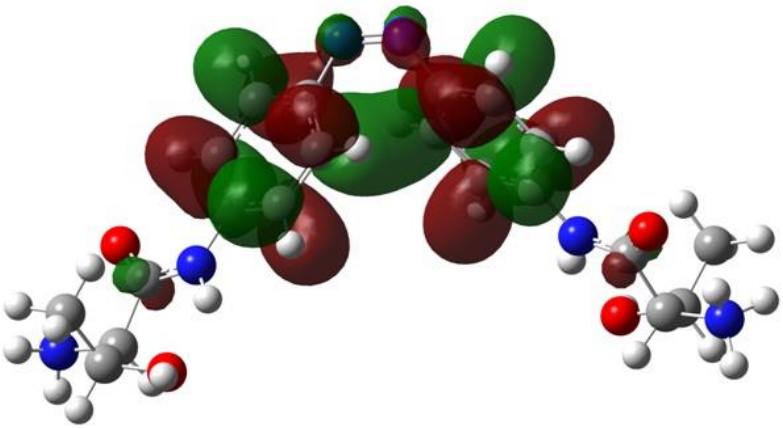

112
LUMO+1

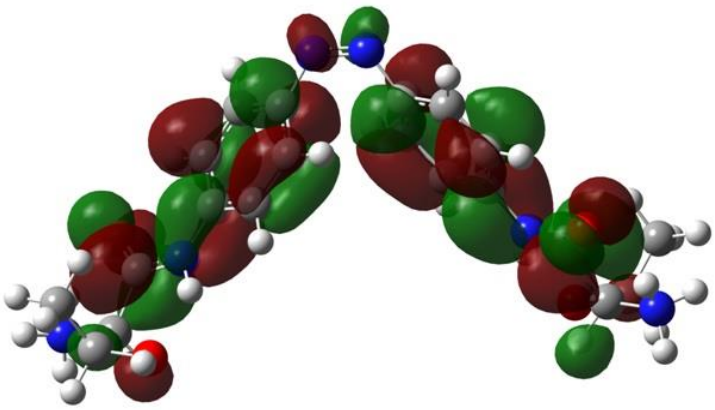

111
LUMO

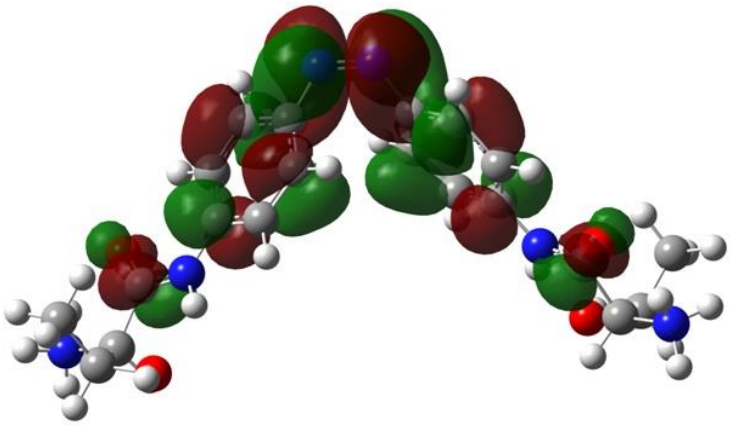

110

HOMO

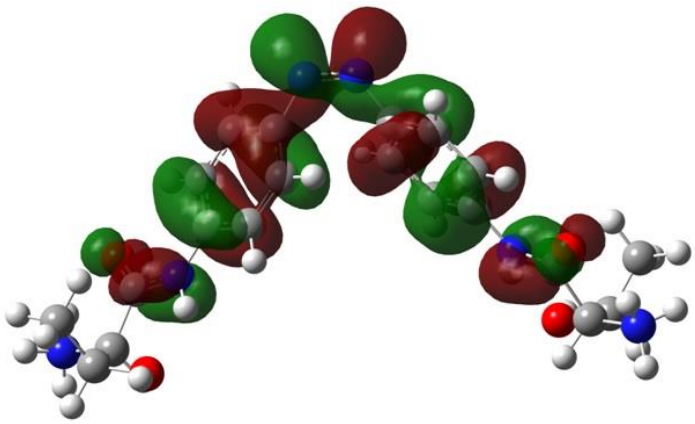

109

HOMO -1

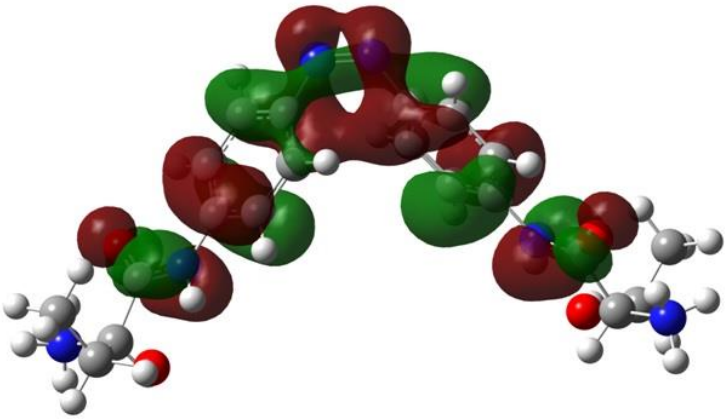

108

HOMO -2

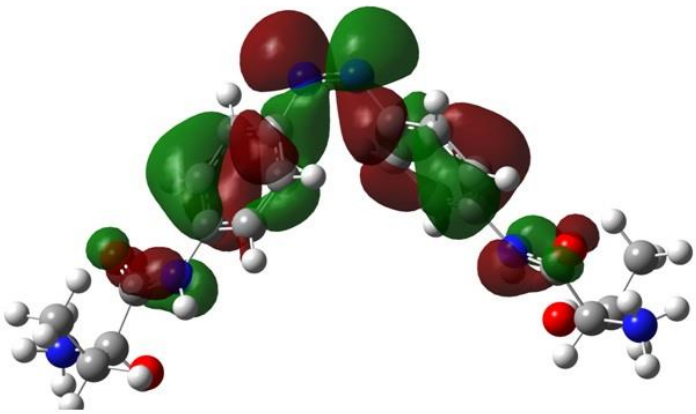

Experimental

Materials

Common reagent-grade chemicals were used without further purification. Salmon sperm double-stranded DNA, guanine-rich oligonucleotides forming quadruplex assemblies (Tel-22 and Z-G4), Ethidium Bromide (EtBr) and Thioflavin T (ThT) were purchased from Sigma Aldrich Chem. Co. Ant-PIm was synthesized according to our previous procedures.[5,6] MilliQ water was used throughout all experiments. Duplex, quadruplexes and **Azo-LL/DD-Lys** were dissolved in water and kept under dark, except during photo-irradiation.[1,7-9] All measurements were performed in 50 mM Tris-HCl buffer (pH 7.5).

Sample irradiation

The photo-induced isomerization reactions of **Azo-LL/DD-Lys** were performed by using a high pressure Hg Oriel lamp equipped with interference filters at 360 and 515 nm. The resulting light intensity was 0.85 mW at 360 nm (*trans*-*cis*) and 0.42 mW at 515 nm (*cis*-*trans*).

The **Azo-LL/DD-Lys** *trans*-to-*cis* and *cis*-to-*trans* ratio was assessed by ^{1}H NMR spectroscopy according to the intensity ratios of the corresponding signals (data not shown). The *trans*:*cis* and *cis*:*trans* composition of the photostationary state was found to be 90:10 and 20:80, respectively.

UV/Vis spectroscopy

The UV-Vis absorption spectra were recorded on a Hitachi U-2900 spectrophotometer at 298 K. The concentration of the photochromes (20 μM) was kept constant while incremental additions of duplex/quadruplex were added into the solution. Quantitative data analysis based on the UV-Vis titration takes into account the composition of the photostationary state.

Fluorescence displacement assays

Fluorescence displacement assays were carried out with a Hitachi F-7000 spectrofluorometer. The site-marker-duplex/quadruplex concentration was kept constant and the binary mixtures were titrated with incremental addition of **Azo-LL/DD-Lys** (no UV/UV) until no appreciable changes on the emission intensity were observed, indicating complete replacement of the duplex/G4-fluorescent probes. Under these circumstances, the quantitative binding data analysis was carried out taking into account not only the composition of the photostationary state but also, when required, the inner filter effect (IFE) as in the case of the replacement of ThT-G4 systems.[1,7,10]

$$F_{corr} = F_{obs} \times 10^{(A_{exc}+A_{em})/2} \quad (1)$$

where F_{corr} is the corrected fluorescence intensity, F_{obs} is the uncorrected fluorescence intensity, A_{exc} and A_{em} are the absorbances of the compounds at the excitation and emission wavelengths used.

Circular dichroism

CD spectra were measured with a Jasco J-815 spectropolarimeter (JascoInc, USA) equipped with the JascoPeltier-type temperature controller (CDF-426S/15) and are presented as a sum of 3 accumulations. CD measurements were performed at 298 K in the wavelength range of 200-600 nm at different duplex or quadruplex/**Azo-LL/DD-Lys** ratios. Before use, the optical chamber of the CD spectrometer was deoxygenated with dry nitrogen and was held under nitrogen atmosphere during the measurements. Appropriate references were subtracted from the obtained CD spectra.

DNA Characterization

Molar extinction coefficients of the following DNA sequences were calculated by using oligo analyzer on the IDT web site and applying the Cavaluzzi-Borer correction:[11-14]

(Tel-22): 5'-AGGGTTAGGGTTAGGGTTAGGG-3' ($\varepsilon_{260\ nm}$ = 233942 M^{-1} cm^{-1});

(Z-G4): 5'-TGGTGGTGGTGGTTGTGGTGGTGGTGTT-3' ($\varepsilon_{260\ nm}$ = 271911 M^{-1} cm^{-1}).

The molar extinction coefficient for genomic salmon sperm *ds*-DNA is expressed in bp units and is taken as 13200 M^{-1} cm^{-1}.

Evidences for G4 folding sequences used in this study were provided by CD measurements and isothermal difference spectra (IDS) defined as the difference between unfolded and prefolded absorbance spectra (Figure S15).[15,16] G4 self-assembly was generated by adding either NaCl or KCl (100 mM) to a buffered aqueous solution (50 mM Tris-HCl, pH 7.5).

The hydrogen bond orientation of Tel-22 originates two types of CD spectra characterized by:[17]

(Type I) a characteristic peak at ≈ 290 nm and trough at ≈ 260 nm (antiparallel basket structure),

(Type II) a characteristic broad peak between ≈ 260 and 290 nm and a trough at ≈ 240 (antiparallel hybrid structure).

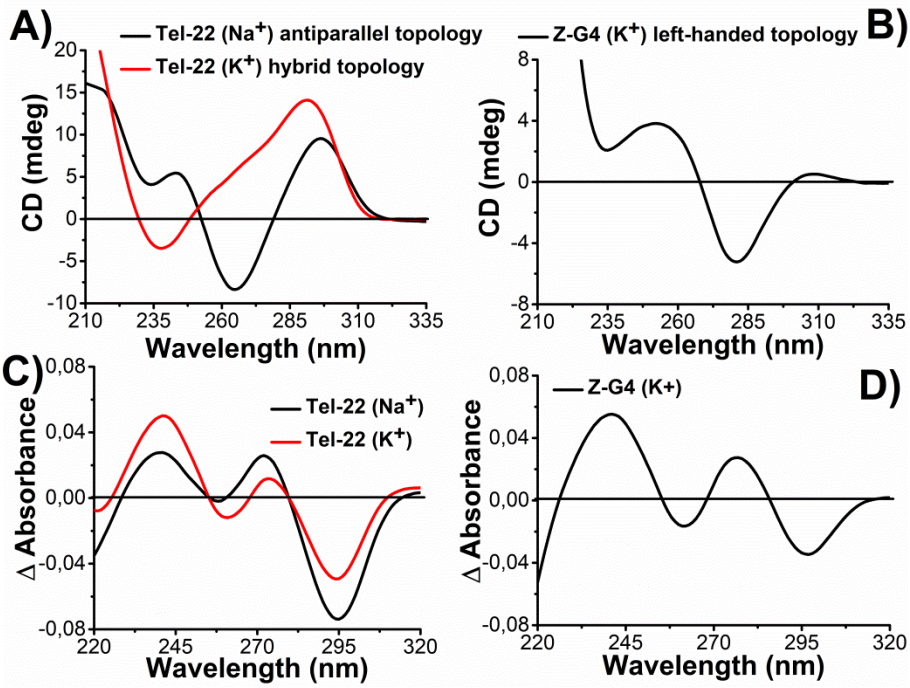

Figure S15. (A) ECD spectra of the telomeric quadruplex Tel-22 in the presence of Na^+ (black line) and K^+ (red line). (B) ECD spectra of the left-handed quadruplex Z-G4 in the presence of K^+. (C) IDS of Tel-22 (Na^+) and Tel-22 (K^+). (D) IDS of Z-G4 (K^+). All the measurements were performed in 50 mM Tris-HCl (pH = 7.5) using either NaCl or KCl 100 mM.

Indeed, while Na^+ induces exclusively antiparallel basket arrangements in Tel-22, K^+ results in a mixed population of both parallel and antiparallel orientations (3+1 hybrid conformation) in agreement with previous studies (Figure S15A and S16).[12,18] On the other hand, Z-G4 in the presence of K^+ folds into a left-handed configuration as showed by the appearance of a negative peak at ≈ 275 nm and a positive peak at ≈ 250 nm in line with the pioneering study of Phan's group (Figure S15B).[19]

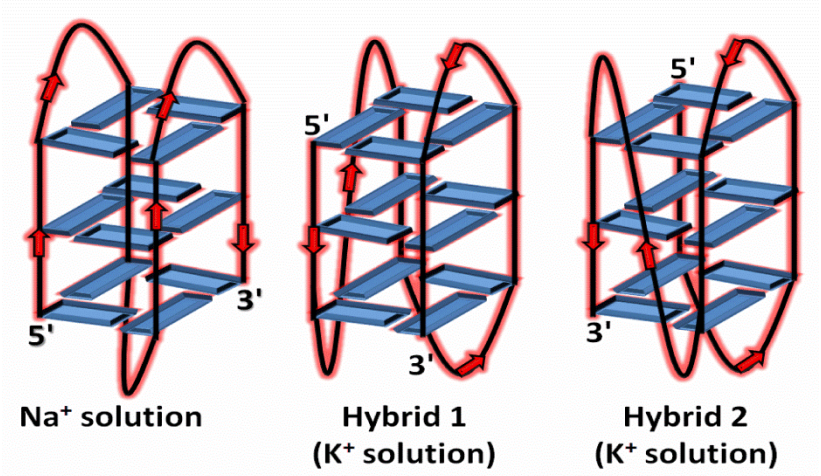

Figure S16. Schematic representation showing the different topologies that Tel-22 assumes in the presence of Na^+ or K^+.

Further evidence for G-quadruplex formation was also provided by analyzing the signature of the IDS spectra. Indeed, the folding process of both Tel-22 and Z-G4 is proved by the appearance of peaks at ≈ 240, 270 and 295 nm in agreement with previous studies (Figure S15C and D).[17]

UV-Vis spectral changes

The ability of the photochromes to bind duplex and quadruplex DNA morphologies was initially investigated by UV-Vis absorption spectroscopy. The optical changes resulting by the complexation of *ds*-DNA/G4-**Azo-LL/DD-Lys** are showed in Figures S17-20 and Table S2.

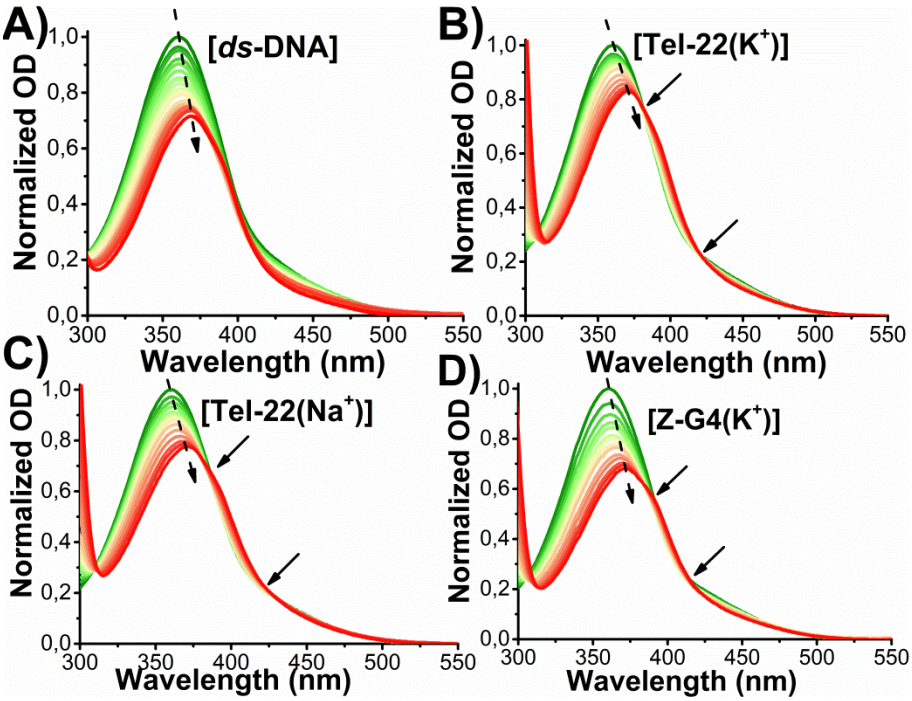

Figure S17. Duplex/quadruplex DNA binding profiles with the molecular photoswitch **Azo-LL-Lys** (no UV). (A) UV-Vis absorption changes of **Azo-LL-Lys** (no UV) with increasing concentration of genomic *ds*-DNA ranging from 0 to 98 μM. (B) UV-Vis absorption changes of **Azo-LL-Lys** (no UV) with increasing concentration of Tel-22 (K^+) ranging from 0 to 22.05 μM. (C) UV-Vis absorption changes of **Azo-LL-Lys** (UV) with increasing concentration of Tel-22 (Na^+) ranging from 0 to 17.55 μM. (D) UV-Vis absorption changes of **Azo-LL-Lys** (UV) with increasing concentration of Z-G4 (K^+) ranging from 0 to 17.55 μM. The dashed and bold arrows aim to show the evolution of the binding profiles and the appearance of isosbetic points, respectively.

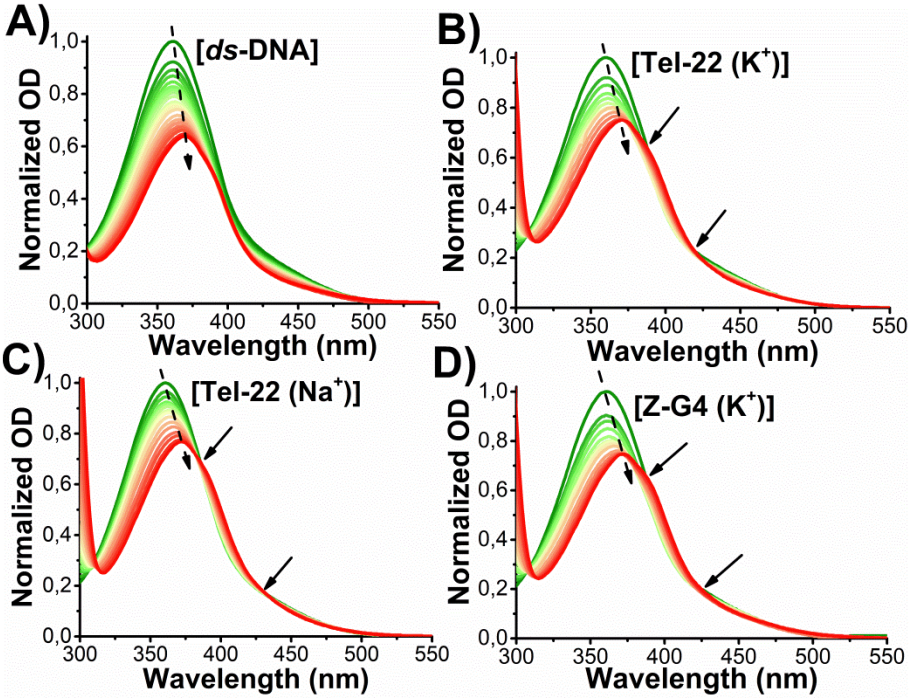

Figure S18. Duplex/quadruplex DNA binding profiles with the molecular photoswitch **Azo-DD-Lys** (no UV). (A) UV-Vis absorption changes of **Azo-DD-Lys** (no UV) with increasing concentration of genomic *ds*-DNA ranging from 0 to 98 μM. (B) UV-Vis absorption changes of **Azo-DD-Lys** (no UV) with increasing concentration of Tel-22 (K^+) ranging from 0 to 17.55 μM. (C) UV-Vis absorption changes of **Azo-DD-Lys** (no UV) with increasing concentration of Tel-22 (Na^+) ranging from 0 to 22.05 μM. (D) UV-Vis absorption changes of **Azo-DD-Lys** (no UV) with increasing concentration of Z-G4 (K^+) ranging from 0 to 17.55 μM. The dashed and bold arrows aim to show the evolution of the binding profiles and the appearance of isosbetic points, respectively.

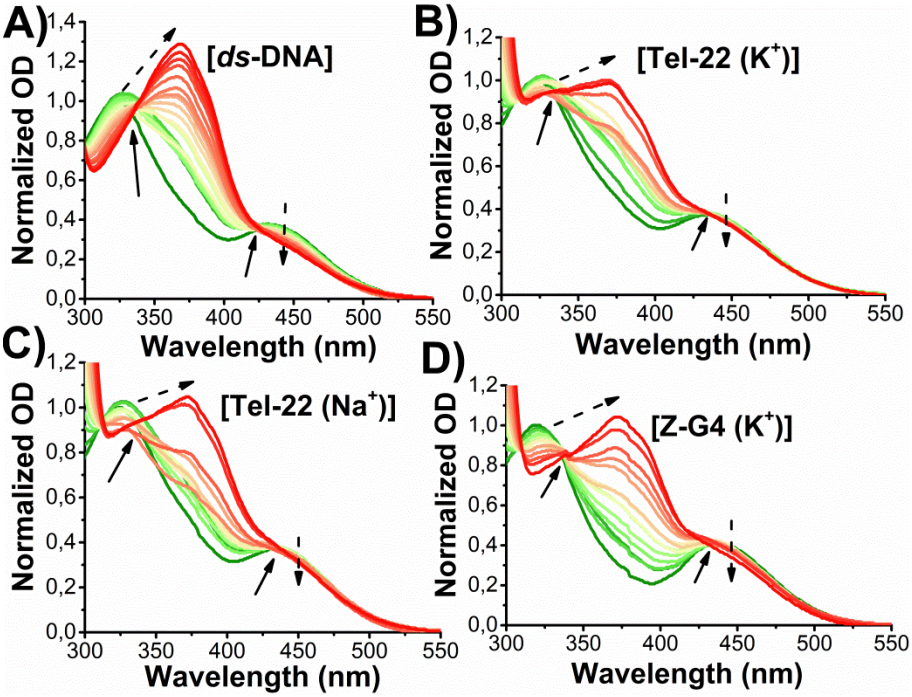

Figure S19. Duplex/quadruplex DNA binding profiles with the molecular photoswitch **Azo-LL-Lys** (UV). (A) UV-Vis absorption changes of **Azo-LL-Lys** (UV) with increasing concentration of

genomic *ds*-DNA ranging from 0 to 98 μM. (B) UV-Vis absorption changes of **Azo-LL-Lys** (UV) with increasing concentration of Tel-22 (K^+) ranging from 0 to 17.55 μM. (C) UV-Vis absorption changes of **Azo-LL-Lys** (UV) with increasing concentration of Tel-22 (Na^+) ranging from 0 to 17.55 μM. (D) UV-Vis absorption changes of **Azo-LL-Lys** (UV) with increasing concentration of Z-G4 (K^+) ranging from 0 to 17.55 μM. The dashed and bold arrows aim to show the evolution of the binding profiles and the appearance of isosbetic points, respectively.

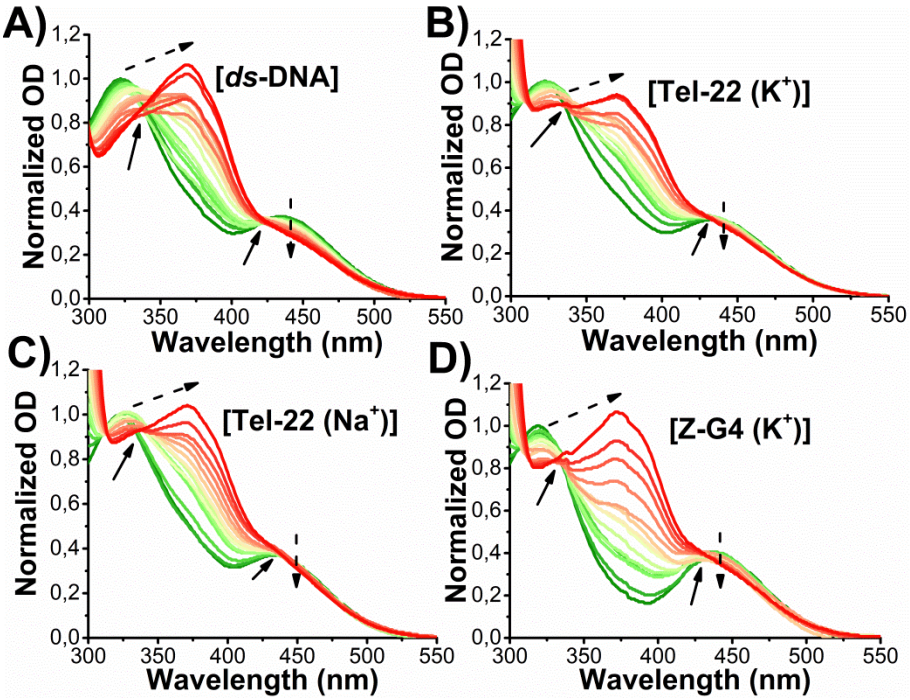

Figure S20. Duplex/quadruplex DNA binding profiles with the molecular photoswitch **Azo-DD-Lys** (UV). (A) UV-Vis absorption changes of **Azo-DD-Lys** (UV) with increasing concentration of genomic *ds*-DNA ranging from 0 to 98 μM. (B) UV-Vis absorption changes of **Azo-DD-Lys** (UV) with increasing concentration of Tel-22 (K^+) ranging from 0 to 17.55 μM. (C) UV-Vis absorption changes of **Azo-DD-Lys** (UV) with increasing concentration of Tel-22 (Na^+) ranging from 0 to 17.55 μM. (D) UV-Vis absorption changes of **Azo-DD-Lys** (UV) with increasing concentration of Z-G4 (K^+) ranging from 0 to 17.55 μM. The dashed and bold arrows aim to show the evolution of the binding profiles and the appearance of isosbetic points, respectively.

Quantification of the association constants between duplex/quadruplex-**Azo-LL/DD-Lys** (no UV) systems follow previously reported protocols.[20] Briefly, the variation of the optical density of **Azo-LL/DD-Lys** was monitored upon addition of duplex and quadruplex DNAs. Plots of the difference between the free and unbound species as a function of the total DNA concentration provide typical saturation curves. Curve analysis was originated based on the semi-log Klotz plot in which the bound concentration is plotted *vs.* log free ligand (duplex or quadruplex) yielding a sigmoidal curve. Non-linear curve fitting procedure based on a growth/sigmoidal bi-dose-response function allow determination of the association constants by converging the binding curves to the best possible

fitting (Figures S21-24). The optical changes and the affinity constants are listed in Table S2. Please note that was not possible to characterize the association strength between **Azo-LL-Lys (UV)** and DNAs due to the non-monotonic and partially-structured band originated at ≈ 360 nm.

Table S2. Spectroscopic data for the titration of the photochromes with the different nucleic acid structures.

Systems	% hypochromicity[a]	Δλ[b] (nm)	K_{a1} (M^{-1})[c]	K_{a2} (M^{-1})[d]
Azo-LL-Lys (no UV)-*ds*-DNA	29	10	2.4 (±0.1) × 10^5	4.3 (±0.1) × 10^4
Azo-DD-Lys (no UV)-*ds*-DNA	36	10	1.9 (±0.1) × 10^5	2.5 (±0.1) × 10^4
Azo-LL-Lys (no UV)-Tel-22 (K^+)	17	12	5.8 (±0.3) × 10^5	1.3 (±0.3) × 10^4
Azo-DD-Lys (no UV)-Tel-22 (K^+)	26	12	6.7 (±0.3) × 10^5	1.2 (±0.3) × 10^5
Azo-LL-Lys (no UV)-Tel-22 (Na^+)	23	12	4.2 (±0.2) × 10^5	1.2 (±0.1) × 10^5
Azo-DD-Lys (no UV)-Tel-22 (Na^+)	23	13	1.7 (±0.1) × 10^5	1.1 (±0.1) × 10^5
Azo-LL-Lys (no UV)-Z-G4 (K^+)	33	13	3.8 (±0.2) × 10^5	/
Azo-DD-Lys (no UV)-Z-G4 (K^+)	25	13	3.8 (±0.2) × 10^5	/

[a]% hypochromicity: is defined as the difference between the absorbances of the free photochrome and the bound photochrome-duplex/quadruplex system. [b]Δλ: is defined as the difference between the maximum of the absorption of the free photochrome and the bound photochrome-duplex/quadruplex system. [c]K_{a1}: association constant reflecting the affinity to the first binding site. [d]K_{a2}: association constant reflecting the affinity to the second binding site. Note that the Azo-LL/DD-Lys (no UV)-Z-G4 (K^+) systems can be fitted with a 1:1 quadruplex:photochrome stoichiometry. All the other systems have been fitted with a 1:2 duplex/quadruplex/photochrome stoichiometry.

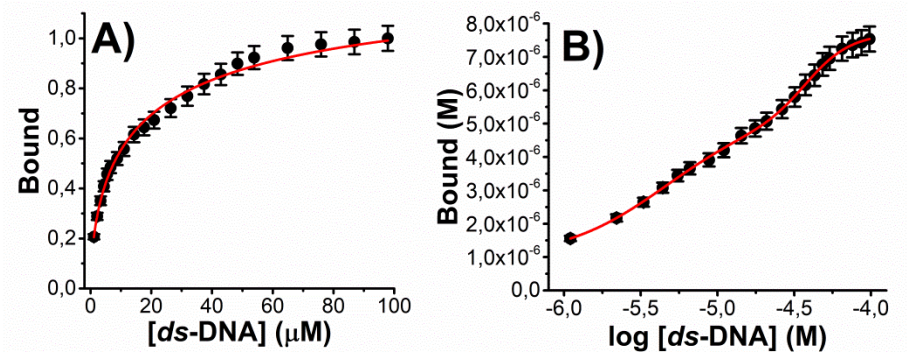

Figure S21. Nonlinear curve fitting analysis. (A) Binding isotherm for *ds*-DNA-**Azo-DD-Lys** (no UV) system. (B) Semi-log plot based on Klotz model plotted as bound (*ds*-DNA-**Azo-DD-Lys** (no UV) complex) *vs.* log free *ds*-DNA. Red lines represent the best data fitting procedure.

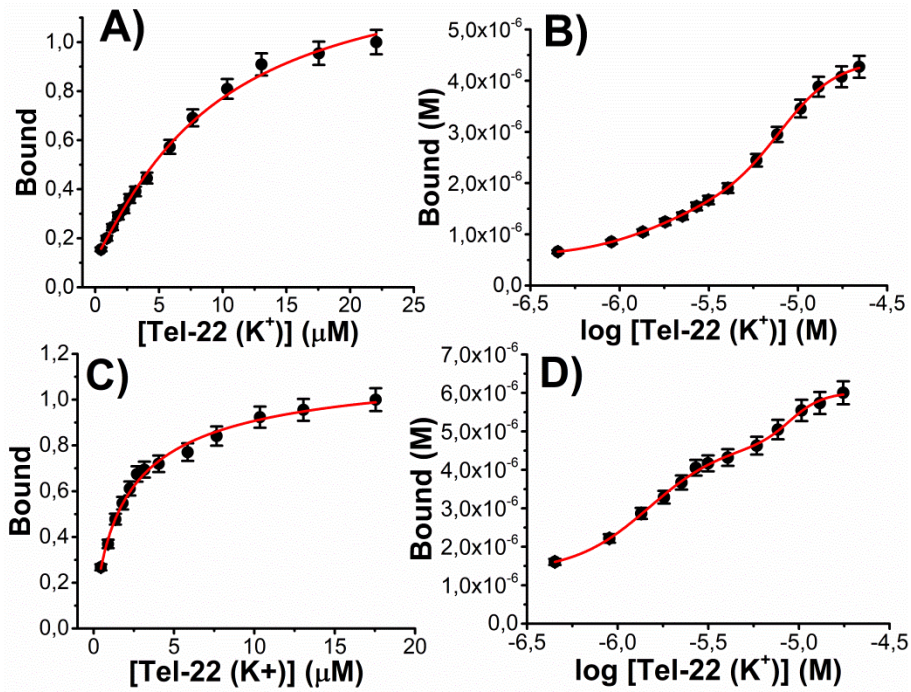

Figure S22. Nonlinear curve fitting analysis. (A) Binding isotherm for Tel-22 (K^+)-**Azo-LL-Lys** (no UV) system. (B) Semi-log plot based on Klotz model plotted as bound (Tel-22 (K^+)-**Azo-LL-Lys** (no UV) complex) *vs.* log free Tel-22 (K^+). (C) Binding isotherm for Tel-22 (K^+)-**Azo-DD-Lys** (no UV) system. (D) Semi-log plot based on Klotz model plotted as bound (Tel-22 (K^+)-**Azo-DD-Lys** (no UV) complex) *vs.* log free Tel-22 (K^+). Red lines represent the best data fitting procedure.

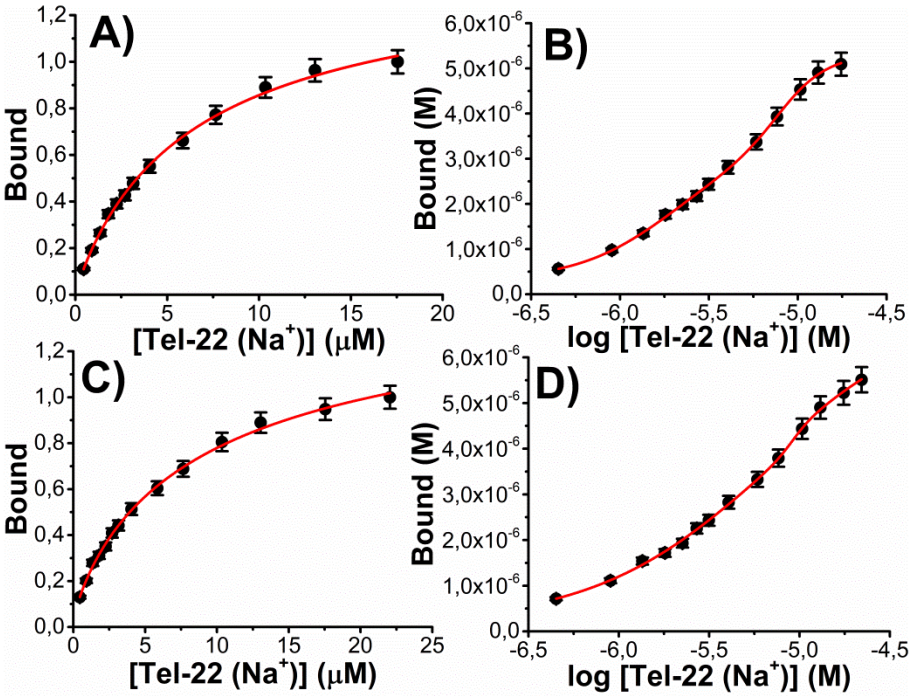

Figure S23. Nonlinear curve fitting analysis. (A) Binding isotherm for Tel-22 (Na^+)-**Azo-LL-Lys** (no UV) system. (B) Semi-log plot based on Klotz model plotted as bound (Tel-22 (Na^+)-**Azo-LL-Lys** (no UV) complex) *vs.* log free Tel-22 (Na^+). (C) Binding isotherm for Tel-22 (Na^+)-**Azo-DD-Lys** (no UV) system. (D) Semi-log plot based on Klotz model plotted as bound (Tel-22 (Na^+)-**Azo-DD-Lys** (no UV) complex) *vs.* log free Tel-22 (Na^+). Red lines represent the best data fitting procedure.

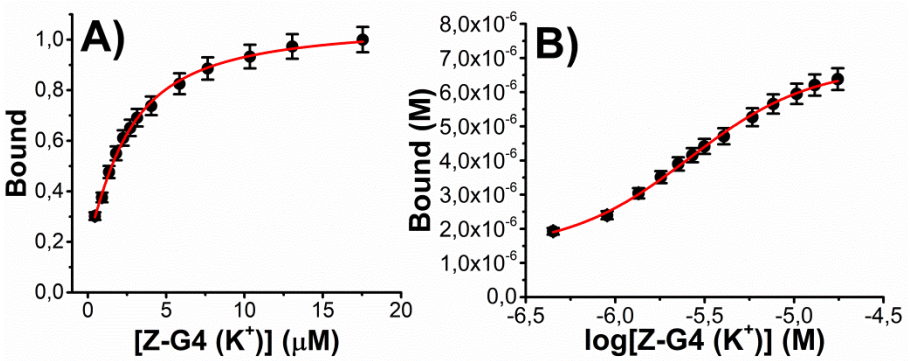

Figure S24. Nonlinear curve fitting analysis. (A) Binding isotherm for Z-G4 (K^+)-**Azo-DD-Lys** (no UV) system. (B) Semi-log plot based on Klotz model plotted as bound (Z-G4 (K^+)-**Azo-DD-Lys** (no UV) complex) *vs.* log free Z-G4 (K^+). Red lines represent the best data fitting procedure.

The best fitting for the telomeric quadruplex (Tel-22)- and *ds*-DNA-photochrome systems is obtained with a binding stoichiometry of 1:2 duplex/quadruplex:photochrome. A rather common ligand binding mode in G4s compatible with 1:2 stoichiometry is the stacking of one ligand at the top and bottom of the tetrads.[21] A schematic representation is shown in Figure S25. The 1:2 binding stoichiometry obtained for duplex-photochrome systems is due to the neighbor exclusion principle (1 ligand every 2 base pairs) that rules the intercalative binding process of the overwhelming majority of the intercalators. Conversely, a 1:1 binding stoichiometry is obtained for Z-G4 (K^+)-photochrome systems. This finding is consistent with the sizeable cavity (≈ 9 Å) described by the Phan's group which provides a matching platform for the stacking of a single photochrome at the bottom of the left-handed quadruplex.[19,22] Similar conclusion were drawn by Qu and co-workers in a recent paper describing the chiral recognition of metal complexes toward Z-G4.[22]

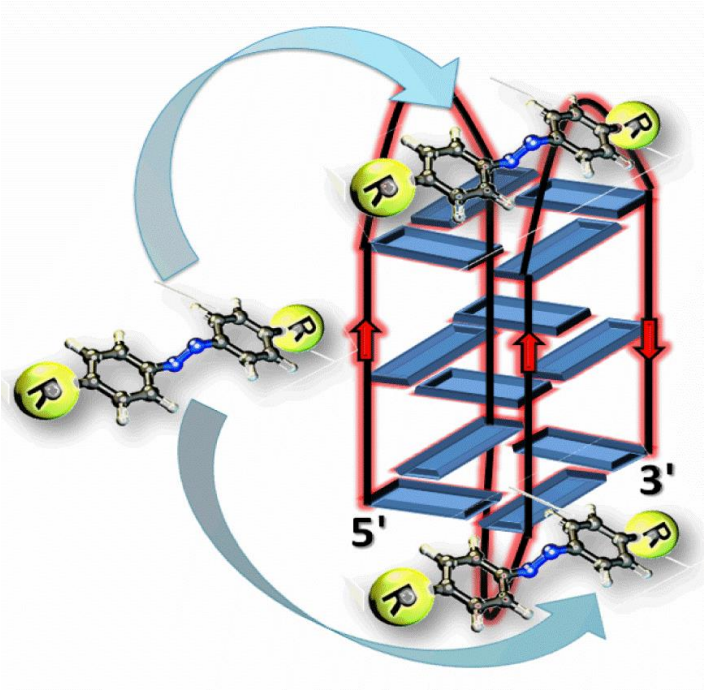

Figure S25. Schematic representation showing the complexation process between the photochrome and the telomeric quadruplex by taking into account a 1:2 (quadruplex:photochrome) binding stoichiometry.

Optical characterization of Azo-LL/DD-Thr

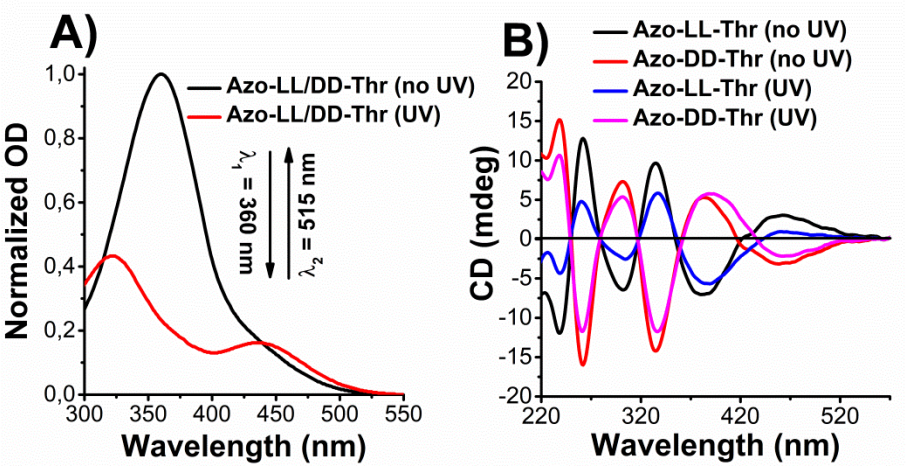

Figure S26. Photochemical reaction of the molecular photoswitches. (A) Photoisomerization process of **Azo–LL/DD–Tyr** after UV (red line) and visible (black line) irradiation. *Trans*-to-*cis* and *cis*-to-*trans* isomerization is accomplished by photon irradiation at 360 and 515 nm, respectively. (B) ECD spectra of **Azo-LL/DD-Tyr** after UV (red line) and visible (black line) irradiation. *Trans*-to-*cis* and *cis*-to-*trans* isomerization is accomplished by photon irradiation at 360 and 515 nm, respectively.

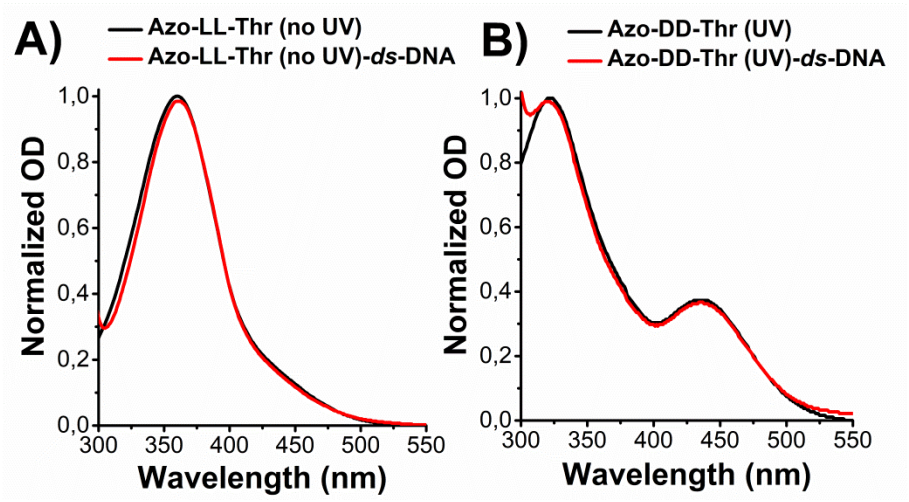

Figure S27. Duplex DNA binding profile. (A) UV-Vis absorption changes of **Azo-LL-Thr** (no UV) in the presence of genomic *ds*-DNA. [**Azo-LL-Thr** (no UV)] = 20 μM and [*ds*-DNA] = 98 μM. (B) UV-Vis absorption changes of **Azo-DD-Thr** (UV) in the presence of *ds*-DNA. [**Azo-DD-Thr** (UV)] = 20 μM and [*ds*-DNA] = 65 μM.

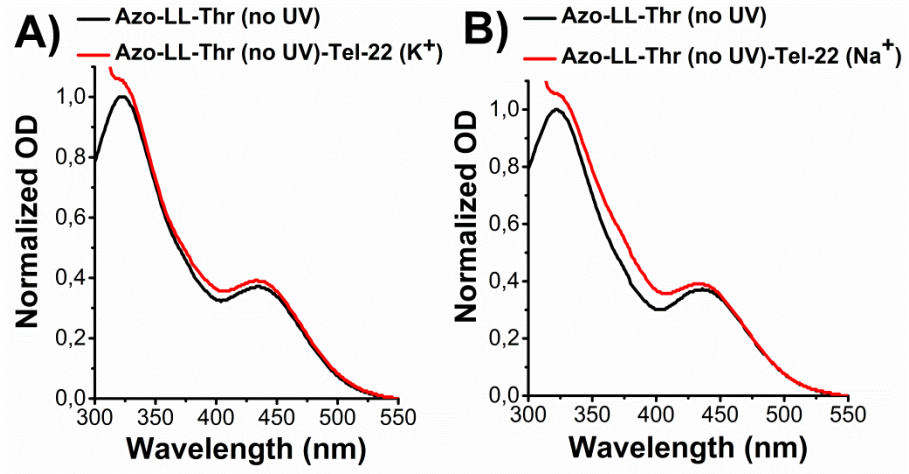

Figure S28. Tel-22 (Na^+/K^+) binding profile. (A) UV-Vis absorption changes of **Azo-LL-Thr** (UV) in the presence of Tel-22 (K^+). [**Azo-LL-Thr** (UV)] = 20 μM and [Tel-22 (K^+)] = 17.55 μM. (B) UV-Vis absorption changes of **Azo-LL-Thr** (UV) in the presence of Tel-22 (Na^+). [**Azo-LL-Thr** (UV)] = 20 μM and [Tel-22 (Na^+)] = 17.55 μM.

Fluorescence displacement assays

Site-localization of the molecular photoswitches was carried out by using fluorescence displacement assays whose mechanism is depicted in Figure S29.

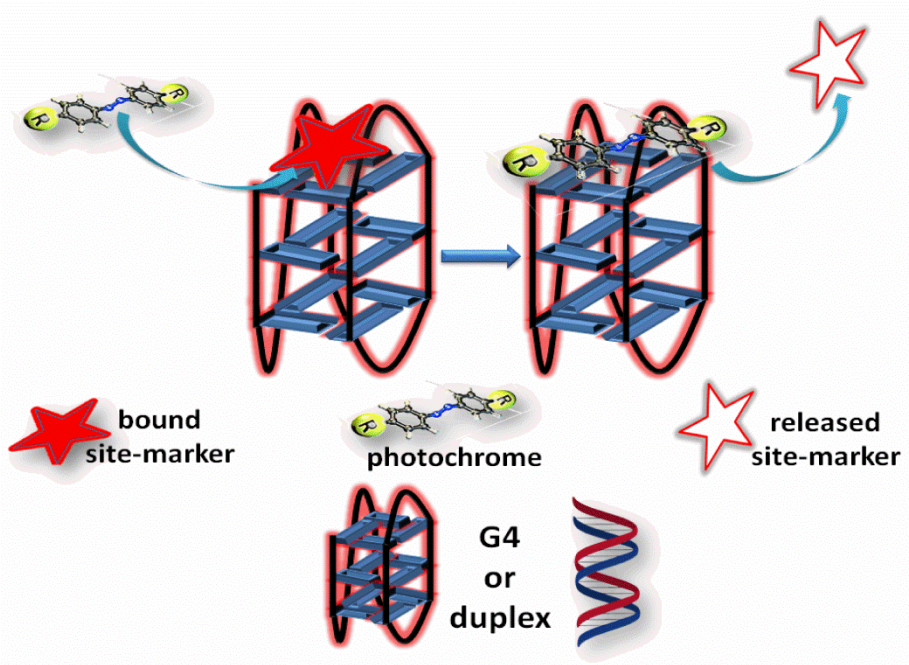

Figure S29. Schematic representation showing the site-marker displacement assays.

In order to distinguish between intercalation and groove binding, two well-known duplex markers were used. Ethidium Bromide (EtBr) is a light-up probe that binds duplex DNA by intercalation whereas, Ant-PIm is a turn-off probe that binds the *ds*-DNA minor groove.[5,11] Please note that Hoechst 33258, a minor groove binder that binds AT-rich tracts, was not used in these experiments due to its excitation (λ_{exc} = 350 nm) and emission (λ_{em} = 460 nm) wavelengths that are strongly overlapped with the absorption spectra of the photochromes. Upon addition of increasing amount of **Azo-LL/DD-Lys** (no UV/UV) to the *ds*-DNA-EtBr systems the fluorescence intensity was gradually quenched indicating the ability of the molecular photoswitches, in both their conformations, to displace the archetypical intercalator from the GC-rich compartments (Figures S30-32). On the other hand, addition of both **Azo-LL/DD-Lys** (no UV) to *ds*-DNA-Ant-PIm systems does not induce modification on the emission maximum, thus, ruling out the association of the light-activated compounds through groove binding mode (Figures S33). Once the coordination mode of **Azo-LL/DD-Lys** (no UV/UV) in the presence of duplex DNA was ascertained, G4 fluorescence displacement assays were also carried out. Ant-PIm binds human telomeric DNA sequences through intercalation and end-stacking mode and in these circumstances behaves as a blue-shifted light-up probe.[11] Indeed, upon addition of **Azo-LL/DD-Lys** (no UV) the emission

intensity of Tel-22 (Na^+/K^+)-Ant-PIm systems is both red-shifted and quenched pointing out the effective replacement of Ant-PIm by the photochromes (Figures S34-36). However, it is important to note that even at high concentration of the photochromes some Ant-PIm molecules remain bound to the G4s as evidenced by the not fully restored bathochromic effects on the emission maximum. This is related to the exotic intercalative mode that Ant-PIm experiences in the presence of G4s that hamper its replacement from the inner G-tetrads.[11] Further evidences for the binding of the photochromes to Tel-22 (Na^+/K^+) were provided by using Thioflavin T (ThT) as a selective G4 fluorescent sensor.[12] ThT is a light-up probe that binds to Tel-22 through end-stacking.[12] Upon addition of **Azo-LL/DD-Lys** (no UV/UV) to Tel-22 (Na^+/K^+)-ThT systems a decrease of the fluorescence intensity was observed indicating the ability of the photochromes to coordinate Tel-22 (Na^+/K^+) mainly *via* stacking on the top/bottom of the G-tetrads (Figure S37).

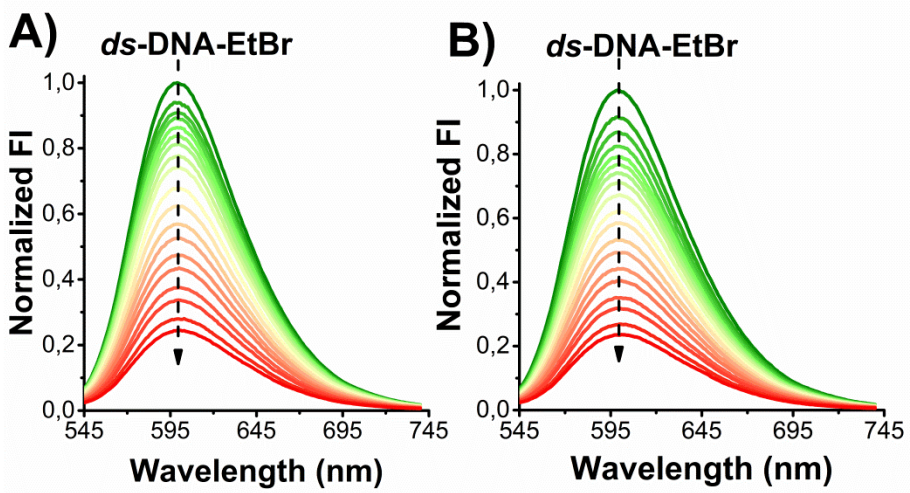

Figure S30. Site-localization of the photochromes resolved by fluorescence displacement assays. (A) Competitive binding interaction between the archetypical intercalator EtBr bound to *ds*-DNA and **Azo-LL-Lys** (no UV). (B) Competitive binding interaction between the archetypical intercalator EtBr bound to *ds*-DNA and **Azo-DD-Lys** (no UV). The turn-on emission profile of *ds*-DNA-EtBr system is gradually quenched by adding incremental amount of **Azo-LL/DD-Lys** (no UV) ranging from 0 to 170 μM. [*ds*-DNA]/[EtBr] = 4 and λ_{exc} = 540 nm.

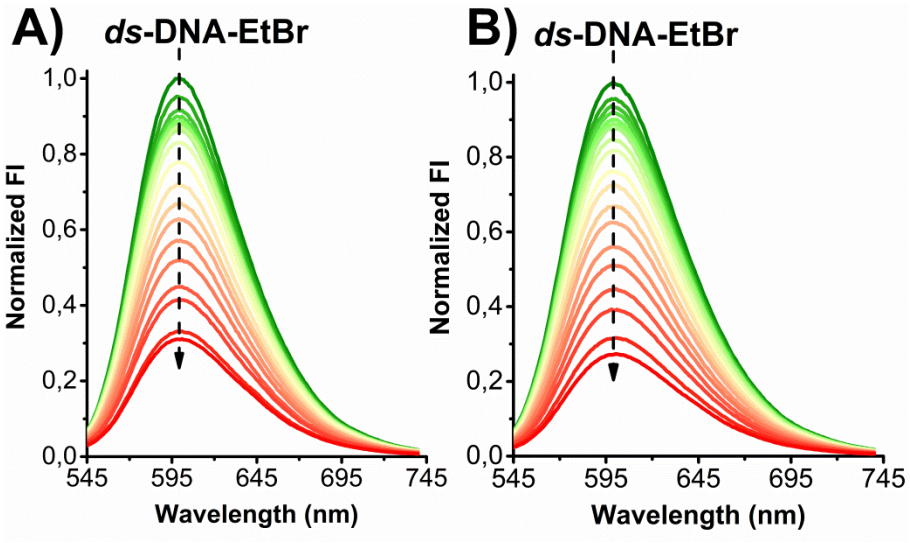

Figure S31. Site-localization of the photochromes resolved by fluorescence displacement assays. (A) Competitive binding interaction between the archetypical intercalator EtBr bound to *ds*-DNA and **Azo-LL-Lys** (UV). (B) Competitive binding interaction between the archetypical intercalator EtBr bound to *ds*-DNA and **Azo-DD-Lys** (UV). The turn-on emission profile of *ds*-DNA-EtBr system is gradually quenched by adding incremental amount of **Azo-LL/DD-Lys** (no UV) ranging from 0 to 170 μM. [*ds*-DNA]/[EtBr] = 4 and λ_{exc} = 540 nm.

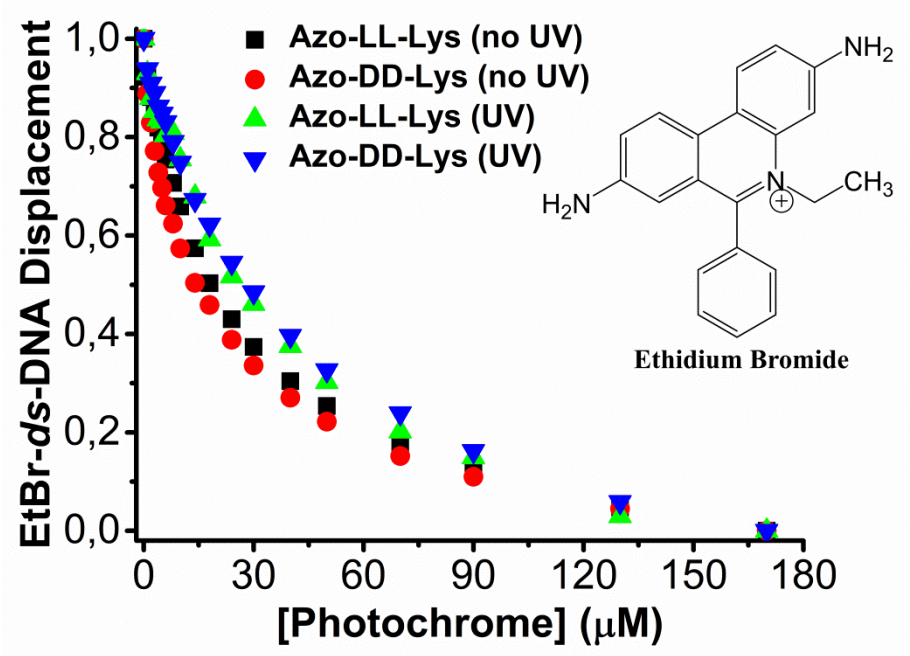

Figure S32. Competitive binding interaction between the duplex site-marker EtBr bound to *ds*-DNA and **Azo-LL/DD-Lys** (no UV/UV).

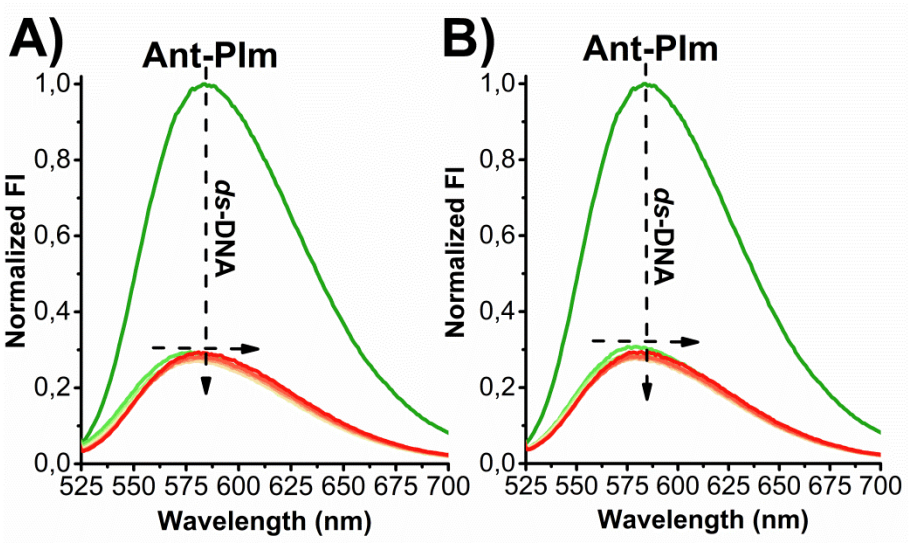

Figure S33. Site-localization of the photochromes resolved by fluorescence displacement assays. (A) Competitive binding interaction between the nonlinear minor groove binder Ant-PIm bound *ds*-DNA and **Azo-LL-Lys** (no UV). (B) Competitive binding interaction between the nonlinear minor groove binder Ant-PIm bound *ds*-DNA and **Azo-DD-Lys** (no UV). The turn-off emission profile of *ds*-DNA-Ant-PIm system is not affected by the addition of increasing concentration of **Azo-LL/DD-Lys** ranging from 0 to 151 μM. [*ds*-DNA]/[Ant-PIm] = 5 and λ_{exc} = 516 nm.

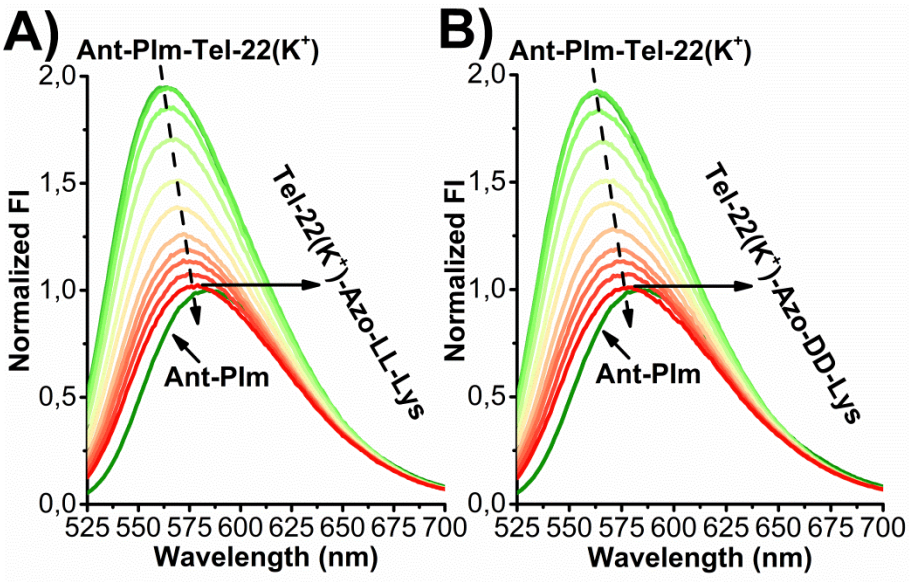

Figure S34. Site-localization of the photochromes resolved by fluorescence displacement assays. (A) Competitive binding interaction between the G4 site-marker Ant-PIm bound to Tel-22 (K^+) and **Azo-LL-Lys** (no UV). (B) Competitive binding interaction between the G4 site-marker Ant-PIm bound to Tel-22 (K^+) and **Azo-DD-Lys** (no UV). The turn-on emission profile of Tel-22-Ant-PIm system is gradually quenched by the addition of increasing concentration of **Azo-LL/DD-Lys** ranging from 0 to 151 μM. [Tel-22 (K^+)]/[Ant-PIm] = 8 and λ_{exc} = 516 nm.

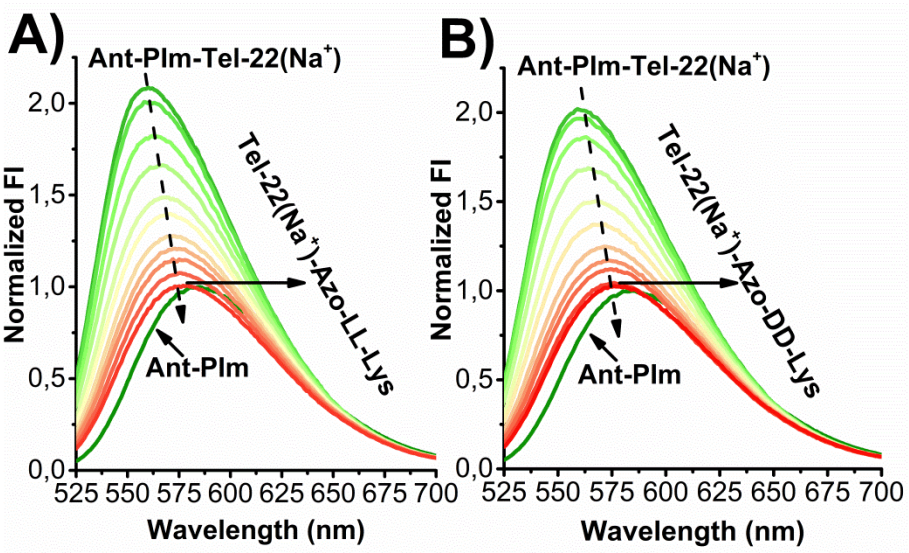

Figure S35. Site-localization of the photochromes resolved by fluorescence displacement assays. (A) Competitive binding interaction between the G4 site-marker Ant-PIm bound to Tel-22 (Na^+) and **Azo-LL-Lys** (no UV). (B) Competitive binding interaction between the G4 site-marker Ant-PIm bound to Tel-22 (Na^+) and **Azo-DD-Lys** (no UV). The turn-on emission profile of Tel-22-Ant-PIm system is gradually quenched by the addition of increasing concentration of **Azo-LL/DD-Lys** ranging from 0 to 151 μM. [Tel-22 (Na^+)]/[Ant-PIm] = 8 and λ_{exc} = 516 nm.

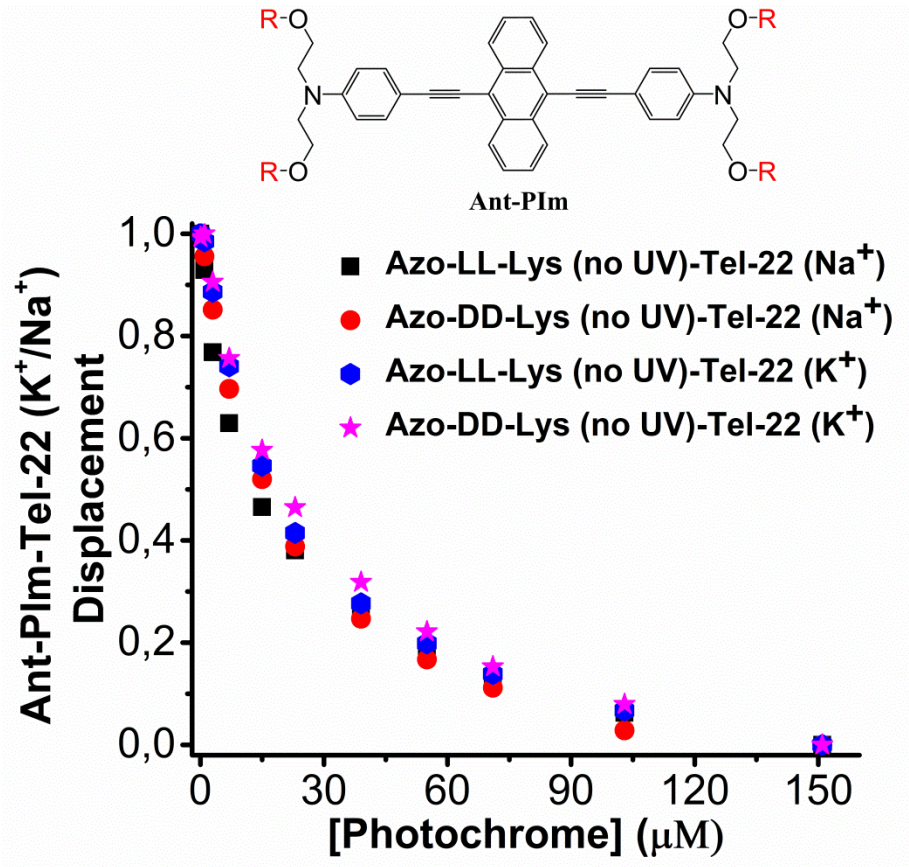

Figure S36. Competitive binding interaction between the G4 site-marker Ant-PIm bound to Tel-22 (Na^+/K^+) and **Azo-LL/DD-Lys** (no UV).

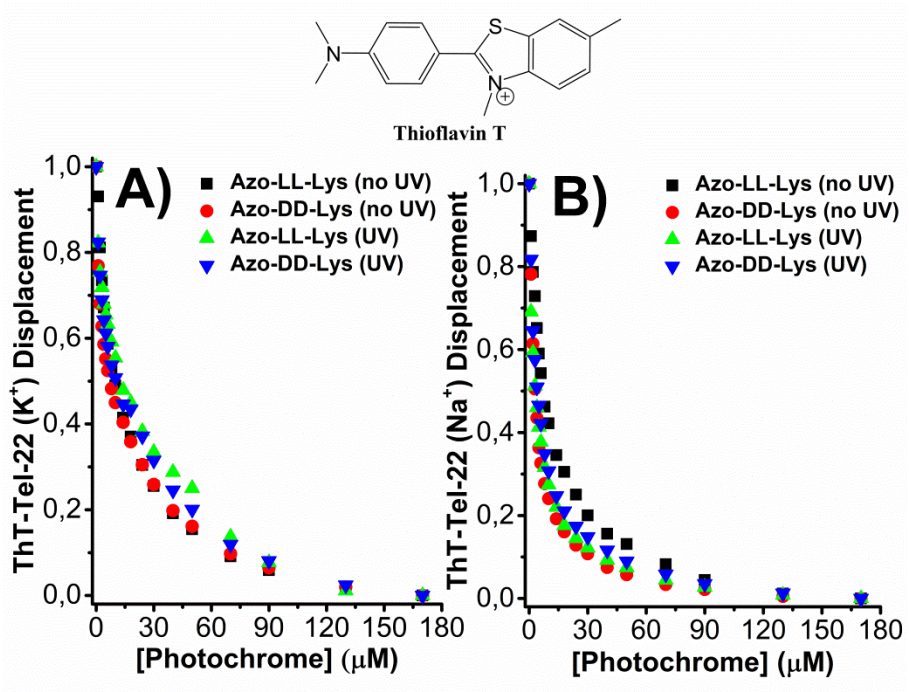

Figure S37. Competitive binding interaction between the G4 site-marker ThT bound to (A) Tel-22 (K^+) and (B) Tel-22 (Na^+) and **Azo-LL/DD-Lys** (no UV/UV).

In order to precisely quantify the photochrome-induced site-marker displacement, $^{ds}DC_{50}$ and $^{G4}DC_{50}$ values were designed as the required concentration to displace 50% of the molecular probes from either duplex or quadruplex DNAs. As shown in Table S3, **Azo-LL/DD-Lys** (no UV/UV) exhibit moderate affinity for duplex and quadruplex morphologies in agreement with the derived association constants.

Table S3. $^{ds}DC_{50}$ and $^{G4}DC_{50}$ calculated based on the fluorescence displacement assays.

Photochrome	System	$^{ds}DC_{50}$ (μM)*	$^{G4}DC_{50}$ (μM)*
Azo-LL-Lys **(no UV)**	EtBr-*ds*-DNA	26.8	/
Azo-DD-Lys **(no UV)**	EtBr-*ds*-DNA	27.1	/
Azo-LL-Lys **(UV)**	EtBr-*ds*-DNA	40.0	/
Azo-DD-Lys **(UV)**	EtBr-*ds*-DNA	47.5	/
Azo-LL-Lys **(no UV)**	ThT-Tel-22 (K^+)	/	8.9
Azo-DD-Lys **(no UV)**	ThT-Tel-22 (K^+)	/	21.0
Azo-LL-Lys **(UV)**	ThT-Tel-22 (K^+)	/	45.7
Azo-DD-Lys **(UV)**	ThT-Tel-22 (K^+)	/	44.1
Azo-LL-Lys **(no UV)**	ThT-Tel-22 (Na^+)	/	7.7

Azo-DD-Lys **(no UV)**	ThT-Tel-22 (Na^+)	/	2.3
Azo-LL-Lys **(UV)**	ThT-Tel-22 (Na^+)	/	4.7
Azo-DD-Lys **(UV)**	ThT-Tel-22 (Na^+)	/	2.6
Azo-LL-Lys **(no UV)**	Ant-PIm-Tel-22 (K^+)	/	21.7
Azo-DD-Lys **(no UV)**	Ant-PIm-Tel-22 (K^+)	/	24.5
Azo-LL-Lys **(no UV)**	Ant-PIm-Tel-22 (Na^+)	/	24.7
Azo-DD-Lys **(no UV)**	Ant-PIm-Tel-22 (Na^+)	/	20.1

* the $^{ds}DC_{50}$ and $^{G4}DC_{50}$ were extrapolated by using a nonlinear fitting procedure based on Hill dose-response model.

ECD spectra of Azo-LL/DD-Lys (no UV/UV)

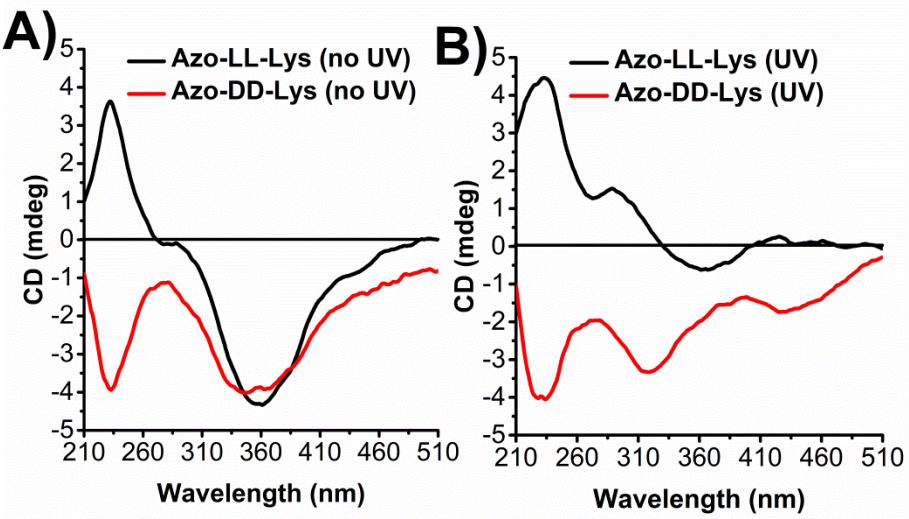

Figure S38. Electronic circular dichroism spectra of the photochromes. (A) ECD spectra of **Azo-LL-Lys** (no UV) and **Azo-DD-Lys** (no UV). (B) ECD spectra of **Azo-LL-Lys** (UV) and **Azo-DD-Lys** (UV).

ECD spectra of Azo-LL/DD-Lys complexed with duplex and quadruplexes

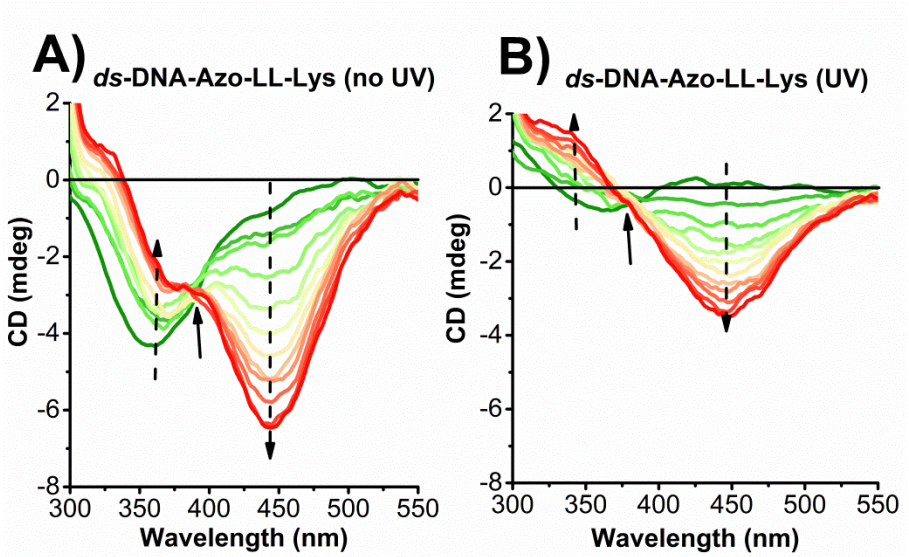

Figure S39. Electronic circular dichroism analysis of **Azo-LL-Lys** (no UV/UV)-*ds*-DNA adducts. (A) ECD spectra resulting from the complexation of **Azo-LL-Lys** (no UV)- and (B) (UV)-*ds*-DNA systems. [**Azo-LL-Lys** (no UV/UV)] = 50 μM and [*ds*-DNA] = from 0 to 440 μM.

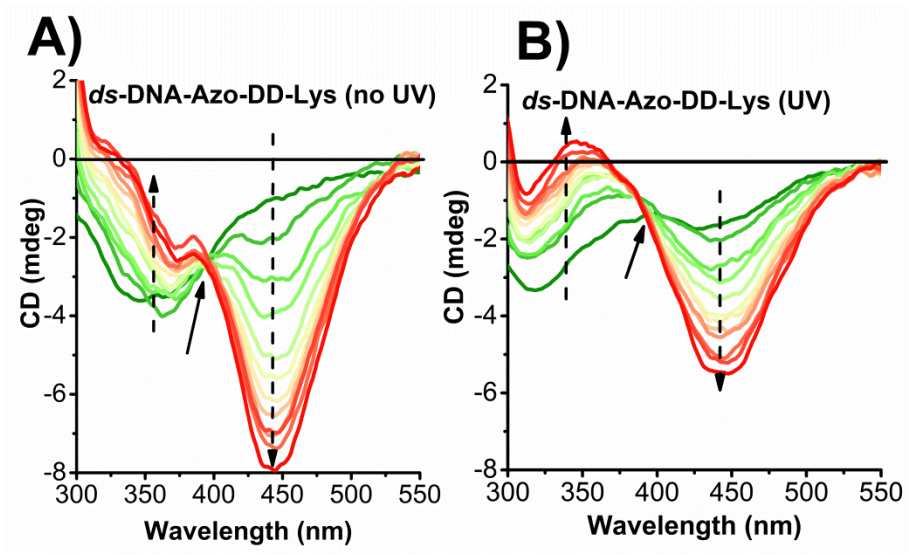

Figure S40. Electronic circular dichroism analysis of **Azo-DD-Lys** (no UV/UV)-*ds*-DNA adducts. (A) ECD spectra resulting from the complexation of **Azo-DD-Lys** (no UV)- and (B) (UV)-*ds*-DNA systems. [**Azo-DD-Lys** (no UV/UV)] = 50 μM and [*ds*-DNA] = from 0 to 440 μM.

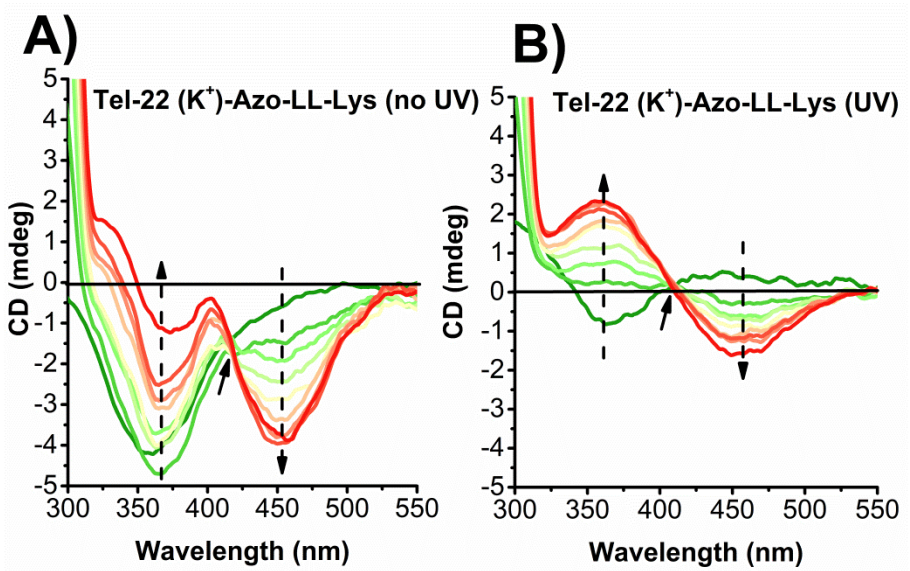

Figure S41. Electronic circular dichroism analysis of **Azo-LL-Lys** (no UV/UV)-Tel-22 (K^+) adducts. (A) ECD spectra resulting from the complexation of **Azo-LL-Lys** (no UV)- and (B) (UV)-Tel-22 (K^+) systems. [**Azo-LL-Lys** (no UV/UV)] = 50 μM and [Tel-22 (K^+)] = from 0 to 20 μM.

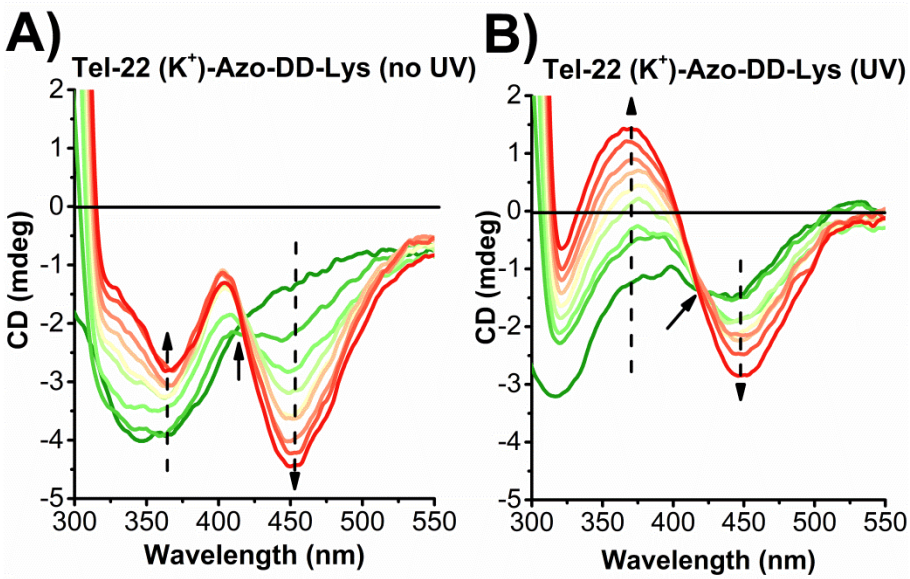

Figure S42. Electronic circular dichroism analysis of **Azo-DD-Lys** (no UV/UV)-Tel-22 (K^+) adducts. (A) ECD spectra resulting from the complexation of **Azo-DD-Lys** (no UV)- and (B) (UV)-Tel-22 (K^+) systems. [**Azo-DD-Lys** (no UV/UV)] = 50 μM and [Tel-22 (K^+)] = from 0 to 20 μM.

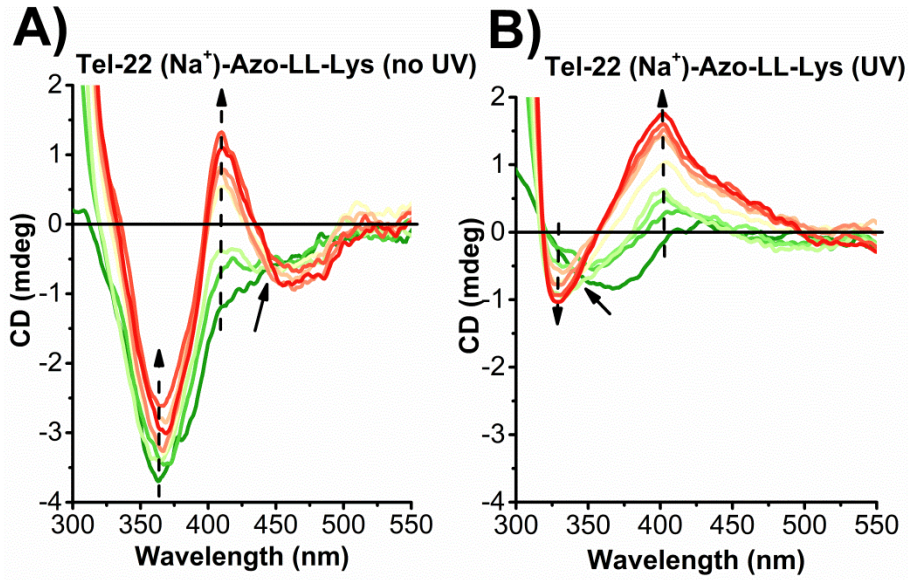

Figure S43. Electronic circular dichroism analysis of **Azo-LL-Lys** (no UV/UV)-Tel-22 (Na^+) adducts. (A) ECD spectra resulting from the complexation of **Azo-LL-Lys** (no UV)- and (B) (UV)-Tel-22 (Na^+) systems. [**Azo-LL-Lys** (no UV/UV)] = 50 μM and [Tel-22 (Na^+)] = from 0 to 20 μM.

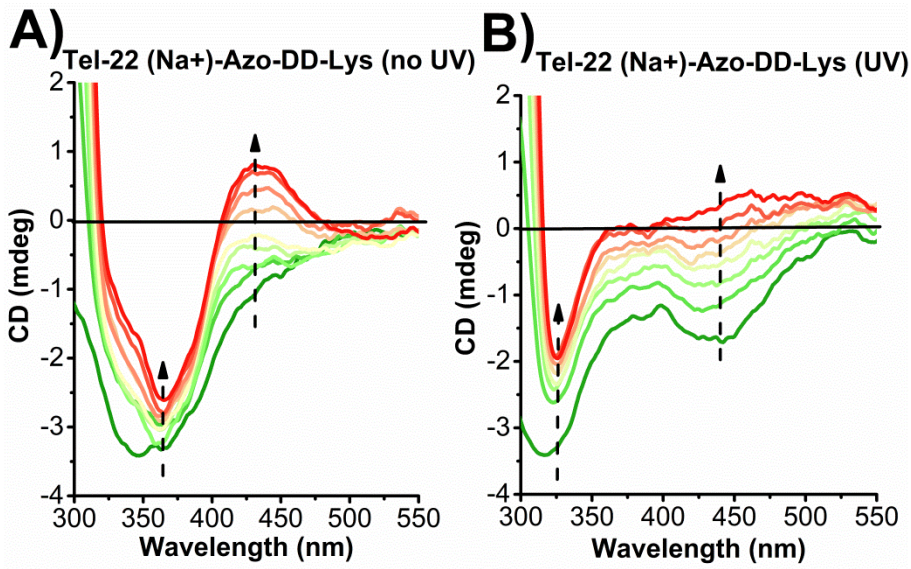

Figure S44. Electronic circular dichroism analysis of **Azo-DD-Lys** (no UV/UV)-Tel-22 (Na^+) adducts. (A) ECD spectra resulting from the complexation of **Azo-DD-Lys** (no UV)- and (B) (UV)-Tel-22 (Na^+) systems. [**Azo-DD-Lys** (no UV/UV)] = 50 μM and [Tel-22 (Na^+)] = from 0 to 20 μM.

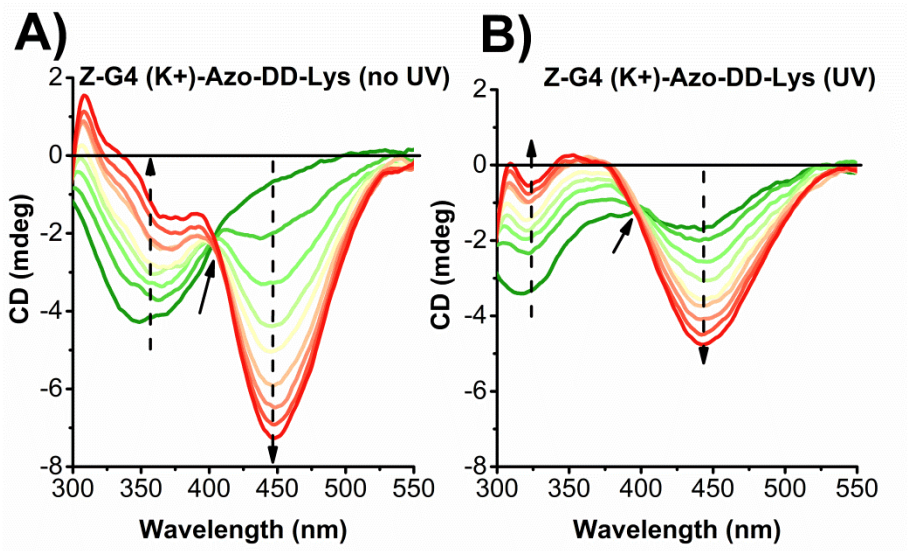

Figure S45. Electronic circular dichroism analysis of **Azo-DD-Lys** (no UV/UV)-Z-G4 (K^+) adducts. (A) ECD spectra resulting from the complexation of **Azo-DD-Lys** (no UV)- and (B) (UV)-Z-G4 (K^+) systems. [**Azo-DD-Lys** (no UV/UV)] = 50 μM and [Z-G4 (K^+)] = from 0 to 20 μM.

Duplex and quadruplexes conformational changes

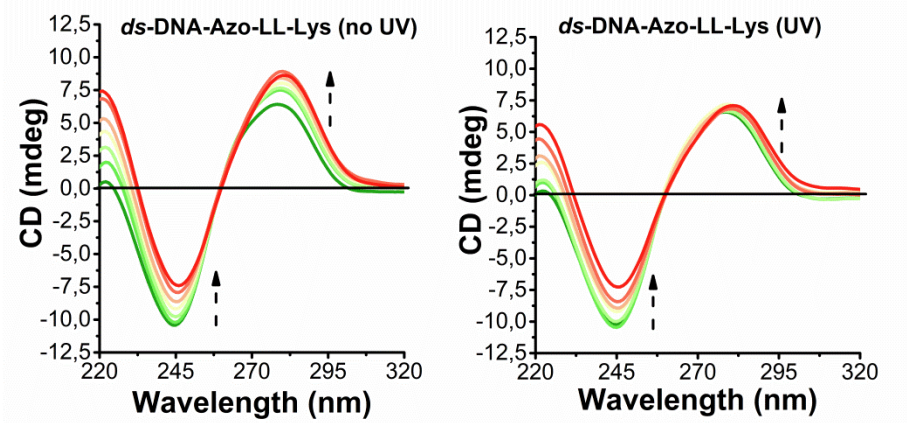

Figure S46. ECD spectra recorded for *ds*-DNA at various **Azo-LL-Lys** (no UV/UV)/*ds*-DNA molar ratios (r). r = 0, 0.05, 0.1, 0.15, 0.2, 0.3 and 0.4. The dashed arrows aim to show the evolution of the binding profiles.

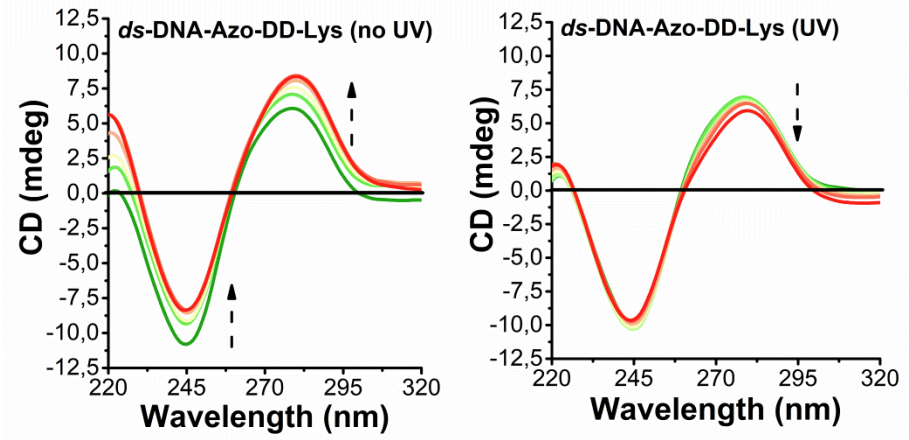

Figure S47. ECD spectra recorded for *ds*-DNA at various **Azo-DD-Lys** (no UV/UV)/*ds*-DNA molar ratios (r). r = 0, 0.05, 0.1, 0.15, 0.2, 0.3 and 0.4. The dashed arrows aim to show the evolution of the binding profiles.

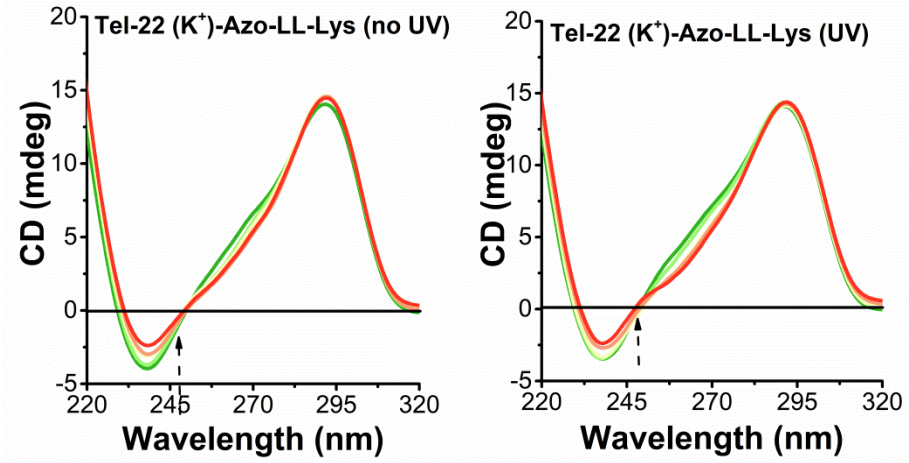

Figure S48. ECD spectra recorded for Tel-22 (K^+) at various **Azo-LL-Lys** (no UV/UV)/Tel-22 (K^+) molar ratios (r). r = 0, 0.5, 1, 1.5 and 2. The dashed arrows aim to show the evolution of the binding profiles.

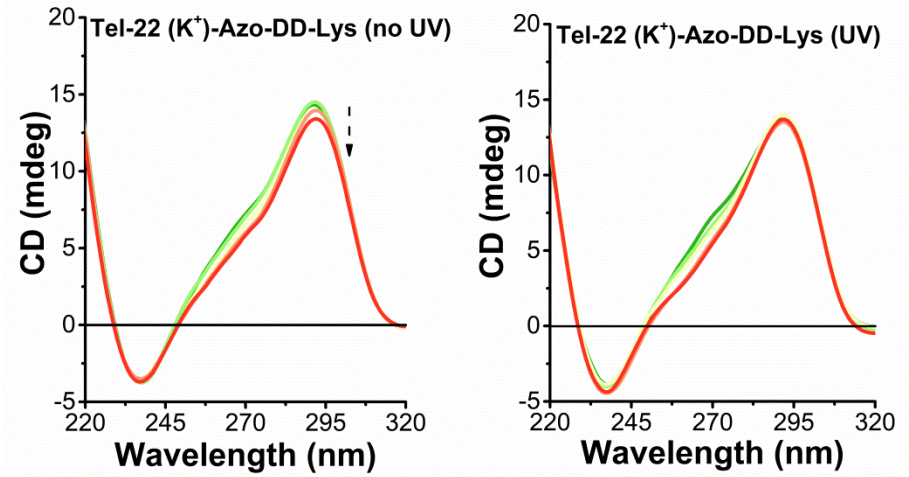

Figure S49. ECD spectra recorded for Tel-22 (K^+) at various **Azo-DD-Lys** (no UV/UV)/Tel-22 (K^+) molar ratios (r). r = 0, 0.5, 1, 1.5 and 2. The dashed arrow aims to show the evolution of the binding profiles.

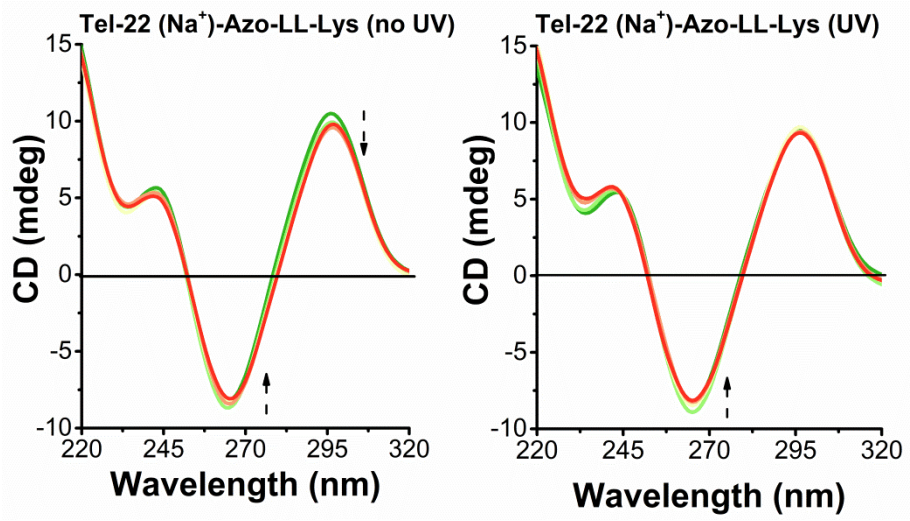

Figure S50. ECD spectra recorded for Tel-22 (Na^+) at various **Azo-LL-Lys** (no UV/UV)/Tel-22 (Na^+) molar ratios (r). r = 0, 0.5, 1, 1.5 and 2. The dashed arrows aim to show the evolution of the binding profiles.

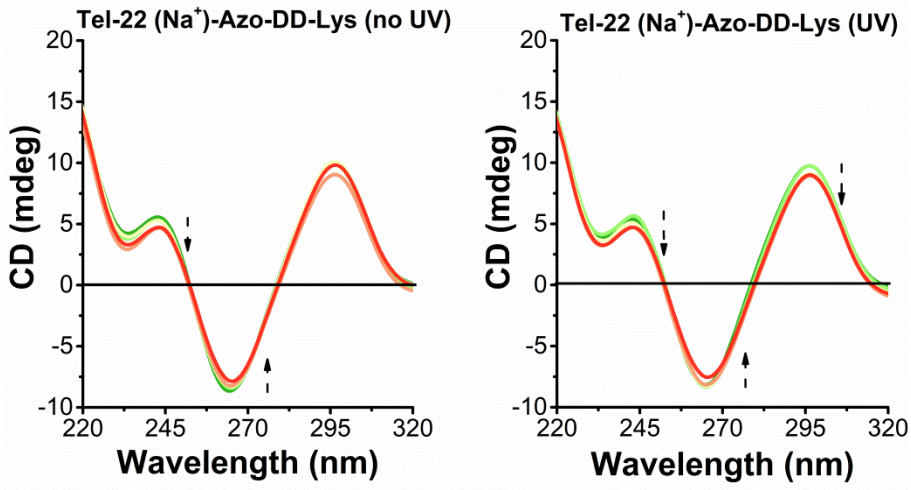

Figure S51. ECD spectra recorded for Tel-22 (Na^+) at various **Azo-DD-Lys** (no UV/UV)/Tel-22 (Na^+) molar ratios (r). r = 0, 0.5, 1, 1.5 and 2. The dashed arrows aim to show the evolution of the binding profiles.

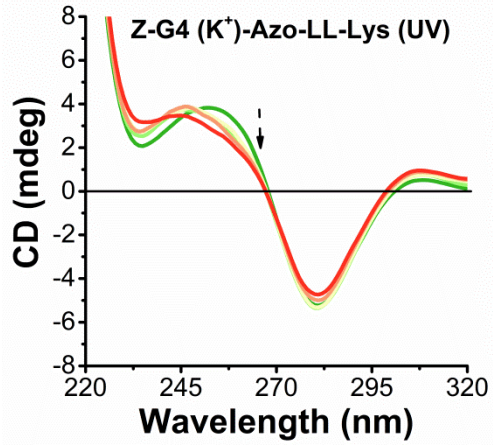

Figure S52. ECD spectra recorded for Z-G4 (K^+) at various **Azo-LL-Lys** (UV)/Z-G4 (K^+) molar ratios (r). r = 0, 0.5, 1, 1.5 and 2. The dashed arrow aims to show the evolution of the binding profiles.

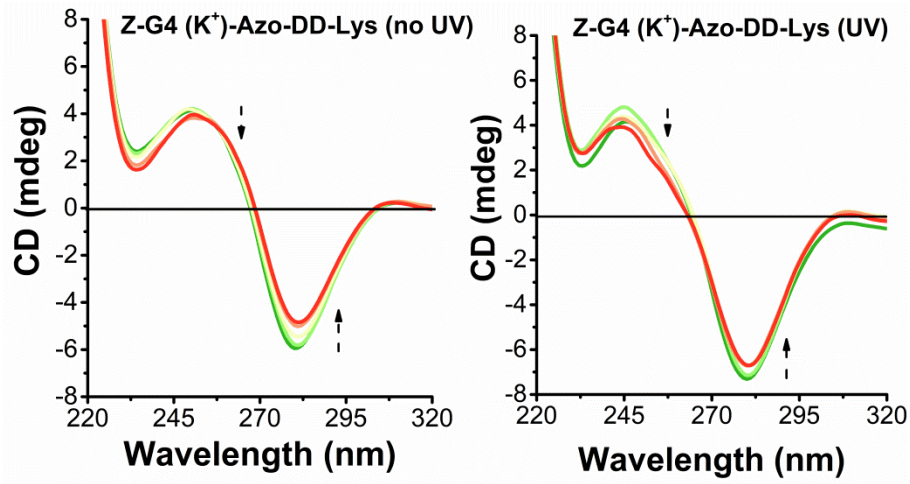

Figure S53. ECD spectra recorded for Z-G4 (K^+) at various **Azo-DD-Lys** (no UV/UV)/Z-G4 (K^+) molar ratios (r). r = 0, 0.5, 1, 1.5 and 2. The dashed arrows aim to show the evolution of the binding profiles.

References

(1) M. Deiana, Z. Pokladek, M. Dudek, S. G. Mucha, L. M. Mazur, K. Pawlik, P. Mlynarz, M. Samoc and K. Matczyszyn, *Phys. Chem. Chem. Phys.*, 2017, **19**, 21272−21275.

(2) Gaussian 16, Revision A.03, M. J. Frisch *et al*. Gaussian, Inc., Wallingford CT, 2016.

(3) A. Austin, G. Petersson, M. J. Frisch, F. J. Dobek, G. Scalmani and K. Throssell, *J. Chem. Theory and Comput*., 2012, **8,** 4989-5007.

(4) J. Tomasi, B. Mennucci and R. Cammi, *Chem. Rev*., 2005, **105**, 2999-3094.

(5) M. Deiana, B. Mettra, K. Matczyszyn, D. Pitrat, J. Olesiak-Banska, C. Monnereau, C. Andraud and M. Samoc, *Biomacromolecules*, 2016, **17**, 3609−3618.

(6) M. Deiana, B. Mettra, K. Matczyszyn, K. Piela, D. Pitrat, J. Olesiak-Banska, C. Monnereau, C. Andraud and M. Samoc, *Phys. Chem. Chem. Phys.*, 2015, **17**, 30318−30327.

(7) M. Deiana, Z. Pokladek, M. Ziemianek, N. Tarnowicz, P. Mlynarz, M. Samoc and K. Matczyszyn, *RSC Adv.*, 2017, **7**, 5912-5919.

(8) M. Deiana, Z. Pokladek, K. Matczyszyn, P. Mlynarz, M. Buckle and M. Samoc, *J. Mater. Chem. B*, 2017, **5**, 1028−1038.

(9) M. Deiana, Z. Pokladek, J. Olesiak-Banska, P. Mlynarz, M. Samoc and K. Matczyszyn, *Sci. Rep.*, 2016, **6**, 28605.

(10) M. Deiana, B. Mettra, L. M. Mazur, C. Andraud, M. Samoc, C. Monnereau and K. Matczyszyn, *ACS Omega*, 2017, **2**, 5715-5725.

(11) M. Deiana, B. Mettra, L. Martinez-Fernandez, L. M. Mazur, K. Pawlik, C. Andraud, M. Samoc, R. Improta, C. Monnereau and K. Matczyszyn, *J. Phys. Chem. Lett.*, 2017, **8**, 5915-5920.

(12) J. Mohanty, N. Barooah, V. Dhamodharan, S. Harikrishna, P. I. Pradeepkumar and A. C. Bhasikuttan, *J. Am. Chem. Soc.*, 2013, **135**, 367-376.

(13) A. Marchand, A. Granzhan, K. Iida, Y. Tsushima, Y. Ma, K. Nagasawa, M. P. Teulade-Fichou and V. Gabelica, *J. Am. Chem. Soc.*, 2015, **137**, 750-756.

(14) M. J. Cavaluzzi and P. N. Borer, *Nucleic Acids Res.*, 2004, **32**, e13.

(15) A. Renaud de la Faverie, A. Guédin, A. Bedrat, L. A. Yatsunyk and J. L. Mergny, *Nucleic Acids Res.*, 2014, **42**, e65.

(16) J. L. Mergny, J. Li, L. Lacroix, S. Amrane and J. B. Chaires, *Nucleic Acids Res.*, 2005, **33**, e138.

(17) P. L. T. Tran, J. L. Mergny and P. Alberti, *Nucleic Acids Res.*, 2011, **39**, 3282-3294.

(18) S. Neidle, *J. Med. Chem.*, 2016, **59**, 5987-6011.

(19) W. J. Chung, B. Heddi, E. Schmitt, K. W. Lim, Y. Mechulam and A. T. Phan, *Proc. Natl. Acad. Sci. U. S. A.*, 2015, **112**, 2729−2733.

(20) A. M. Rossi and C. W. Taylor, *Nat. Protoc.*, 2011, **6**, 365-387.

(21) A. Marchand, D. Strzelecka and V. Gabelica, *Chem. Eur. J.*, 2016, **22**, 9551-9555.

(22) A. Zhao, C. Zhao, J. Ren and X. Qu, *Chem. Commun.*, 2016, **52**, 1365-1368.